Numerical Modelling for Alternative Solution Designs of Steel and Timber Structures in Fire

Kathryn Chin

A Thesis submitted to the Faculty of Graduate Studies in Partial Fulfillment of the Requirements for the Degree of Master of Science

Graduate Program in Civil Engineering

York University

Toronto, Ontario

August 2025

Abstract

The objective of this thesis is to increase confidence in alternative solution designs, since its use has increased. Through experimental data collection, a better understanding of steel and timber behaviour in fire was gained and the knowledge was transferred to numerical model development. A validated modelling methodology allows designers to predict structural performance in fire which can then be used to justify decision making and as a method to show the design is code compliant. This thesis examined the performance of steel trusses exposed to a localized fire with a complementary heat transfer and thermal deformation model. For timber, cone calorimeter experiments were completed on various timber products with complementary heat transfer models followed by an exploratory study on thermal parameters in modelling. The thesis provides recommendations for best practices and future research regarding finite element modelling of steel and timber to further develop tools for alternative solution designs.

Acknowledgements

First and foremost, I'd like to thank my supervisor Dr. John Gales. I'm so grateful for all his support and guidance. His openness to always have a conversation, the opportunities he's provided whether it be through travel or support in scholarship applications, his encouragement in my research but most of all, the knowledge he so freely gives. I've learned so much from him and I'm so glad he took a chance on a high school summer student who knew nothing at all except that she was curious to learn.

I would also like to thank past and current research team members Ethan, Chloe, Tim, Anne, Hannah, Pina, and Bronwyn. I'm so grateful to be a part of a team that is so generous with their time and advice. Thank you for all your help and the conversations we've had. To Riad Rajab who always helped me in the lab with a smile on his face and Sindy Mahal who made sure everything was in order, answering all my questions, thank you.

I would like to thank Dr. Panos Kotsovinos and Dr. Rwayda Al Hamd for being mentors, guiding and assisting in my research, bringing new perspectives and alternative approaches. I'd like to thank everyone at the University of Waterloo Fire Research Group for their lab, assistance and overall guidance. I would like to recognize ARUP for their technical support and the in-kind support of Benson Steel. York University and Next Generation Wood Construction are acknowledged for their financial support.

To my friends and family, thank you the endless support. Without you, this would not have been possible. To Jenn, Steph, Christopher, and Matthew, thank you for matching my crazy. Thank you for understanding me, I wouldn't be me without you. To Betty, for being the best dog and always greeting me with a wagging tail. And finally, thank you to my parents. Thank you for everything you've done for me. For loving me, for supporting me, for letting me dream big and never once thinking I'd fail. Thank you.

Declaration

The work presented follows a modified manuscript format in which all work, with the exception of Chapter 5, has been published, submitted to, or presented at a journal or conference. Each chapter is modified or adapted from the research articles, all of which were completed during the author's Master's degree at York University. All research articles were developed and influenced by several co-authors with the author being the primary author for majority of the research articles. For research articles where the author is not the primary author, only their contributions to the study will be included in the thesis herein. Within the declaration and thesis, a clear statement will be made regarding the author's contributions for studies where they are the second author.

Chapter 3 is adapted from:

- Jeanneret, C., **Chin, K.**, Kotsovinos, P., and Gales, J. (2023) Chord Shielding Effect in Steel Trusses when Exposed to a Localized Fire. CSCE Annual Conference (2023). Moncton, Canada
- **Chin, K.**, Jeanneret, C., Kotsovinos, P., and Gales, J. (2024) Experimental and Numerical Response of Steel Trusses Exposed to a Localized Fire. Proceedings of the 13th International Conference on Structures in Fire. 1127-1136
- **Chin, K.**, Jeanneret, C., Kotsovinos, P., Al Hamd, R., and Gales, J. (2025) Modelling Thermal Deformation of a Steel Truss. 16th International Conference and Exhibition on Fire Science and Engineering. Royal Holloway College, Windsor, United Kingdom.

The first study is an experimental study with the primary author Jeanneret being the lead on the project. The author of the thesis assisted in testing (from setting up the experiment and instrumentation to recording data) and completed the literature review section.

Chapter 4 is adapted from:

- Philion, E., **Chin, K.**, Kostovinos, P., Weckman, B., and Gales, J. (2024) An Analysis of the Fire Performance of Small-Scale Canadian Heritage Hardwood and Softwood. Structural Engineering International, DOI: 10.1080/10168664.2024.2340566

- **Chin, K.**, Lau, A., Lacroix, D., and Gales, J. (2025) Numerical Modelling of Charring in Engineered Timber. International Fire Safety Symposium (IFireSS 2025) - 5th Edition. Ulster University Belfast, Belfast, United Kingdom

In the first study where Philion is the primary author, the thesis author was responsible for the modelling portion of the paper. This included gathering model input values such as density and moisture content information through furnace drying, building the model, analyzing the results, and writing the modelling section of the study.

Table of Contents

Abstract ii

Acknowledgements iii

Declaration iv

Table of Contents vi

List of Tables ix

List of Figures x

Chapter 1 : Introduction 1

1.1 General 1

1.2 Motivation 3

1.3 Scope of Project 3

1.4 Research Objectives 5

1.5 Outline of Thesis 6

Chapter 2 : Literary Basis 9

2.1 Prescriptive Design Versus Alternative Solutions 9

2.2 Heat Transfer 11

2.3 An Overview of Steel and Timber 13

2.3.1 Steel 13

2.3.2 Timber 16

2.4 The Finite Element Method 20

2.4.1 Pre-Processor: User Specifications 21

2.4.2 Solver Method 22

2.4.3 Post-Process and Validation 24

2.5 Summary 24

Chapter 3 : Experimental Testing and Numerical Modelling of Steel Trusses Exposed to a Localized Fire 26

3.1 Introduction 26

3.2 Background 29

3.3 Experiments on Steel Trusses Under Localised Fire 31

3.3.1 Methodology 32

3.3.2 Results 36

3.4 Numerical Models 38

3.4.1 Methodology 38

3.4.2 Results 42

3.5 Discussion 46

3.5.1 Experiment 46

3.5.2 Heat Transfer Model 48

3.5.3 Thermal Deformation Model 50

3.6 Conclusion 51

Chapter 4 : Cone Calorimeter Testing and Numerical Modelling of Sawn Lumber and Engineered Timber 54

4.1 Introduction 54

4.2 Background 55

4.2.1 Moisture Evaporation 55

4.2.2 Char Formation 57

4.2.3 Summary 58

4.3 Experimental and Numerical Methodology 59

4.3.1 Experiment 59

4.3.2 Model 64

4.4 Experimental and Numerical Results 66

4.4.1 Experimental ... 66
4.4.2 Numerical Model Results ... 69
4.5 Discussion ... 73
4.6 Conclusions ... 77
Chapter 5 : Exploratory Modelling Analyses of Thermal Material Parameters ... 78
5.1 Introduction ... 78
5.2 Thermal Material Properties ... 79
5.3 Methodology ... 82
5.3.1 Summary of Experiments ... 82
5.3.2 Modelling Scenarios ... 83
5.3.3 Model Parameters ... 86
5.4 Results ... 87
5.5 Discussion ... 90
5.6 Conclusions ... 91
Chapter 6 : Conclusions and Recommendations ... 93
6.1 Summary ... 93
6.2 Conclusions ... 95
6.3 Research Recommendations ... 97
6.4 Design Recommendations ... 98
References ... 99

List of Tables

Table 3.1: Description of the location of thermocouples. 34
Table 3.2: Percent difference between model and experimental results at peak thermal strain. .. 45
Table 3.3: Coefficient of thermal expansion based on DIC results. 46
Table 4.1: Cone calorimeter test matrix. 59
Table 4.2: Average and CoV of material properties per test type. 61
Table 4.3: Average char depth and charring rate for the heritage hardwood and softwood samples. 68
Table 4.4: Average and CoV of char depth and average charring rate for the engineered timber glulam and CLT samples. 69
Table 5.1: Summary of the simulations conducted. 83
Table 5.2: Example of model input specific heat capacity curve after density modification. 86
Table 5.3: Average factor between experimental and numerical results. 89

List of Figures

Figure 1.1: Examples of modern steel and timber construction in Canada (Author's photos)....... 1
Figure 1.2: Process of structural fire modelling... 4
Figure 1.3: Overview of thesis chapters and their interconnectivity. 6
Figure 2.1: The standard fire time-temperature curve used for the standard fire test as per ISO 834 [15]. 9
Figure 2.2: Fire triangle diagram adapted from [20]. 12
Figure 2.3: Phase diagram of steel with respect to the carbon weight (adapted and replicated from [27], [28]). 14
Figure 2.4: Annex K reduced elastic modulus, yield strength, and ultimate strength values at increased temperatures. 15
Figure 2.5: Drawing indicating the location of bound and free water. 16
Figure 2.6: Diagram of laminates for glulam (left) and CLT (right). 18
Figure 2.7: Cross section of burned timber showing the char layer.. 19
Figure 2.8: Examples of solid elements and beam elements. 20
Figure 2.9: Finite element software's used in the thesis herein (adapted from [47]). 20
Figure 2.10: Example of a truss element in the FEM. 22
Figure 3.1: Experimental setup and truss dimensions. 33
Figure 3.2: Location of thermocouples. 34
Figure 3.3: Images of a truss exposed to a localized fire before (left) and after (right) using narrow spectrum illumination. 36
Figure 3.4: Time-temperature experimental data from the thermocouples.................................. 37
Figure 3.5: Strain over time experimental data using DIC. 38
Figure 3.6: Time-temperature curve of thermocouple tree experiment. 39
Figure 3.7: Corresponding thermocouple data to the area of applied boundary conditions for the heat transfer model. 40
Figure 3.8: Model beam numbering (left) and side view of members (right). 41
Figure 3.9: Averaged input time-temperature curves applied to each beam section.................... 42
Figure 3.10: Comparison of model versus experimental results for the heat transfer model (L1 to L3). 43

Figure 3.11: Comparison of model versus experimental results for the heat transfer analysis (L4 to L6). 43
Figure 3.12: Top chord (L7) experimental and model results comparison. 44
Figure 3.13: Diagonal chord (L3) experimental and model results comparison. 44
Figure 3.14: Bottom chord (L5) experimental and model results comparison. 45
Figure 3.15: DIC validation against Eurocode 3 [97] using strain over temperature. 47
Figure 3.16: Comparison of the experimental steel temperatures versus the calculated steel temperatures using the Eurocode 3 method for steel temperature development. 49
Figure 4.1: Latent Heat method [106] modified specific heat capacity over time. 56
Figure 4.2: Prepared glulam sample prior to cone calorimeter testing. 60
Figure 4.3: Prepared CLT sample prior to cone calorimeter testing. 61
Figure 4.4: Cone calorimeter apparatus. 62
Figure 4.5: Cone calorimeter heating mechanism. 63
Figure 4.6: Char depth measuring apparatus and measurement locations. 64
Figure 4.7: Mesh sensitivity analysis of hardwood at 50 kW/m^2 for 3 minutes. 65
Figure 4.8: Time sensitivity analysis of hardwood at 50 kW/m^2 for 3 minutes. 65
Figure 4.9: Examples of adhesive bleeding occurring during the CLT cone calorimeter tests (circled in red). 67
Figure 4.10: Charred glulam sample (left) and charred CLT sample (right) after a six-minute test. 68
Figure 4.11: Numerical heat transfer of CLT tested for three minutes (temperature in Kelvin)... 70
Figure 4.12: Experimental versus model charring rate for hardwood. 70
Figure 4.13: Experimental versus model charring rate for softwood 71
Figure 4.14: Experimental and model charring rates for the glulam samples. 71
Figure 4.15: Experimental and model charring rates for the CLT samples. 72
Figure 4.16: Comparison of experiment and model charring rates for 30 kW/m^2 heat intensity. 72
Figure 4.17: Comparison of experiment and model charring rates for 50 kW/m2 heat intensity. 73
Figure 4.18: Temperature versus node depth at the end a 3-minute CLT simulation with varied density. 76
Figure 5.1: Comparison of the specific heat capacity over temperature curves for Eurocode 5 [107] and König and Walleij [123]. 80

Figure 5.2: Comparison of density over temperature curves for Eurocode 5 [107] and König and Walleij [123] assuming a dry density of 425 kg/m^3 and a moisture content of 12%. 81
Figure 5.3: Comparison of thermal conductivity over temperature curves for Eurocode 5 [107], König and Walleij [123] and Fredlund [124]. 82
Figure 5.4: Comparison of charring rates from glulam experiments and simulations................. 88
Figure 5.5: Comparison of charring rates from CLT experiments and simulations...................... 88
Figure 5.6: Temperature over time at various nodes for a 3-minute CLT test using Simulation 1C (left) and 6C (right). 89

Chapter 1: Introduction

1.1 General

With over 700,000 fires in Canada between the years 2005 and 2021 (approximately 45,000 per year) [1], Fire Safety Engineering is a necessary practice. Of these fires, most were categorized as structural fires which includes all building types. The fires span small scale events such as residential fires, to major, devastating wildfires. Given the prevalence and hazard of fire disasters, the true objective of Fire Safety Engineering is to limit fire risks and ensure life safety. In recent years, the industry has seen an increase in innovative structures, with designers pushing boundaries, striving towards unique, sustainable and complex structures, ultimately increasing the need for alternative solutions such as performance-based design (see Figure 1.1 for examples of modern Canadian structures).

Figure 1.1: Examples of modern steel and timber construction in Canada (Author's photos).

Performance-based design allows for more flexibility, requiring structures to achieve a particular performance result, rather than prescribing a set procedure [2]. Additionally, performance-based design shifts the focus to fire resilience, rather than the prescriptive solution which uses fire resistance. Fire resilience is an all-encompassing term, focusing on a structure's ability to withstand a fire, and the ease in which the structure can recover from a fire. Fire resistance on the other hand uses the standard fire test to determine the fire resistance rating (time of structural stability) of a particular system or member. Because of its focus on the result and not the process, alternative solutions such as performance-based design are more conducive to the optimization of resources such as the amount and location of fire protection and/or materials. This means that designs can be more sustainable, efficient, and economical, as well as use new technology and materials [3]. However, there are challenges that arise, particularly when designing from a fire safety perspective.

The thesis herein will focus on steel and timber behaviour at elevated temperatures. Concrete is not being considered because of its benefits to cost ratio. When designing concrete in fire, additional fire protections are rarely used since concrete is non-combustible with a low thermal conductivity. Instead, the size or geometry of the concrete member is adjusted [4]. Therefore, the cost of needing a Fire Safety Engineer to conduct performance-based fire design for concrete will likely outweigh the cost saved by any reduction in the required amount of concrete. However, the optimization of the amount of steel and fire protection material can provide more impactful financial incentives, hence its consideration in this study.

Therefore, steel and timber have a basis for alternative solutions though for different reasons. Being able to optimize fire protection on steel members would be beneficial as it does not face the same drawbacks as concrete. Furthermore, recent years have seen and increase in innovative design in the geometry of structures being built. This innovation often results in the use of prescriptive designs being inappropriate, thus requiring alternative solutions. However, it is important that there is research and knowledge behind these decisions. Steel has complex behaviour in fire and improper fire safety design can result a failure at the localized scale to a complete collapse.

From a fire perspective, timber was heavily used historically until the emergence of steel and concrete. However, starting in 2021, countries and industry leaders in engineering attended the Conference of the Parties in which they committed to reduce their carbon emissions by 2030 [5], [6]. Therefore, timber construction has reemerged because it is a viable solution to build more sustainably. Unlike concrete or steel, timber is compelling because it is a carbon sink (can sequester carbon), it is a renewable resource and is abundant in Canada [7]. Developments have led to the creation of engineered timber such as glulam or cross-laminated timber (CLT), which allows mass timber construction. However, unlike steel, timber is a combustible material. This means that when timber burns, it becomes fuel, increasing the intensity and complexity of the fire. Pyrolysis occurs during this burning process; a chemical reaction in which a layer of char (having no structural strength) and volatile gases are produced [8]. The combustibility of timber often requires designers to move towards performance-based fire design because, as stated in a study by Gales et al., prescriptive designs using fire resistance principles are not applicable for combustible materials [9]. Evidently, an increase in complexity of the types of structures being built, material behaviour and new technologies has led to a need for performance-based fire design of steel and timber structures.

1.2 Motivation

In Canada, the steel industry has Annex K (CSA-S16), a normative part of the steel design standards which provides alternative design guidance regarding steel and fire design [10]. Similarly, the Wood Design Manual has Annex B, which is an informative (not mandatory) section regarding the fire resistance design of timber [11]. The novelty of timber design means that fire safety codes are much more generalized (hence the fact that Annex B is informative rather than normative) due to significant knowledge gaps in this field.

Overall, current codes and guidelines predominantly use the prescriptive design approach as the default approach. While steel and timber have some guidance within codes and standards for alternative solutions, the push for performance-based design has resulted in the need for risk-based analysis as a tool in fire safety design. Therefore, the motivation of this thesis is to advance modelling technologies and methodologies to more accurately simulate material behaviour when exposed to fire scenarios. Risk-based analysis can use modelling technology such as finite element analysis to predict how various structural systems, geometries and fire scenarios will impact structural strength before and after a fire event. This will inform whether a structure is stable, for how long it will remain stable in a given fire exposure and identify vulnerable areas of the system where fire protection measures should be optimized. Hence, reliable modelling tools can assist in safe, efficient, and sustainable performance-based fire resilient design.

1.3 Scope of Project

While the development of these numerical models can assist in limiting fire risks, it is important to note that research gaps for fire dynamics and steel and timber material behaviour in fire hinder the development of accurate design tools. Designing without having a comprehensive understanding of the heat exposure and materials used can be dangerous in terms of life safety and evacuation. Therefore, the following thesis will conduct experimental testing prior to model development to better understand the materials, as well as use the data for model validation.

Structural fire modelling can be done in three phases: the fire model, a heat transfer model, and a mechanical model [12]. The fire model is typically done in a separate, fire dynamics software, while heat transfer and mechanical models can be conducted using finite element software. While all three models are not always completed, they must be done in consecutive order with results from the previous model being used as inputs in the next model (see Figure 1.2). A literature review of numerical models for various steel members and systems published within the last five years at the time of writing found common challenges in fire modelling [13]. These included the application of boundary conditions in the heat transfer model and inaccuracies in modelling results and methodology in a phase of the model being transferred to the final results. The study also found the importance of model validation, a step in which the simulated results can be compared to experimental data to evaluate the accuracy of the modelling methodology.

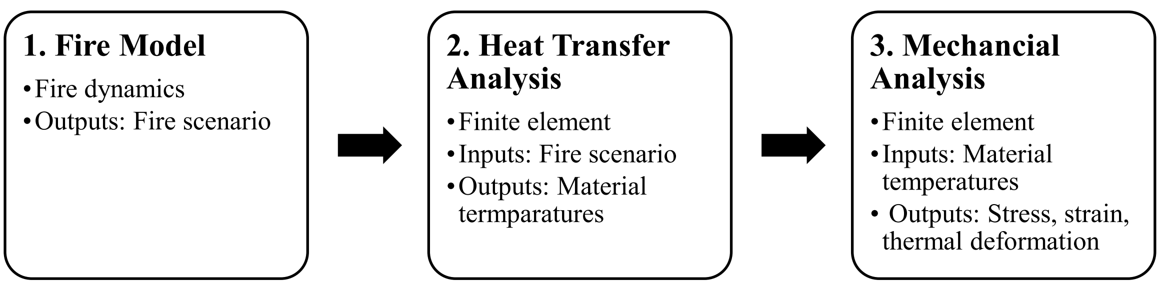

Figure 1.2: Process of structural fire modelling.

The scope herein will focus on developing finite element modelling tools. For steel, as a more researched and well understood building material, the thesis will develop both heat transfer and mechanical analysis models. Research gaps have been found in the fire design of stadium roof trusses. The amount of fire protection required, if any, is often left to up to the discretion of the designer, and will therefore, be the structural steel system considered. For timber, because of its novelty, it is under researched, leading to significant knowledge gaps. Therefore, only a heat transfer model will be developed for timber elements. Specific focus will be placed on various timber products, sawn heritage lumber and engineered timber, to determine key parameters that impact charring rates and heat transfer mechanisms.

To develop these models, a strong understanding of steel and timber behaviour is required. Therefore, the thesis will include a series of experiments to generate both input data and validation data. Different modelling methodologies and exploratory studies will be developed, compared and tested. Therefore, the thesis herein will explore three major themes:

1. Experimental testing of steel and timber exposed to non-standard fire heating exposures;
2. The development of numerical, heat transfer and mechanical modelling tools to be validated using experimental data; and,
3. Exploratory analyses of varying timber properties to understand which parameters are important in modelling, and how they impact the accuracy of the results.

Non-standard heating exposures will be used for the research herein due to the focus on performance-based design and resilient structures. A more in-depth analysis of timber behaviour will be performed since it is an understudied material with significant research gaps. Specific focus will be placed on the charring behaviour of various timber specimens including heritage hardwood and softwood, and mass timber elements glulam and CLT. Exploratory analyses of timber will also be conducted, changing thermal material parameters and various input methodologies to determine the limitations of the model as well as alternative methodology approaches. While not in the scope of this project, the research establishes the base for possible modelling of hybrid timber-steel structures, another movement currently in industry. With a better understanding of how each material behaves when isolated, a more informed modelling methodology can be developed. Overall, developing finite element heat transfer and/or mechanical modelling methodology of steel and timber exposed to fire can be used by industry when conducting performance-based fire design.

1.4 Research Objectives

The recent push for sustainability, economic construction and innovative design has led to a rise in performance-based design. From a fire perspective, numerical modelling tools have been identified as a useful aid in using alternative solutions for fire design and analysis for industry use, especially since the codes provide detailed guidance for prescriptive design only. Simulated results can be used in risk-based analyses, assisting in informed decision making. However, research is required to determine how to develop these tools and more specifically, what parameters are important to generate accurate predictions. With the overarching research question of "What input parameters are required to develop modelling tools that accurately represent steel and timber behaviour in fire?", this thesis aims to build further understanding of these research questions through the following objectives:

1. Increase knowledge of timber and steel fire resilience through non-standard fire testing;
2. Develop design and analysis tools for industry use to promote using alternative solutions to design steel and timber structures in the future;
3. Develop and validate a modelling methodology that can predict heat transfer, deformation and/or residual strength during and after a fire event;
4. Determine best practices for numerical modelling as well as identify key parameters that are necessary for accurate modelling results; and,
5. Identify remaining literary gaps hindering the use of alternative solutions.

1.5 Outline of Thesis

This thesis uses a modified manuscript-based style. Chapters 3 and 4 contain text from submitted or published conference and journal peer-reviewed papers. Text has been modified to represent the authors contributions to each study, as well as to ensure a unified body of research. All research was conducted during the author's Master of Applied Science degree at York University. The following section will briefly describe the contents of each thesis chapter. Figure 1.3 illustrates an overview of the thesis chapters as well as how they are connected.

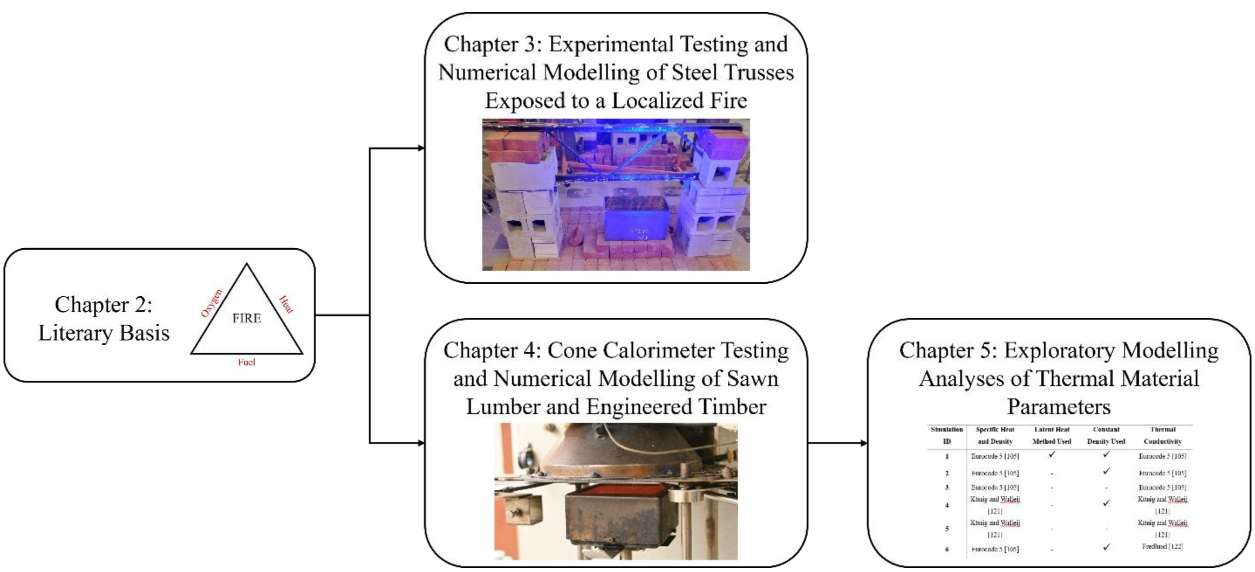

Figure 1.3: Overview of thesis chapters and their interconnectivity.

Chapter 2: Literary Basis provides the reader with background information required to understand subsequent thesis chapters. The chapter will describe performance-based design versus prescriptive design, discussing the use of the standard fire test in the prescriptive approach. Next, a brief description of heat transfer mechanisms relevant to the thesis herein will be explored followed by an overview of steel and timber as materials, as well as their behaviour in fire. Finally, the section will provide an overview of the finite element method.

Chapter 3: Experimental Testing and Numerical Modelling of Steel Trusses Exposed to a Localized Fire conducts experimental testing on small-scale steel trusses to determine its thermomechanical behaviour when exposed to non-uniform, non-standard fire testing. Focus was placed on the presence of a chord shielding effect in which exposed portions of the truss redirected heat and flames, limiting the heat exposure of protected truss sections. Time-temperature data was collected using thermocouples and thermal strain data was collected using digital image correlation. From there, a heat transfer and mechanical model were developed to predict temperatures, thermal strains, and residual strength during and after a fire event. The model results were validated using the experimental data. The purpose was to establish finite element modelling methodologies for performance-based design assistance, and to provide additional guidance and tools for stadia roof fire design.

Chapter 4: **Cone Calorimeter Testing and Numerical Modelling of Sawn Lumber and Engineered Timber** explores the heat transfer mechanism of various timber products when exposed to a controlled heating source. To determine the differences between material behaviour, boundary conditions, geometry, and scale all remained the same. Heritage softwood and hardwood, and mass timber glulam and CLT elements were tested using a cone calorimeter, which provides a constant heat flux exposure. Tests were conducted using various time durations to track the formation of the char layer to gain a better understanding of pyrolysis for model validation. The model was made using an apriori methodology in another study. Therefore, the objective of the chapter was to assess the accuracy of the model for the given scenario, as well as identify key parameters affecting heat transfer which require further research.

Chapter 5: Exploratory Modelling Analyses of Thermal Material Parameters expands upon Chapter 4 in which the thermal material parameters used in the previous chapter were modified and analyzed. Additionally, the methodology used in Chapter 4 was modified to explore alternative approaches given the software limitations. The purpose of this chapter is to analyse how the accuracy of the model is impacted when these parameters and methods are changed. It allows for recommendations for modelling methodology to be given and continues to identify and further provide information on key parameters for timber in fire modelling. Overall, Chapter 5 aims to explore the bounds of finite element modelling for timber in fire, highlighting limitations and research gaps.

Chapter 6: Conclusions and Recommendations will summarize key findings from the previous chapters as well as their novelty. Chapter 6 will discuss the applicability of the research conducted in the thesis herein, as well as highlight future research areas required to further the development of numerical modelling of steel and timber in fire.

Chapter 2: Literary Basis

This chapter will aim to inform the reader of topics and concepts necessary to understand the thesis herein. The chapter will review the differences between prescriptive design and alternative solutions such as performance-based design, heat transfer, steel and timber material properties and their behaviour in fire, and the finite element method.

2.1 Prescriptive Design Versus Alternative Solutions

This section will further discuss the differences between prescriptive and performance-based design. In the context of prescriptive design, the basis for fire design relies on the standard fire test. Per ASTM E119 the standard fire test is a procedure in which specimens are placed in a furnace and exposed to the standard fire time-temperature curve [14]. The standard time-temperature curve (illustrated in Figure 2.1) resembles a logarithmic function, increasing infinitely, excluding the cooling phase. From literature, the standard fire test was developed between 1890 and 1916 and was made to represent a worst-case scenario fire according to knowledge at that time. However, research developments within the fire safety engineering field illustrate that this testing methodology is now considered unrepresentative of a real fire heat exposure [9]. In a real fire, temperatures can reach higher maximum temperatures in a shorter period of time (faster heating rate and higher intensity) and include a cooling phase.

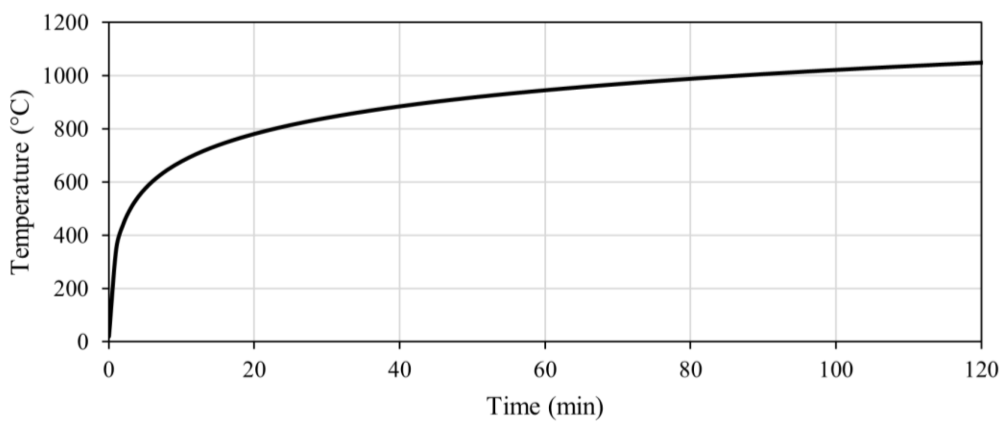

Figure 2.1: The standard fire time-temperature curve used for the standard fire test as per ISO 834 [15].

Using the standard fire test, a fire resistance rating can be assigned. According to the National Fire Code of Canada, the fire resistance rating indicates "the time in minutes or hours that a material or assembly of materials will withstand the passage of flame and the transmission of heat when exposed to fire under specified conditions of test and performance criteria" [16]. From there, codes can prescribe fire protection based on the required fire resistance rating. However, in the standard fire test, instrumentation such as thermocouples and/or plate thermometers measure the temperature within the furnace to ensure it matches the specified standard fire time-temperature curve. If a combustible material is tested, it releases its own heat energy, potentially increasing the temperature within the furnace and decreasing amount of additional energy needed to sustain the curve. This leaves uncertainty in if the fire resistance rating is accurate or comparable to the results of other materials.

While it is important to have standardized testing, it is also important to understand their limitations and restrictions. With more complex structures and materials as well as developments within research, code guidance and testing procedure should continue to adapt. This has led to the increase in the use of alternative solutions such as performance-based design. Alternative solutions often focus on fire resilience which is a broader term. According to Himoto, fire resilience is a function of the ability and time of a structure to be rehabilitated post fire event and the severity of the fire damage [17]. Therefore, assessing the fire resistance requires exposing materials and specimens to realistic fire conditions and monitoring factors that affect structural integrity throughout both the heating and cooling phases.

Alternative solutions have less emphasis on the process of design and more on the quality of the final design. As discussed in Chapter 1, steel and timber contain additional Annex's which provide basic information on alternative solutions. For example, Annex K, part of the steel standard, provides reduction factors for structural properties (for example the elastic modulus and yield stress) of steel at elevated temperatures, which can be factored into performance-based fire designs (this will be elaborated upon in Section 2.3.1) [10]. For timber, Annex B provides modified "k" factors, charring rates for cross-sectional area reduction, and information regarding gypsum board as fire protection amongst other information [11].

When conducting alternative design, code compliance has been met if a performance-based design meets or exceeds the performance criteria as the prescriptive design [10]. Assessment of performance can be done through three main methods, numerical modelling, fire testing, or other calculations. As an example, a design can have reached the acceptable solution if it is fire tested to a greater severity than what is prescribed in the code (the standard fire) for the same duration. For the thesis herein, focus will be placed on the numerical modelling method. A validated model based on a wide variety of experiments allows the methodology to be used in predictive scenarios required for alternative solutions. Within a range of validated exposures, designers can confidently estimate the expected deformations or temperature profile of the particular component or system. This limits the need for more costly experiments and allows the solution to be benchmarked and compared to the prescriptive solution to prove it meets code compliance. [18]

Overall, alternative solutions are beneficial because they allow for more freedom and flexibility, allowing designers to optimize material use such as the amount or placement of fire protection measures. This can lower financial and environmental costs, however further development of guidance, especially within Canada, is necessary. If the cost of the alternative solutions is higher than the savings from the alternative solutions, then the prescriptive design is more reasonable [18], [19]. Therefore, the focus of the thesis herein is developing easy to use and widely accessible numerical modelling tools to assist in alternative solutions.

2.2 Heat Transfer

When discussing fire safety design and material behaviour in fire from a realistic heat exposure perspective, it is important to understand basic fire dynamics and heat transfer mechanisms. A fire is comprised of three necessary elements: oxygen, heat and fuel, known as the fire triangle (see Figure 2.2) [20]. If one of these elements is not present, the fire will extinguish. In terms of timber in fire, complexity occurs because timber is combustible, thus acting as fuel. When the timber begins to burn, it also releases heat, providing two elements of the fire triangle. Unlike steel, timber can sustain a fire by itself if oxygen is present.

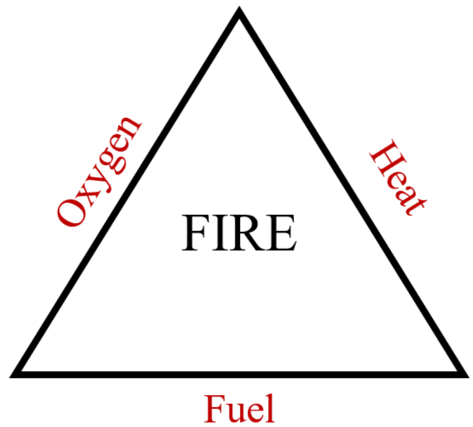

Figure 2.2: Fire triangle diagram adapted from [20].

With a fire or heat source, there are three basic heat transfer mechanisms: conduction, convection, and radiation. Heat transfer is often represented as a heat flux which is a measure of energy over area (W/m^2). Per Drysdale [21], conduction is the transfer of heat through contact between solid surfaces. As seen in Equation 2.1, conduction is a function of thermal conductivity, temperature difference and the distance in which the temperature difference occurs. Convection is heat transfer through a fluid medium (air for this thesis) and is a function of temperature and the convective heat transfer coefficient (Equation 2.2). Finally, radiation transfers energy through electromagnetic waves without requiring a medium (see Equation 2.3 for factors impacting radiative heat transfer). During a fire, all three heat transfer mechanisms may be present with the total heat flux equaling the sum of conduction, convection and radiation as seen in Equation 2.4; however, one will often be more prevalent than the other two at a given time or location.

$$\dot{q}''_{conduction} = -\frac{\kappa \Delta T}{\Delta x} \tag{2.1}$$

Where,

$\dot{q}''_{conduction}$ is the heat flux caused by conduction (W/m^2)

κ is the thermal conductivity (W/mK)

ΔT is the temperature difference (K)

Δx is the distance in which the temperature difference occurs (m)

$$\dot{q}''_{convection} = h\Delta T \tag{2.2}$$

Where,

$\dot{q}_{convection}''$ is the heat flux caused by convection (W/m^2)

h is the convective heat transfer coefficient (W/m^{2}K)

$$\dot{q}''_{radiation} = \phi\varepsilon\sigma T^4 \tag{2.3}$$

Where,

$\dot{q}''_{radiation}$ is the heat flux caused by radiation (W/m^2)

ϕ is the configuration factor

ε is the emissivity of the surface

σ is the Stefan-Boltzmann constant (5.67E-8 W/m^{2}K^4)

T is the temperature (K)

$$\dot{q}'' = \dot{q}''_{conduction} + \dot{q}''_{onvection} + \dot{q}''_{radiation} \tag{2.4}$$

Where,

$\dot{q}''$ is the total heat flux (W/m^2)

2.3 An Overview of Steel and Timber

With an understanding of heat transfer, the impact of fire on steel and timber will be reviewed next. This section will discuss the structural properties of steel and timber as well as relevant products for the thesis herein. From there, the materials' behaviour in fire will be reviewed.

2.3.1 Steel

Steel is a non-combustible material and is a good heat conductor. As a high-level overview, it is made from iron ore which is placed in a blast furnace where it is melted down before impurities can be removed through a refinement process. From there, the molten steel can be formed into various shapes [22]. It is important to understand the microstructure of steel considering its impact on structural properties. During manufacturing, the heating and cooling treatments applied to the steel members will impact the microscopic grain structure. Residual stresses (stresses within a member without the presence of external loads) are created. This is caused by uneven heating or cooling during the manufacturing process as the outer portion of the steel member will both heat and cool at faster rates due to it is exposure to the environment [23].

Concerns with steel in fire include how these residual stresses and overall structural properties are impacted when the steel is heated and cooled once again. Since increases in temperature results in changes of steel grain size and shape, "chaotic grain reordering" can occur [24]. Changes in steel microstructure occurs in various phase changes including several in the solid form. An overview of the various phases steel undergoes at different temperatures with respect to the carbon weight of the steel (amount of carbon) can be seen in Figure 2.3. Each phase has different material properties. A study by Pańcikiewicz et al. indicated that unloaded, there are no significant changes to steel microstructure which would impact steel resistance to brittle failure observed when the temperature remains under 600 °C [24]. Changes in material behaviour and properties such as a weakening the member and loss of ductility, toughness, stiffness, and hardness compared to its originally manufactured state were seen 800 °C [24], [25], [26].

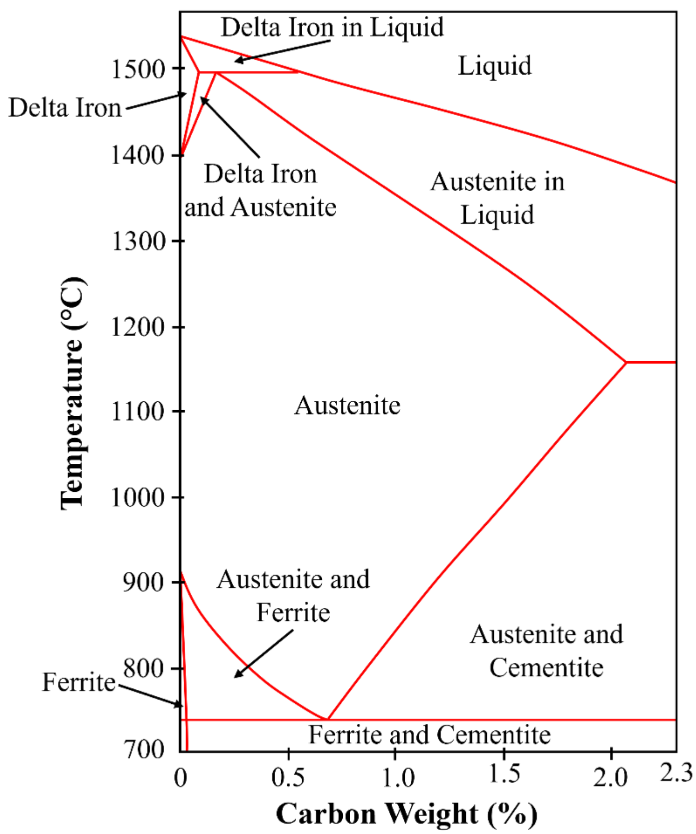

Figure 2.3: Phase diagram of steel with respect to the carbon weight (adapted and replicated from [27], [28]).

To account for this change in structural properties, Annex K of the CSA S16:19 standard for the design of steel structures provides modified elastic modulus, yield stress, ultimate tensile strength, proportional limit and shear modulus values. These are represented as a ratio of the ambient value with respect to the elevated temperature [26], [29] (see Figure 2.4).

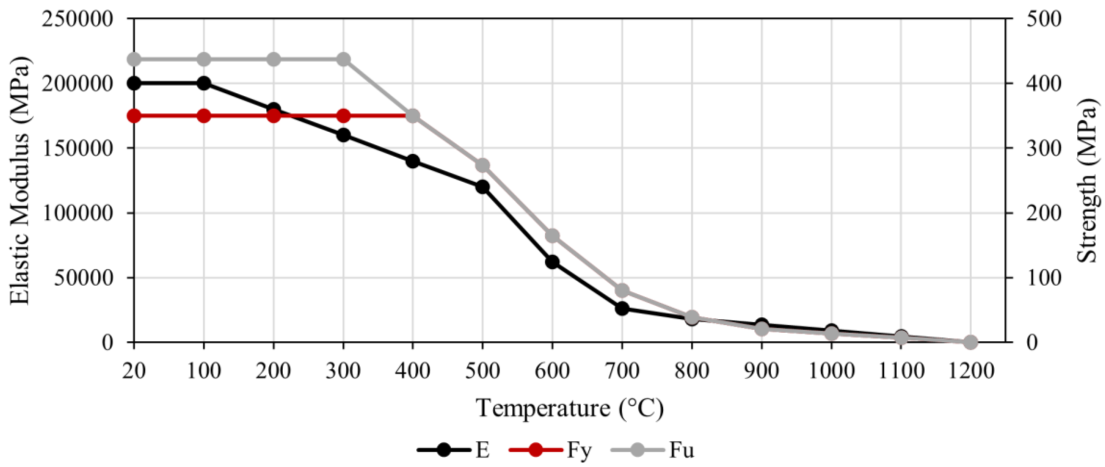

Figure 2.4: Annex K reduced elastic modulus, yield strength, and ultimate strength values at increased temperatures.

Other processes that occur when steel is heated is thermal expansion and contraction. When steel is heated, it undergoes thermal expansion and as it cools, the steel will contract. This follows the relationship seen in Equation 2.5 in which the change in length is dependent on a thermal expansion coefficient, the original length and the temperature change. This thermal expansion and contraction results in thermal strains, again impacting structural stability.

$$\Delta L = \alpha L_0 \Delta T \tag{2.5}$$

Where,

ΔL is the change in length (m)

α is the coefficient of thermal expansion (°C^{-1})

L_0 is the original length of the member (m)

ΔT is the temperature difference (°C)

The ability of the steel member to return to its original shape (elastic versus plastic behaviour) is dependent on both the amount of heat applied and the load applied [30]. Once loads and reaction forces are present, transient creep strain is introduced, beginning to develop at 400 °C [31]. Creep strain is defined as deformation caused by constant loading and is a function of time, the amount of stress or load applied, and the temperature at which it occurs [32]. This coupled with the loss of strength and stiffness can lead to localized failure or complete collapse of the structure. Overall, the behaviour of steel highlighted in the section herein indicate that steel is vulnerable in fire.

2.3.2 Timber

There are two main categories of wood: hardwood and softwood. These are broad categories of various wood species, separated by the cell type composition [33]. Softwoods are better suited for timber construction because they have a faster growth rate and are more affordable, thus are used today as both sawn lumber products and engineered timber products [34]. However, older heritage structures have used hardwood. Because of their different compositions, they do have different behaviour in fire scenarios. Further discussion regarding softwood and hardwood can be found in Chapter 4.

At a microscopic level, all wood contains a series of tube-like cells oriented vertically, parallel to the tree trunk axis [33]. In terms of structural stability, this means that timber is an anisotropic material, performing stronger under loading parallel to the cell direction compared to radially or tangentially (perpendicular to the cell direction). Water or moisture (used interchangeably in the thesis herein) is contained either within the cell walls (bound water) or within the cavity of the cells (free water) (see Figure 2.5). The amount of moisture within the cells is presented as a moisture content, which is the ratio of water to dry mass (see Equation 2.6).

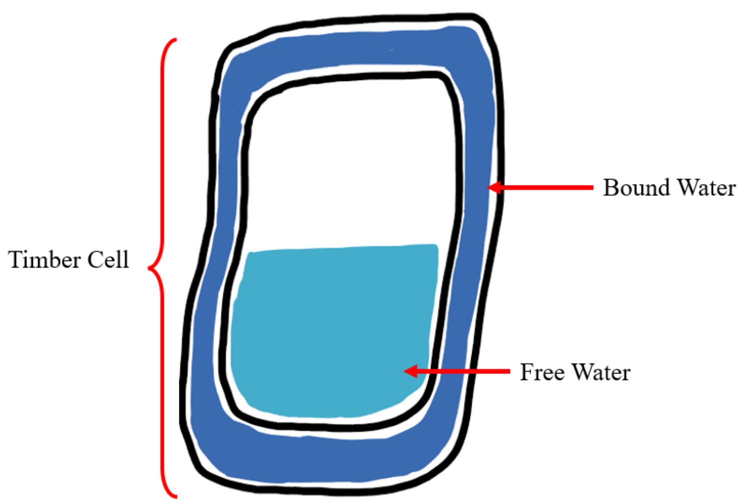

Figure 2.5: Drawing indicating the location of bound and free water.

$$MC = \frac{M_{wet} - M_{dry}}{M_{dry}} * 100\% \quad (2.6)$$

Where,

MC is the moisture content (%)

M_{wet} is the wet mass (g)

M_{dry} is the dry mass (g)

While free water only adds to the wet mass, bound water impacts overall volume of a member [33]. Increases or decreases in the amount of moisture held within the cell walls can lead to swelling or shrinkage of timber. During a fire, additional energy is required to evaporate the water leading to shrinkage. This is much more significant than swelling that may occur due to heating (similar to the thermal expansion discussed for steel previously). Shrinkage is a significant phenomenon not only because it impacts overall heat transfer, but because it can result in cracking, which during a fire, can lead to deeper penetration of heating and char formation [35]. Therefore, similar to steel, timber at a microscopic level is incredibly complex with research gaps and unquantified behaviours.

Moving on from the composition of timber at a microscopic view, there are a wide variety of timber products. For the thesis herein, sawn lumber and engineered timber will be discussed. Sawn lumber is the wood product after a tree trunk has been to the sawmill, essentially removing bark and shaping the log into usable construction products [36]. Dimensional lumber can then be made from sawn lumber, which are members that are less than 89 mm thick [37]. Engineered timber on the other hand, is a composite material, bonding dimensional lumber using adhesives or other mechanical fastening methods (ex. nails) to form larger, more sustainable wood products [38]. The materials tested in this thesis include glulam and cross-laminated timber (CLT), which both use adhesives to bond the products together.

Sawn lumber members are assigned a grade stamp, which provides information regarding where the member was processed, the species combination, seasoning designation (how it was conditioned and insight into moisture content) and its overall grade or structural properties (information provided dependent on if it was visually graded or machine stress rated) [37]. This allows sawn lumber to be categorized according to its species type and strength. These categories also exist for engineered timber (glulam and CLT); however, it becomes more complicated since the member is composed of a combination of dimensional lumber members.

Figure 2.6 illustrates an example of glulam and CLT, specifically showing how the product is made. Glulam is comprised of dimensional lumber oriented parallel to each other and is predominantly used as beams and columns. CLT alternates directions, with each layer or ply perpendicular and is predominantly used for floors walls and roofs. The outer ply's are the longitudinal layers while the ply's perpendicular are the transverse layers.

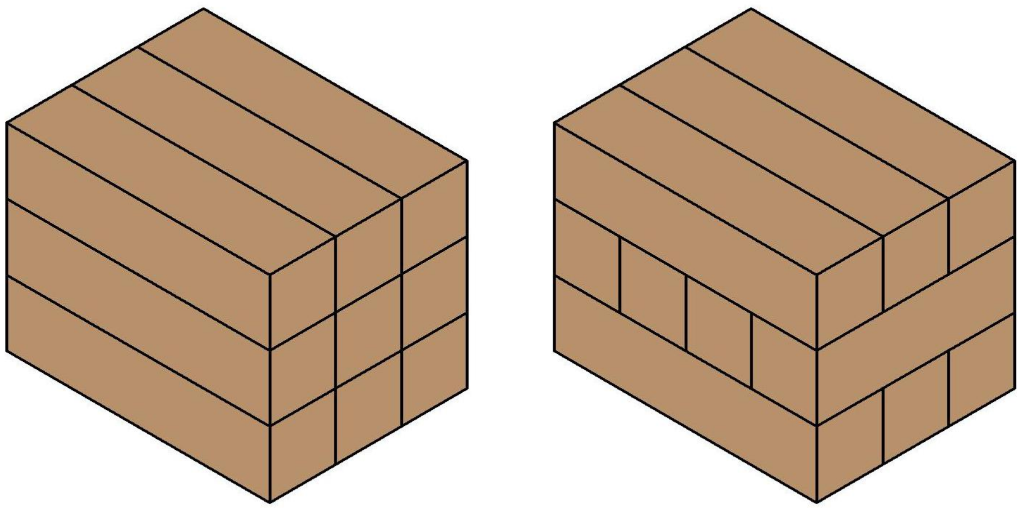

Figure 2.6: Diagram of laminates for glulam (left) and CLT (right).

For glulam, members are once again assigned a species combination but are further broken down into their primary application: bending, compression or tension [39]. This is because timber is an anisotropic material, meaning its properties vary with loading direction. From there, the members are then assigned a stress grade. Focusing on bending as the primary application (used in the study herein), four stress grades are found: 20f-E, 24f-E, 20f-EX, and 24f-EX [36]. The number (20 or 24) is the allowable bending stress in imperial units, the "f" means it is a flexural member, and the "E" indicates that the laminations are mostly machine stress rated. The "EX" means that the member will have equal resistance in positive and negative bending [39]. To do so, the outer laminates are of higher quality (more structural strength) than the inner laminates.

CLT members are divided into five stress grades: E1, E2, E3, V1, and V2. The "E" indicates the laminates are machine stress rated while the "V" means it was visually graded. Differences in the various "E" and "V" stress grades are the species combination used in the longitudinal and transverse layers. Similar to glulam, CLT is often a proprietary product so information regarding individual ply's or laminates can be difficult to obtain. The Canadian Wood Council suggests that for a "product evaluation report", specimens should be taken to the Canadian Construction Materials Centre [40]. From a fire perspective, this lack of knowledge regarding individual laminate grades and properties is concerning. If the fire reaches inner laminates, especially the "EX" glulam members where inner laminates are weaker, the remaining structural strength of these members is unknown. Ultimately, this is a research gap within fire safety engineering that needs to be addressed.

Expanding more upon timber's behaviour in fire, timber is combustible. When timber burns, it undergoes pyrolysis, which according to the government of Canada, is defined as the "chemical decomposition of organic materials induced by heat" [41]. Essentially, when timber is heated, chemical reactions occur to change the wood into volatiles and char (see Figure 2.7). Included in the volatiles category are combustible gasses which act as fuel and can combine with oxygen and heat to ignite and further propagate the fire [42], [43]. Note however, that ignition does not always occur and is dependent on the environmental conditions. If there are no flames but pyrolysis is still occurring, this is called smouldering. This can occur if no ignition occurs, or after the flames are extinguished but residual heat results in continued char formation [44]. Char is a porous carbon layer which has no structural strength but does have insulating properties (lower thermal conductivity) [45]. This means that the char layer can slow heat transfer through the remaining unburned wood.

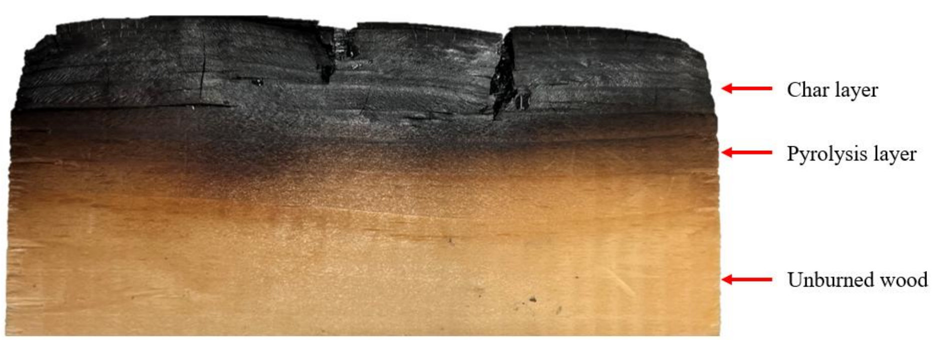

Figure 2.7: Cross section of burned timber showing the char layer.

To summarize, as wood burns, it loses depth in the cross-sectional area of unburned, structurally strong wood. However, while the char layer has no structural strength, it can slow heat transfer reducing the amount of further loss of strength. The Wood Design Manual (CSA-O86) specifies charring rates and estimations of char depth [36]. However, the impact of char fall off, crack formation and its impact are largely unquantified still.

2.4 The Finite Element Method

The final topic discussed in Chapter 2 is a description of the finite element method. Again, the thesis aims to develop and explore modelling of steel and timber in fire with the objective of being a tool for alternative solution designs. The finite element method (FEM) is a mathematical methodology which reduces or "discretizes" large, complex systems into a series of smaller "elements" (see Figure 2.8). The elements are connected at nodes. The FEM can be used to predict structural and thermal behaviour.

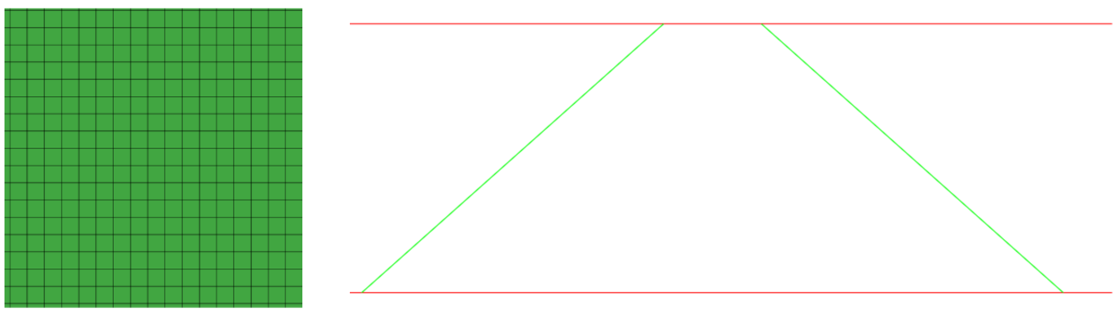

Figure 2.8: Examples of solid elements and beam elements.

Generally, a pre-processor is used to specify input parameters and boundary conditions, a solver is used to run the simulation, and post-processors used to read, output, and visualize the results. The software's used for the thesis herein include the Oasys LS-DYNA suite (Primer, D3Plot and T/HIS) [46] and Ansys' LS-DYNA (see Figure 2.9).

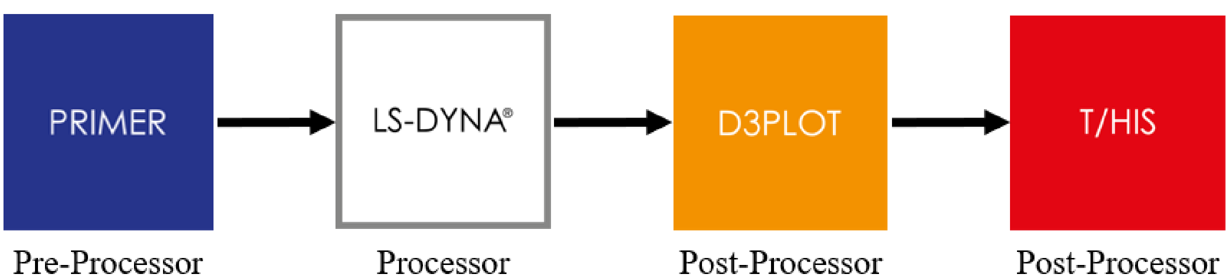

Figure 2.9: Finite element software's used in the thesis herein (adapted from [47]).

2.4.1 *Pre-Processor: User Specifications*

When creating a finite element model, the geometry is first created and then divided into a mesh. This mesh size is important since it determines how many elements the simulation will have. Generally, the more elements used, the more data will be produced resulting in more accurate results. However, it will also increase computational time and cost. If too many elements are used and the mesh size is too small, this can also result in unusual behaviour predictions [48]. Therefore, it is user's responsibility to determine the appropriate mesh size for each project through mesh sensitivity analyses.

From there, material properties and boundary conditions are assigned to the elements. For a heat transfer analysis, required material properties include density, specific heat capacity, and thermal conductivity. For timber latent heat and phase change temperature may also be required to account for moisture evaporation. Boundary conditions will include the thermal energy applied to the system from the heat source. This can be specified as a heat flux, convective and/or radiative heat exposures. The initial temperature is set to ambient temperature. For a structural analysis, material properties would include the modulus of elasticity, density, Poisson's ratio, yield strength, and coefficient of thermal expansion. Boundary conditions would include specifying the supports (fixed, pinned or roller for example), restricting movement. Then loads (thermal and/or structural) should be applied to the system.

Finally, output specifications and convergence requirements are inputted. This informs the software what information the user would like output as well as the accuracy and stability of the solution required to move onto the next timestep. One criterion that must be met by the solver is a convergence tolerance which checks the stability of the solution at each timestep. The solver will iterate on the same timestep to achieve the final solution which, compared to the previous iteration has the same values up to the set tolerance [49]. For example, if the tolerance is set to 1E-6, the solution must have the same first six decimal places compared to the previous iteration to move onto the next timestep. Additionally, the maximum temperature change between each timesteps can be specified [50]. This, combined with a set range of allowable timesteps allows the solver to optimize computational time while maintaining accurate results. The solver is free to fluctuate the timestep between the range given that the temperature change remains below the maximum.

2.4.2 Solver Method

The solver will then conduct the finite element method. For structural applications, software will solve a series of force, displacement and stiffness equations to calculate the displacement at each node. In a two-dimensional analysis, a single node can experience rotation, and displacement in the x and y direction. For a two-dimensional truss element as will be discussed in Chapter 3, there is no rotation, and the degrees of freedom would be as seen in Figure 2.10. To calculate the forces or displacements for a single truss element, Equations 2.7 and 2.8 will be used. For a system of members, the software will form the individual stiffness matrices of each member and place them into a global stiffness matrix. The global stiffness matrix will account for how nodes attached to the same member will interact and affect each other. From there, the solver will work, using the specified boundary conditions, to calculate the forces and displacements in the x and y direction for each node at each timestep. This information is then used to calculate stresses and strains experienced by the system.

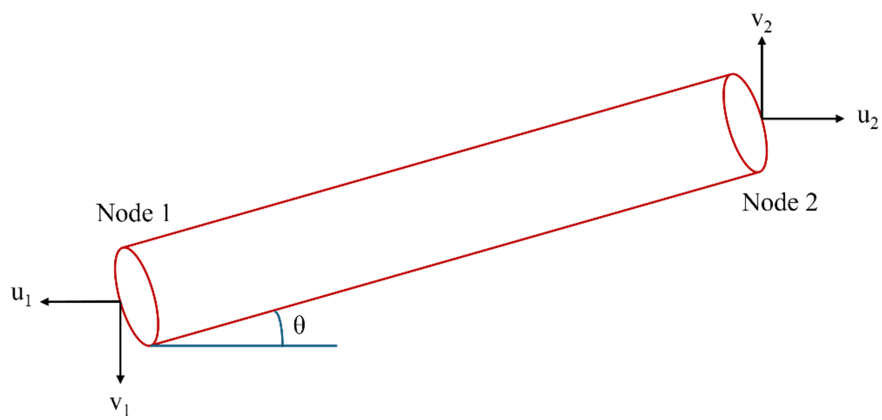

Figure 2.10: Example of a truss element in the FEM.

$$\begin{Bmatrix} F_{1x} \\ F_{1y} \\ F_{2x} \\ F_{2y} \end{Bmatrix} = [K] \begin{Bmatrix} u_1 \\ v_1 \\ u_2 \\ v_2 \end{Bmatrix} \tag{2.7}$$

Where,

$[K]$ is the stiffness matrix seen in Equation 2.8 (N/m)

$\begin{Bmatrix} F_{1x} \\ F_{1y} \\ F_{2x} \\ F_{2y} \end{Bmatrix}$ is the horizontal and vertical forces for each node (N)

$\begin{Bmatrix} u_1 \\ v_1 \\ u_2 \\ v_2 \end{Bmatrix}$ is the horizontal and vertical displacements for each node (m)

$$[K] = \frac{EA}{L}\begin{bmatrix} \cos^2\theta & cos\theta sin\theta & -\cos^2\theta & -cos\theta sin\theta \\ cos\theta sin\theta & \sin^2\theta & -cos\theta sin\theta & -\sin^2\theta \\ -\cos^2\theta & -cos\theta sin\theta & \cos^2\theta & cos\theta sin\theta \\ -cos\theta sin\theta & -\sin^2\theta & cos\theta sin\theta & \sin^2\theta \end{bmatrix} \quad (2.8)$$

Where,

E is the elastic modulus (Pa)

A is the cross-sectional area (m^2)

L is the length of the member (m)

θ is the angle of the member (rad)

For heat transfer applications, instead of aiming to calculate displacements, the output instead is a temperature gradient. Similar to a structural application, the software will calculate the temperature experienced by each element at each timestep. First, the boundary conditions will be applied, in this thesis, they will be convection and radiation, or a heat flux. Instead of the forces of elements interacting with each other, heat through conduction will be the dominant factor. The temperatures can be calculated for a three-dimensional heat transfer problem using Equation 2.9 [51]. Once again, the interaction between elements means a system of equations is generated as the individual temperature calculations are placed into a global matrix for the software to solve.

$$\rho C\frac{\partial T}{\partial t} - \left[\frac{\partial}{\partial x}\left(k_{xx}\frac{\partial T}{\partial x}\right) + \frac{\partial}{\partial y}\left(k_{yy}\frac{\partial T}{\partial y}\right) + \frac{\partial}{\partial z}\left(k_{zz}\frac{\partial T}{\partial z}\right)\right] = Q \quad (2.9)$$

Where,

ρ is the density (kg/m^3)

C is the specific heat capacity (J/(kgK))

T is the temperature (K)

t is the time (s)

x is the x direction (m)

y is the y direction (m)

z is the z direction (m)

k is the thermal conductivity (W/mK)

Q is the amount of heat per volume (W/m^3)

There are two categories of methods to solve these systems of equations: implicit and explicit analysis. In the thesis herein, all simulations will be solved using explicit analysis, a more direct method in which known values from previous timesteps are used to inform the calculation of an unknown in the current timestep [52]. This was decided based on previously validated studies using the same software for different problems.

2.4.3 Post-Process and Validation

From there, the user should analyze and interpret the results. Due to the volume of data generated, this is often done using a post-processor. To check the accuracy of the results, validation studies should be completed. This is the process of comparing the simulated results to experimental data, examining and explaining discrepancies. Once a level of accuracy has been met, parametric models can be created. Parametric studies are used to vary specific parameters within a validated model to gain an understanding of the behaviour that would occur in that scenario. This is useful for designers to justify decision making through risk-based analysis and be used as evidence that the alternative solution meets the prescriptive-based design criteria.

2.5 Summary

This chapter provided an overview of important information required to better understand this thesis. The literary basis spanned the difference between prescriptive design and alternative solutions, heat transfer, overall steel and timber composition and behaviour at elevated temperatures, and how the finite element method works.

With a focus on developing modelling methodologies and tools for the application of alternative solutions, it was important to understand the limitations of prescriptive design. For fire safety engineering, prescriptive design follows a set procedure, testing through the standard fire test and designing to achieve a desired heat resistance rating. This limits structures to be fire resistant and not fire resilient (the objective of alternative solutions). Alternative solutions allow the focus to be shifted towards optimizing designs while ensuring it reaches the same or greater performance as the prescriptive solutions. Another concept discussed in Chapter 2 is the methods of heat transfer. Fires require three elements: fuel, heat, and oxygen. Heat is then transferred using three mechanisms: conduction, convection and radiation which can be added to calculate the total heat transfer.

From there, an overview of steel and timber were provided, starting with their microstructure and expanding into its structural properties and behaviour in fire. Steel begins to weaken at around 800 °C, experiencing a loss of ductility, toughness, stiffness, and hardness. It also experiences thermal expansion and contraction, resulting in thermal strains. Timber consists of tube-like cells which contain moisture both within the cell cavity and the cell walls. This moisture is an important consideration in fire since the evaporation of water requires heat energy. Sawn lumber can be used as structural members by themselves or can be manufactured to form engineered timber products such as glulam or CLT. Furthermore, timber is a combustible material that undergoes pyrolysis, in which unburned wood changes into char and volatiles. This char layer has no structural strength; however, it does have some insulating properties, slowing further heat transfer to unburned wood.

Finally, this thesis focuses on numerical modelling tools using the finite element method. Therefore, a review of the method from the pre-processor, solver, post-processor, and validation was provided. During the pre-processor stage, the user will input geometry, material properties, boundary conditions, and convergence requirements. The solver will then take the user inputs and solve the forces and displacements for a mechanical model or the temperatures for a heat transfer model at each node and timestep. From there, the results will be exported to a post-processor so the data can be analyzed and compared to experimental results for validation. Validation indicates the accuracy of the model and its ability to realistically capture behaviours. It also can highlight limitations or areas of future work.

Chapter 3: Experimental Testing and Numerical Modelling of Steel Trusses Exposed to a Localized Fire

3.1 Introduction

In traditional fire safety engineering research, the three primary knowledge specialist fields, structural fire resilience, human behaviour, and fire dynamics, are often considered separately and in an isolated manner. However, in real life and in fire safety design these specialisms coexist, therefore there are advantages to considering them concurrently when developing fire research programs. This chapter focuses specifically on the integration of structural fire resilience and human behaviour within the application of high occupancy, large scale structures: stadia.

When designing stadia, there is a lack of guidance and codes for determining the adequate structural fire resistance of roofing systems. In the UK, the Approved Document B, that is the relevant guidance for buildings including stadiums, states that 'roofs' do not require fire resistance on loadbearing components with the exception that roof collapse would lead to overall building structural collapse [53]. The Green Guide, a widely used fire safety engineering guide for stadiums, states that a risk assessment should be completed to determine if fire protection is required [54]. No further information on how to conduct the risk assessment or required criteria is provided. Furthermore, the 2022 Australia building code, states that fire protection and resistance is not required if the materials are incombustible [55], thus, a commonly used steel roofing system would not require any fire protection. And finally, the NFPA 101 Life Safety Code provides guidance for assembly seating facilities, stating that fire protection in the form of sprinkler systems is not required if the roof construction is more than 15 m above the floor level and use is restricted to low fire hazard uses, nor are they required over the floor area of the stadium and any other place where an engineer determines ineffectiveness of sprinkler protection due to the height of the building or combustible loading [56]. Similar to the Green Guide, no further detailing regarding engineering judgement is provided. Further, the NFPA states that the ventilation system of structures such as stadia needs to maintain a smoke level higher than 1.83 m above the floor of egress paths [56]. Evidently, these codes and guidelines are generalized requirements, often unable to capture the complexity of actual fire hazards and rely solely on the designer's judgement.

Therefore, current guidance leaves roof stadium structures vulnerable to fire exposure. This can be seen through numerous stadium roof fires, including New Orleans in 2021 [57], Texas in 2019 [58], and Helsinki in 2024 [59], which led to injuries and structural damage. A more in-depth analysis can be performed on a fire that occurred in a Toronto, Canada, stadium in March 2022 during a professional basketball game. This event will be used as a case study and referenced for the research herein as it justifies the possibility of a similar event occurring in the future. During the event, an electrical fire was caused by an overhead speaker in the rafters adjacent to the structural roofing system, a steel truss. The fire was localized, eventually leading to a phased evacuation. First, those directly underneath the speaker were asked to evacuate so that firefighters could extinguish the fire; this occurred approximately 15 minutes after the fire was identified. The fire was extinguished after another 15 minutes, followed by a full evacuation beginning 50 minutes after the fire's identification [60].

The evacuation caused a significant financial loss, estimated to be approximately $1.6 million USD in ticket sales alone [61], [62]. Additionally, two years after the fire, the owner of the stadium is reportedly seeking $3 million CAD for the damages to the building and the required inspection, cleaning and repair (replacement and rebuilding) post fire [63]. Other factors such as television revenue, merchandise and concessions sales also increase the financial cost. For example, television accounts for most of the revenue of major sporting events, with the National Basketball Association having signed media agreements averaging to be just under $7 billion USD per year [61]. Therefore, while only a fraction of the total losses can be estimated, this event demonstrates that significant economic losses that can occur from even a small, localized fire event.

This case study of fire safety in stadia highlights a real situation in which there is an intersection between the areas of human behaviour and structural fire resilience. Because of the fire's location, it took time for the firefighters to evacuate those directly under the fire and then to reach the roof to extinguish the fire resulting in a time from identification to extinguishment of 30 minutes. The start of the full evacuation was lengthy (nearly an hour) due to the uncertainty of the situation. This time should be considered within the stability of the stadium roof structure. From the case study, it is clear that stadium roof fires are a unique scenario and that currently, this is not explicitly being considered within structural design and evacuation planning. Additional time having occupants in the building during a fire means that the structure must remain stable for unanticipated time. If this is not possible, then there is a credible life safety hazard.

While the fire was small and the spectators were safe through the duration of the event, this is not always the case as seen through the other stadium roof fires mentioned above. Therefore, questions arise such as:

1) What happens from a structural and evacuation perspective if the fire is more severe?

2) How can one determine structural resilience and residual strength of systems during and after a fire event? And,

3) How does one limit uncertainty regarding life safety and structural resilience in a stadia roof fire event?

All the research questions indicate a clear need for additional fire considerations in stadia roof design. The challenge is that if fire safety engineering is completed for these stadia, it will require an alternative solution such as performance-based design since prescriptive guidance (per a review of current codes and guides) is generally unavailable. The Canadian steel design standard contains Annex K, which is a normative part of the standard providing methods for alternative solutions for steel design in fire [29]. This standard is used not only in Canada, but internationally as well. One of the ways to conduct alternative solution designs is the development of validated numerical models, which can then be used in predictive simulations for specific structural elements in risk-based analysis frameworks. Therefore, as in line with the objective of this thesis, the chapter herein aims to develop numerical modelling tools for necessary alternative solution designs of stadium roof structures in fire.

In order to develop validated models however, experimental data is needed. Prior to modelling, it is important to first understand how a localized fire can impact a common structural system such as a truss roofing system to ensure safe egress. Because it has been seen that Annex K requires further Canadian experimental data for model validation in order to develop and encourage the use of alternative solutions [64], Canadian steel specimens will be tested herein and the data supplied to the models.

To summarize, the aim of this chapter is to better understand the behaviour of steel trusses are exposed to a localized fire as well as distribution of heat and the development of thermal strains. Through experimental testing, additional Canadian experimental data will be collected with the results to be used to supply information to numerical models. At a big picture level, the aim is to facilitate the interaction of design and analysis tools, such as modelling softwares for both human behaviour and structural fire resilience to determine the stability of a structure in a fire and allow for safe egress during the fire scenario. More resilient structures will lower environmental and financial costs of a fire as well as promote life safety.

3.2 Background

As discussed in Section 1.3, structural fire modelling consists of three phases: a fire model, a heat transfer model, and a mechanical model. The research in the chapter herein will conduct phases two and three models, using experimental data to bypass the need for a fire model. Therefore, a review of current literature regarding stadium fire numerical studies, stadium steel truss systems in fire, and fire modelling studies of steel trusses was conducted to determine current research gaps.

Clifton et al. [65] and Muñoz Blanc et al. [66] conducted post-fire evaluations on large scale structures (a convention centre and a stadium respectively). Following the three phases discussed above, both studies conducted fire simulations, heat transfer analyses and structural analyses. The numerical models along with material testing were used to assess the existing fire damaged structure. From there, a rehabilitation plan was developed. The methodologies from these studies were used to create a framework for post-fire evaluations of large-scale structures and processes for rehabilitation.

Research into design found performance-based solutions and the development of modelling tools. Studies by Block and Butterworth [67], and Lu et al. [68] highlight how prescriptive guidelines for stadia (Approved Document B) are inapplicable, specifically due to the use of the ISO 834 standard fire [15]. The standard fire test is not representative of a real fire event as it involves a gradual increase in temperature and no cooling period. Therefore, there is a need for alternative solutions, which can benefit from the development of design and analysis tools as previously discussed. Block and Butterworth created a risk-based approach for designing large-scale roof structures (not specific to steel trusses) which considers the frequency, probability and consequences of a particular fire scenario [67]. Lu et al. did not consider a stadium specifically; instead, they studied a large-scale exhibition centre with a steel truss roofing system [68]. A case study was modelled, ultimately finding that the behaviour of these large-scale truss systems, particularly in the cooling phase, is complex. This highlights the inappropriateness of the use of the standard fire within prescriptive guidance for stadium roof structures since it ignores the cooling phase.

Other studies found were non-validated stadium roof models. Salminen and Hietaniemi developed a phase one fire model and a phase two heat transfer model using finite element analysis [69]. Focus was placed on predicting horizontal heat transfer between truss chords. Zhang et al. focused on how water as a fire suppression method would impact the structural integrity of steel trusses [70]. The study found that cooling specific members will result in permanent deformation in surrounding, hotter members. This added challenges when specifying constraints in the model. This illustrates the challenge with non-uniform heating and cooling; complex thermal behaviour will translate to complex structural behaviour. Ozyurt and Wang studied internal truss forces when heating and modelled a variety of truss sizes and compositions [71]. Because high temperatures can cause large displacements and increased forces, it was determined that ambient temperatures cannot be used to calculate forces in fire. Finally, Kubicka and Radoń proposed an assessment methodology for determining the stability of a steel truss [72]. The method used a reliability index to predict failure in a fire scenario. It was noted that this study used the standard fire as the heat exposure and that the method should be validated using a more realistic fire scenario.

Jiang et al. conducted an experimental fire study on a full-scale steel truss roof system [73], with data being used to create two early-warning systems [74], [75]. The experimental study did non-destructive localized fire tests and destructive wood crib fuel tests. Failure modes for the destructive tests were noted. Note that this study was intended for high-occupancy structures and not solely stadia.

For steel truss models in fire in general, not specific to stadia or high-occupancy structures, several studies were considered. The first was conducted by Sibil and Ozyurt in which finite element modelling was used in 330 parametric analyses of steel truss compositions in various fire scenarios [76]. The methodology was first validated using a separate experiment's results. Key findings include that the natural frequency of the trusses decreased with increased fire damage.

This was more significant in uniform fires rather than localized fires. From the perspective of the study herein, localized fire being the less critical case can lead to more confusion regarding next steps after a steel truss non-uniform fire (evacuation or repair) since there is more variability in residual strength. In another study, Kallada et al. focused on developing a fire model and a finite element model (heat transfer and mechanical) to predict structural behaviour of steel trusses exposed to a travelling fire [77]. Results showed that non-uniform heating results in complex behaviours which can include bowing, oscillations, redistribution of loads, and both local and global deformations leading to failure. The behaviours also varied with the orientation of the fire path and the truss.

To summarise, there is a clear need for the development of stadium roof fire resistance guidance. A favoured approach in literature is to develop tools for alternative solutions which will also be followed in the chapter herein. However, there are few studies within current literature that both did experimental testing and validated numerical simulation models within the scope of stadium truss roof fire design. Validation is an integral part of identifying the applicability and accuracy of the simulations. In addition, another research gap that was highlighted through the literature review, is the lack of integration between structural resilience and human behaviour. Except for the studies used to provide early-warning systems, most studies only focus on structural implications. Therefore, the aim of this chapter is to create tools for steel truss design with the context of how much time one actually has to evacuate given the likely protection mechanisms present and the credible fires that may be present. Findings from the reviewed codes and guidance and literature were used to shape the chapter and address the identified research gaps.

3.3 Experiments on Steel Trusses Under Localised Fire

A series of four experiments of steel trusses under localised fire were conducted with the purpose of providing data for model validation. The experiments were used to understand and document the behaviour of steel trusses that would be commonly seen in stadium roof structures. Specific focus was placed on heat transfer, thermal expansion and strain, and the presence of a chord shielding effect. All fire testing was performed with supervision by the first author Jeanneret with assistance from the author of this thesis.

3.3.1 Methodology

For the experiment, two open web steel joists (OWSJs) were tested using a methanol pool fire. OWSJ sections are commonly used in Canada because their lightweight nature allows for long spans. Each truss was tested twice each for repeatability and were heated for thirty minutes. The duration selected was similar to the response time observed in the case study to extinguish the fire and the intensity was estimated to be similar in heat release to the case study. Data was collected for the heating duration and continued into the cooling phase until temperatures reached below 100°C. Past this was structurally insignificant since according to CSA S16:19 [10], the steel has regained all of its properties as per ambient temperature.

The trusses were also unloaded in the experiments such that no permanent/plastic deformation occurred to the structure. The primary objective of the experiments was to determine how thermal strains and forces are developed and how they impact the global structure of the truss system. In addition, by isolating the thermal behaviour, the data would be more appropriate for validating numerical models as less uncertainty is introduced. Loaded truss experiments are outside of the scope of this project because it introduces creep strain which is an incredibly complex concept. The research gaps of understanding and modelling creep strain have been highlighted in [78], [79], [80], with parts of the creep model often unrepresented (the tertiary phase) or requiring several assumptions. With the basis of unloaded truss system behaviours and confidence in a thermal strain model, future studies can be used to explore the impacts of mechanical deformations due to applied loads. Finally, unloaded tests mean that multiple tests can be conducted on different days with the same specimens, allowing for lower experimental cost while increasing the amount of data generated.

3.3.1.1 Experimental Setup

Figure 3.1 illustrates the experimental setup and truss dimensions. These trusses are smaller than a stadium system, with a total size of approximately 2200 mm in length and 360 mm in height. The cylindrical diagonal chords (with a diameter of 20 mm) were welded to the top and bottom chords. Each horizontal member was composed of two 38 x 38 x 4.8 angle members. Since the aim was to develop modelling tools for heat transfer and deformation, the smaller sections were determined to be sufficient as a preliminary study.

The truss was secured 200 mm above the fuel pan using concrete and clay masonry units. This created the realistic fire exposure, with an incident heat of 700 to 800 °C (characterized in [81]). The supports were set in a way to prevent torsional effects while allowing thermal expansion along the length of the OWSJs to be mostly free (partially constrained). The fuel pan's dimensions were 480 by 600 mm, with the fuel pan centred under the middle diagonal chord of the truss.

As seen in the case study, a localized fire near the roofing system is a credible scenario due to the fuel nearby (a speaker in this case). To represent the case study event, a pool fire was chosen as it provides both convective and radiative heating, and realistic heating and cooling phases. Methanol was chosen as the fuel type because of its ability to burn cleanly, releasing less particulates into the atmosphere compared to other commonly used fuels [82]. Also, given the fuel material properties, the characteristics of a localized pool fire can be easily predicted since tests are consistent and repeatable [21], [83]. Therefore, it was determined that eight litres of fuel were required for each test to ensure an approximately 30-minute burn.

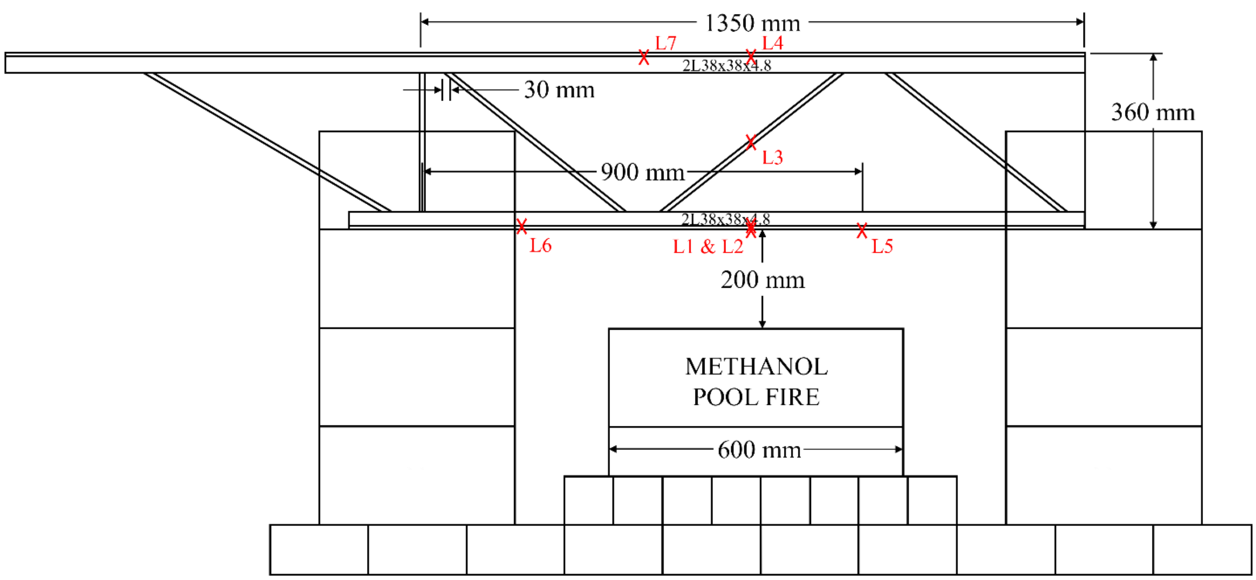

Figure 3.1: Experimental setup and truss dimensions.

3.3.1.2 Instrumentation and Equipment

On each of the OWSJs, two unloaded fire tests were performed using equipment to monitor the chord shielding effect, heat transfer, and thermal strain. Starting with the chord shielding effect and heat transfer measurements, sixteen K-type thermocouples were placed along the trusses in set locations to identify specific effects (see Figure 3.2). These included putting the thermocouples on both angle members' exposed and protected sides (above and below the flanges) (see Table 3.1 for the full description). Note that TC 8 was moved from location A (along the top chord) to B (along the bottom chord) after the first experiment. This was done to capture a location which would experience significantly less thermal exposure for tracking heat transfer.

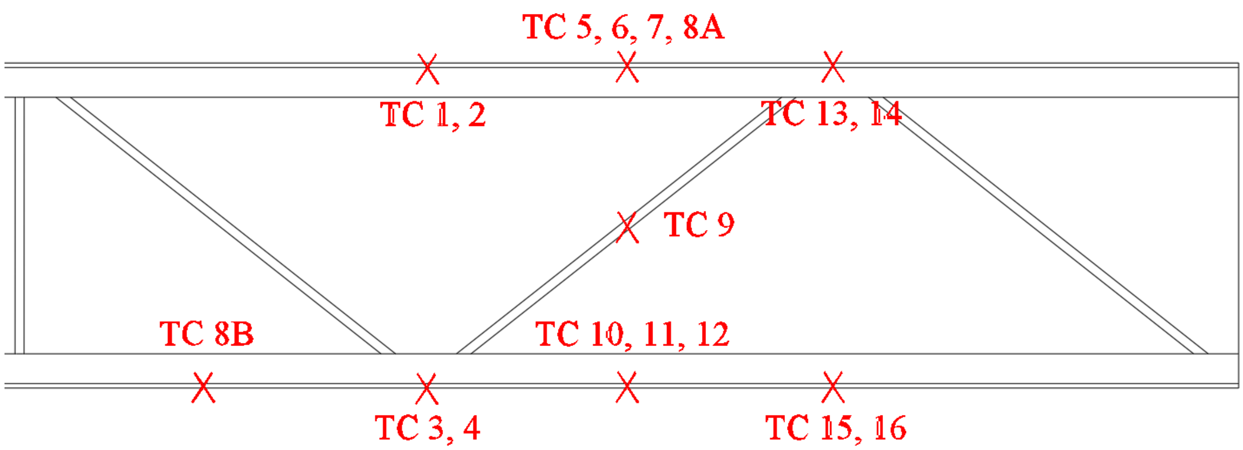

Figure 3.2: Location of thermocouples.

Table 3.1: Description of the location of thermocouples.

Thermocouple ID	Location Description			Location ID
	Angle (w.r.t. front view)	Chord	Surface of angle	
TC 1	Near	Top	Protected	
TC 2	Far	Top	Exposed	L7
TC 3	Near	Bottom	Exposed	
TC 4	Far	Bottom	Protected	
TC 5	Near	Top	Protected	
TC 6	Far	Top	Protected	
TC 7	Near	Top	Exposed	L4
TC 8A	Near	Top	Exposed	L4
TC 8B	Far	Bottom	Protected	L6
TC 9		Diagonal		L3
TC 10	Far	Bottom	Protected	L2
TC 11	Near	Bottom	Exposed	L1
TC 12	Far	Bottom	Exposed	L1
TC 13	Far	Top	Protected	
TC 14	Near	Top	Exposed	
TC 15	Near	Bottom	Protected	L5
TC 16	Far	Bottom	Exposed	

All thermocouples were placed directly onto the steel with the objective of recording the actual steel surface temperature. Then, they were insulated using a small amount of fibre wool to prevent the gas temperatures from impacting the reading and secured to the truss using nickel-chromium wire and aluminum tape [84].

For the purpose of model validation, only the eight thermocouples at the locations denoted in Figure 3.1 will be discussed (descriptions can be found in Table 3.1). Locations one through four (L1 to L4) are all located along the centerline of the fuel pan. These tracked the vertical heat transfer, with the location moving further from the heat source as the location identification number increases. L1 is the average of the thermocouples on the exposed side of the bottom chord flange, and L2 is the protected side. L3 is at the midpoint of the diagonal chord and L4 is the average of the thermocouples on the exposed side of the top chord. L5 is located on the exposed side of the L-shaped member and L6 is on the protected side. L1, L2, L5 and L6, were used to track horizontal heat transfer.

Thermal expansion and strain will be measured at locations L3, L5 and L7, the midpoints of three chords: the top, bottom and diagonal. This will be done using narrow spectrum illumination and digital image correlation (DIC). Narrow spectrum illumination is a technology which filters out smoke and flames, allowing photos to be captured without anything impeding the view of the specimen. The technology uses high intensity blue LEDs (shone onto the specimen), a camera filter, and specific camera settings. These allow for all wavelengths above blue to be filtered out, thus providing clear imaging of the specimen. Figure 3.3 shows a comparison of photos of the trusses taken with and without narrow spectrum illumination. Further information can be found in References [82], [85], [86], [87] which describe this technology in depth as well as provide validation. This method has been used for a variety of experiments including steel, timber and concrete; however, to the author's knowledge, it has not been used for steel trusses and thus adds to the novelty of the study. Therefore, this technology will be validated for the chapter herein requiring additional temperature data from L7 (which is not considered in the heat transfer analysis).

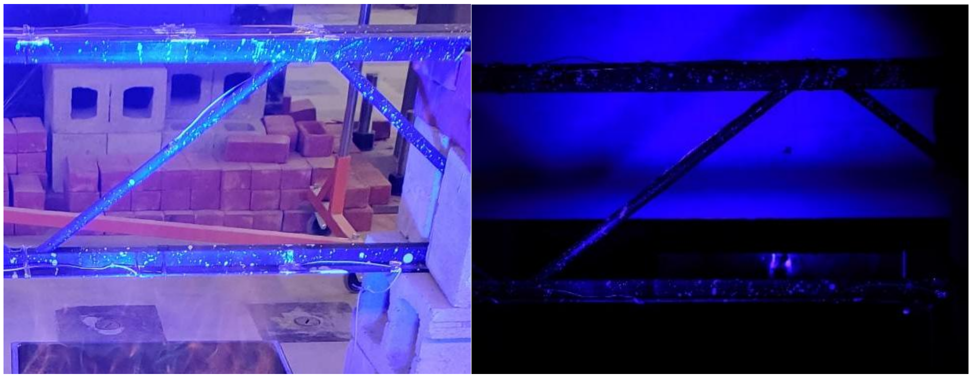

Figure 3.3: Images of a truss exposed to a localized fire before (left) and after (right) using narrow spectrum illumination.

Photos were taken using a high-resolution camera every five seconds during the test with the intention of using DIC to track thermal expansion and strain. DIC requires a visual aid to track specific points. Therefore, the truss specimens were painted black, with a random white speckle pattern; the paints were capable of high temperature use. The DIC technology uses MATLAB to run an image analysis module GeoPIV-RG [88] which inputs the photos in chronological order and tracks specific points using pixels and the pattern. This outputs the distance the point moves between images and thus the strain caused by thermal expansion can be calculated. An accuracy of 0.001 pixels can be achieved [81], [85].

Note that DIC was used instead of strain gauges because of their reliability in fire conditions, and the financial cost. Strain gauges have been said to be unreliable in fire testing, requiring high temperature strain gauges to gain reliability up to 400 °C which then increases financial cost and is not the maximum temperature expected in the project herein [89], [90], [91]. Additionally, the National Institute of Standards and Technology (NIST) has stated suggested that DIC is more useful and appropriate compared to strain gauges hence its use in this chapter [89].

3.3.2 Results

Figure 3.4 shows the averaged time-temperature data from all four truss tests at the six locations highlighted in Figure 3.1. As expected, the temperatures captured by the thermocouples decreased the further the instrument was from the heat source. The heating pattern generally has a sudden increase in temperature at the start, followed by more constant temperatures, and ending with a cool down period. An interesting observation was the difference in temperature between L1 and L2. While they were only separated by 4.8 mm of steel, there is over a 50 °C difference between the two. This may be because of a chord shielding effect being present, in which the steel, to some degree, prevents the flames from touching the protected flange of the member, instead redirecting the flames around it. When looking at horizontal heat transfer, L5 experienced lower temperatures when compared to L1 through L4. L6 experienced little heat transfer as predicted. This was because of its distance to the heat source, and because the diagonal chords of the truss impeded some of the heat transfer to L6.

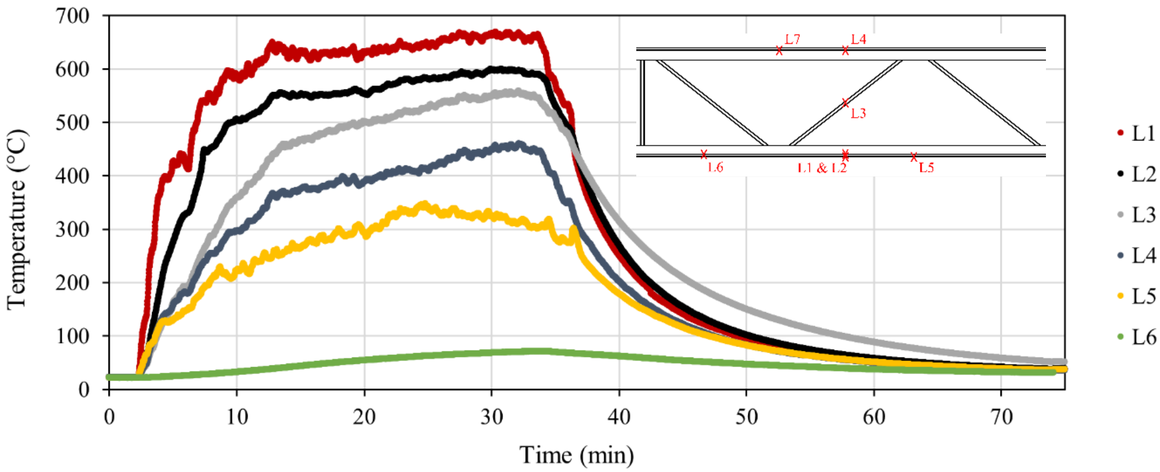

Figure 3.4: Time-temperature experimental data from the thermocouples.

Figure 3.5 shows the average strain data collected from using DIC during the experiments. The strain was calculated at L3, L5 and L7 (along the centreline of each chord) following the methodology by Gatien et al. [86]. The bottom chord, L5, experienced the highest strain in general (maximum strain of 0.00766 mm/mm), with the top chord, L7, experiencing the least (maximum strain of 0.00565 mm/mm). This aligns with predictions, since the members closer to the heat source experienced high temperature changes. All the curves follow the same general trend with a rapid increase in strain, followed by a slower strain rate and then a return to zero after cooling. The timing aligns with the experiment with heating concluding after half an hour. Strains return to zero since no mechanical loading was applied.

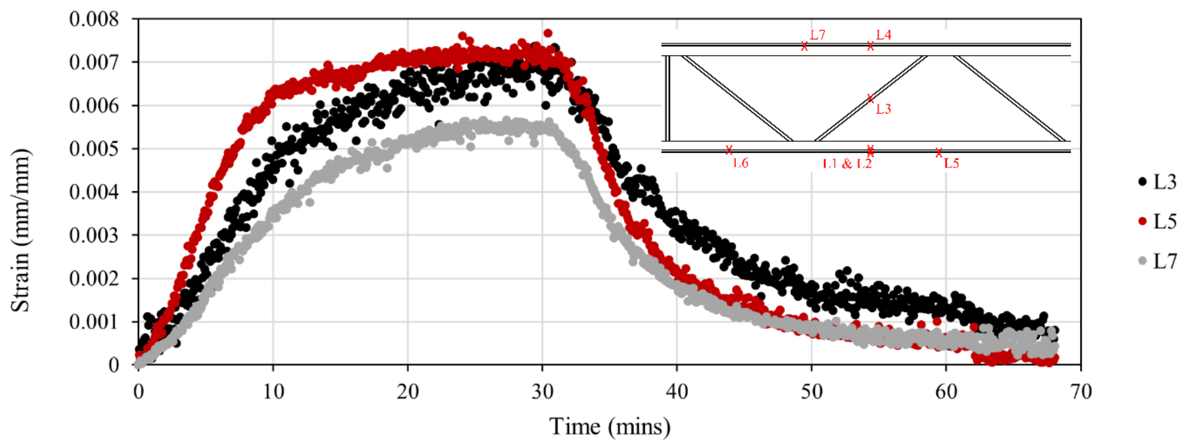

Figure 3.5: Strain over time experimental data using DIC.

3.4 Numerical Models

Following the experiment, a heat transfer and a deformation analysis model were created in LS-DYNA to determine the model's capability to compute temperature and thermal strains as a first stage of research. The models' aim was to provide design and analysis tools for practitioners during and after a fire for steel truss roofing systems and thus purposely remained simple and easily reproduced in practice.

3.4.1 Methodology

Both models were created using Primer as the pre-processor and D3PLOT and T/HIS as the post-processors. LS-DYNA was chosen as the solver because of its common use, and prior validation for modelling steel in fire. Various studies, including References [92], [93], [94], [95] have conducted heat transfer and deformation analyses for steel in different applications. These methodologies will be closely followed and further discussed.

3.4.1.1 Heat Transfer Model

The first model completed was the heat transfer analysis model. The methodology closely follows the processes described by Watson et al. [94], in which a steel bridge cable was modelled over a localized fire, and Temple et al. [95] which provided two verification heat transfer models.

Like the reference studies, this problem was simplified into a two-dimensional model. This means that the top and bottom chords were represented by rectangles the width of the flange (4.8 mm) and parallelograms represented the diagonal chords. Solid elements with a mesh size of 1 mm by 1 mm were chosen. The elements were set to be a thermal isotropic material with thermal properties density, specific heat capacity, and thermal conductivity being inputted. The density value came from the section properties described in the Canadian Steel Design Handbook [96], while the other two curves were taken from Eurocode 3 [97]. All nodes were initially set to ambient temperature (20°C).

Boundary conditions for this model included both convective and radiative heating as per the fire dynamics of the experimental pool fire. Both boundary conditions require the input of heat transfer coefficients, and a time-temperature curve. The convective heat transfer coefficient and emissivity constant were taken from Eurocode 3 as 25 W/m^2K and 0.7, respectively [97]. The time-temperature curves inputted for the heat transfer model were taken from a previously conducted experiment which used a thermocouple tree over a methanol pool fire. This meant that a fire model was not required. The thermocouples were placed every 100 mm above the centreline of the pool fire. As seen in Figure 3.6, the inputted gas temperatures over time start with an immediate increase in temperature followed by a fairly constant temperature profile until extinguishment where cooling occurs, as would be expected in a real fire scenario. Note that a more detailed description and results of the methanol pool fire test with no specimen can be found in [98], [99].

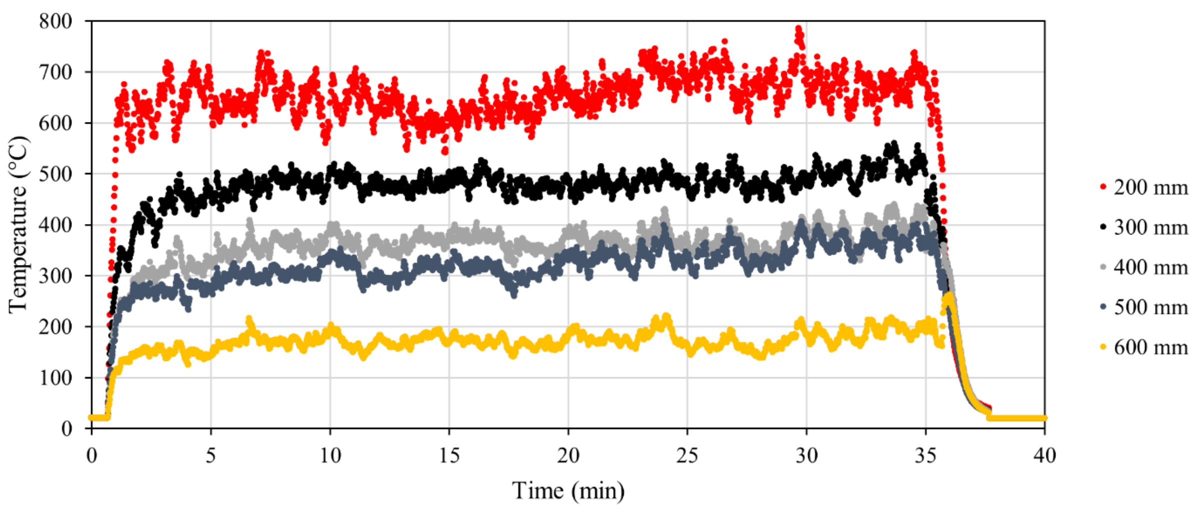

Figure 3.6: Time-temperature curve of thermocouple tree experiment.

Two different approaches to applying boundary conditions were considered with a full comparison described in [99]. The method found to be most accurate was one in which boundary conditions were applied using tributary areas. This was in line with research such as the LOCAFI project, where the heat and flames were found well beyond the base of the fire [83]. Rather than applying only a single boundary condition, five boundary conditions were applied to various sections of the truss. Figure 3.7 shows an illustration of how the truss was divided and their corresponding boundary conditions. The truss was divided based on the thermocouple locations from Figure 3.6, since they were the input data. Therefore, the bottom 100 mm of the truss was assigned the time-temperature curve corresponding to the 200 mm data from Figure 3.6. Note that the bottom of the truss was located 200 mm above the fuel pan. The following sections were 200 mm in height and were assigned their respective time-temperature curve from the thermocouple tree experiment when applying radiative and convective boundary conditions. The width of the section was the width of the fuel pan (600 mm) for simplicity. The author recognizes that this may be a source of error since the flames would take a conical shape as it burned, which was not accounted for here.

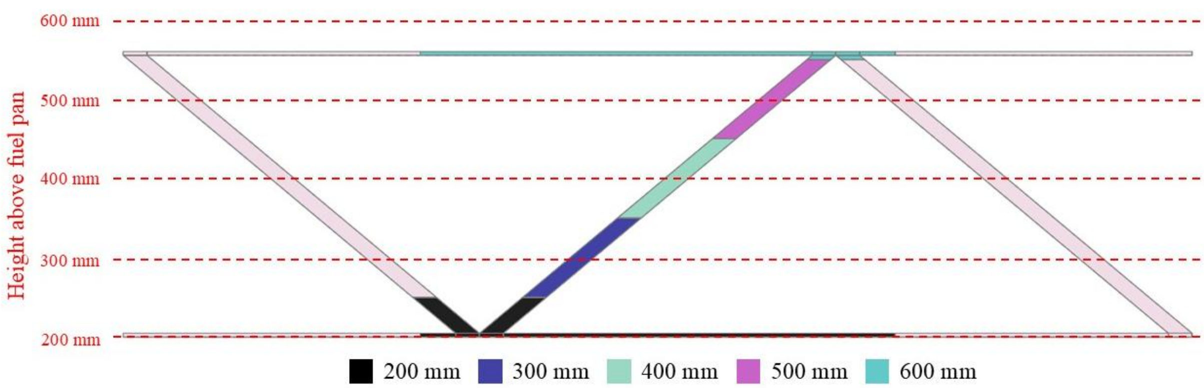

Figure 3.7: Corresponding thermocouple data to the area of applied boundary conditions for the heat transfer model.

The simulation was run using an explicit, non-linear solution, analysed using a diagonal scaled conjugate gradient iterative solver for 4750 seconds (approximately 80 minutes). The duration was set longer than the experiment, however, this only provided additional cool down predictions. The initial timestep was set to one second, with the ability to increase or decrease each timestep depending on the convergence level of the results and while ensuring changes in temperature were not too large (within a set range).

3.4.1.2 Thermal Deformation Model

Following the heat transfer model, a deformation model was conducted using LS-DYNA to assess the capability of the software to compute thermal strains. LS-DYNA has been used in various validated modelling studies which are referenced in the study herein [92], [93]. Hughes-Liu beam types were used to create a total of 11 beams (note that truss elements were not a provided option at the time the model was developed). Beams 1 through 3 (diagonal chords) are cylindrical members with a diameter of 20 mm and beams 4 through 11 (horizontal chords) are T shaped members (see Figure 3.8). T shaped members were chosen to represent the two angles for the horizontal chords to ensure proper fixity of beam elements. Per the LS-DYNA manual, two integration refinement parameters were used [50].

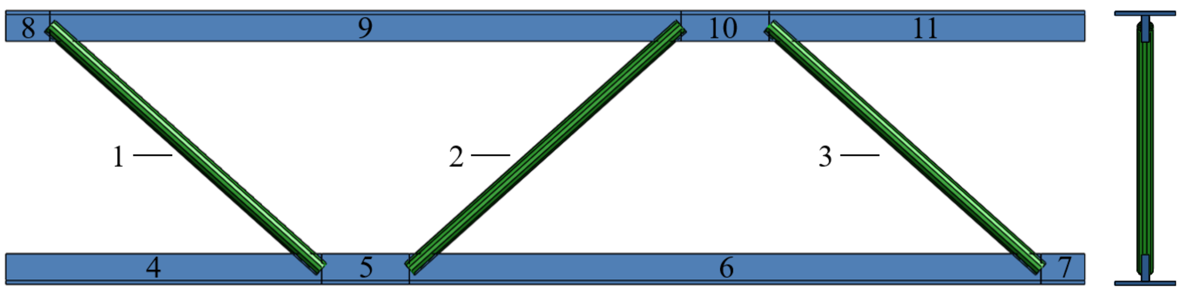

Figure 3.8: Model beam numbering (left) and side view of members (right).

Thermal loads were applied to each beam using the thermocouple data from each set of tests. While the deformation model can use the results of the heat transfer model to predict thermal strain, for the purpose of validation, it was decided to use the experimental thermocouple data to gain a true representation of the thermal deformation model alone. The thermocouple data for each set of truss experiments was averaged with the highest temperature curve from each location was applied to the beam section to be conservative. If a beam section had no thermocouple data, the nearest beam time-temperature curve was applied. The overall averaged input time-temperature curves applied to each beam section can be seen in Figure 3.9.

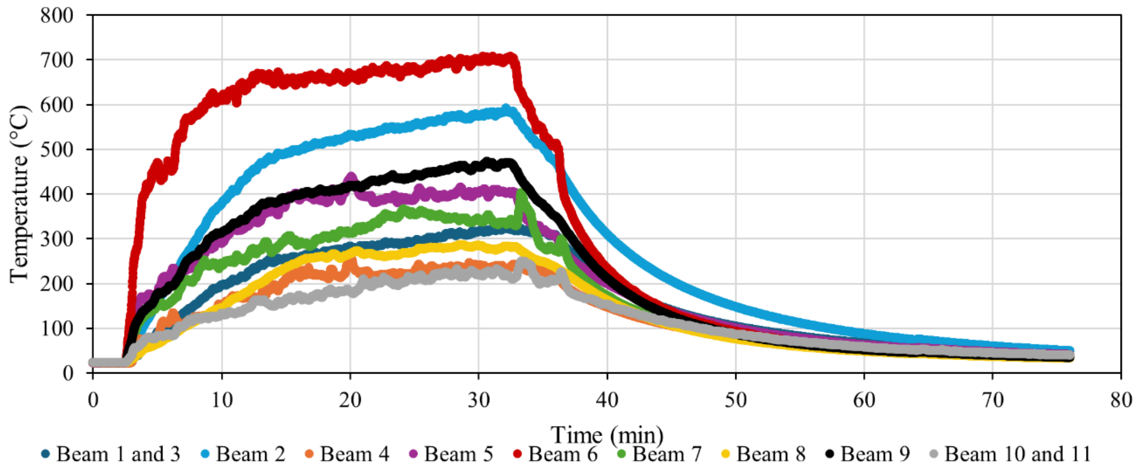

Figure 3.9: Averaged input time-temperature curves applied to each beam section.

Two versions of the model were created because of the partial horizontal restraint of the bottom chord in the experiment. The first version completely fixed both bottom chord corner nodes resisting all movement. The second version had one fixed support and one roller, allowing for translational movement (thermal expansion and contraction). Both versions were run to determine how strain predictions will vary and best practices. The simulation was run for a total duration of 4750 seconds (approximately 80 minutes) and used an explicit solver.

3.4.2 Results

Figure 3.10 and Figure 3.11 show the comparison of experimental and modelling results for the heat transfer model. Unlike the experimental results, the model data at L1 and L2 do not have the same difference in temperature. The heat transfer model predicts nearly the same maximum temperature (690°C versus 700°C). Other observations from the data comparison are that in general, the model underestimates vertical heat transfer, but overestimates horizontal heat transfer. For example, the difference in maximum temperature between experiment and model for L3 to L6 is 179°C, 266°C, -352°C and -156°C respectively. Overall, while the magnitude of temperatures experienced varied in accuracy, the heating trends of the model followed the experimental data.

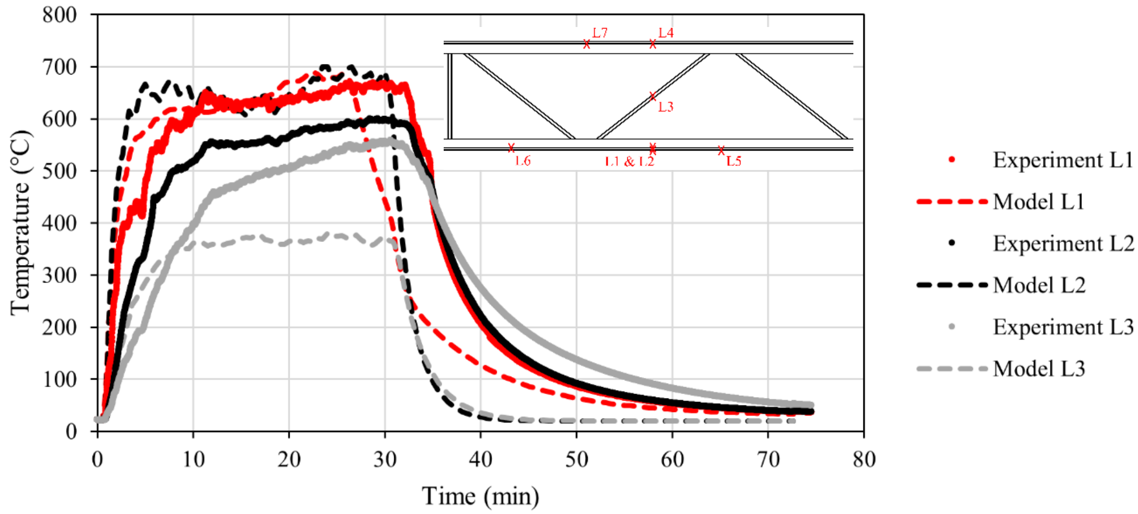

Figure 3.10: Comparison of model versus experimental results for the heat transfer model (L1 to L3).

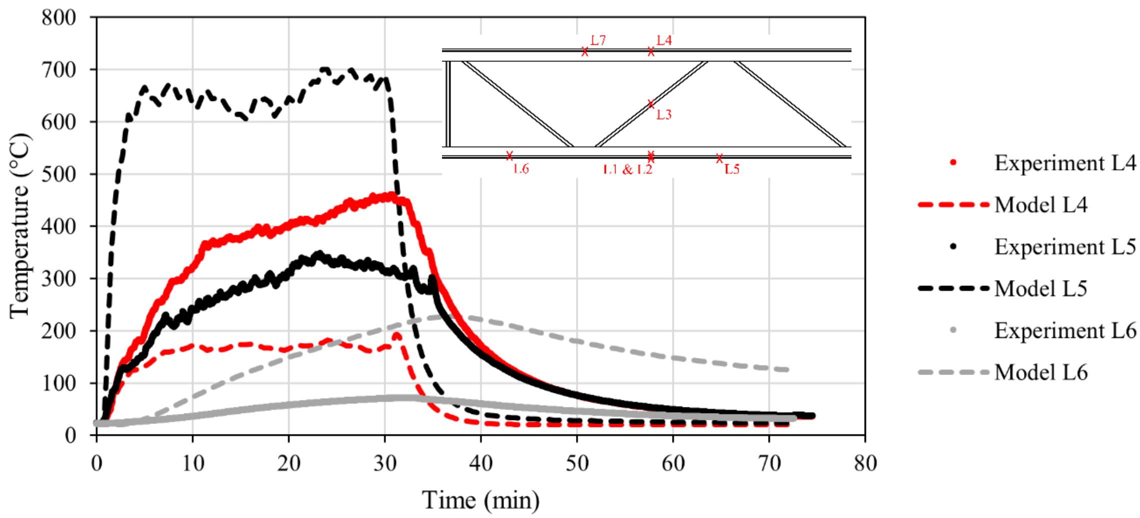

Figure 3.11: Comparison of model versus experimental results for the heat transfer analysis (L4 to L6).

For the mechanical model, the results of the experiment, free end model and fixed end model were compared at each location (Figure 3.12 to Figure 3.14). The model data was shifted 90 seconds forward to align the data's start with the experimental results. Table 3.2 summarizes the percent difference of peak thermal strain between each model and the experimental results. Except for the fixed end model at the bottom chord location, all predictions follow the correct trends and magnitudes seen in the experiments. The thermal strain increases quickly at the start of the simulation (phase one), has a period of slower, more gradual increase in thermal strain (phase two), followed by a cooling period in which the strains return to zero (phase three). These three phases of thermal strain behaviour occur at the correct time for each simulated prediction.

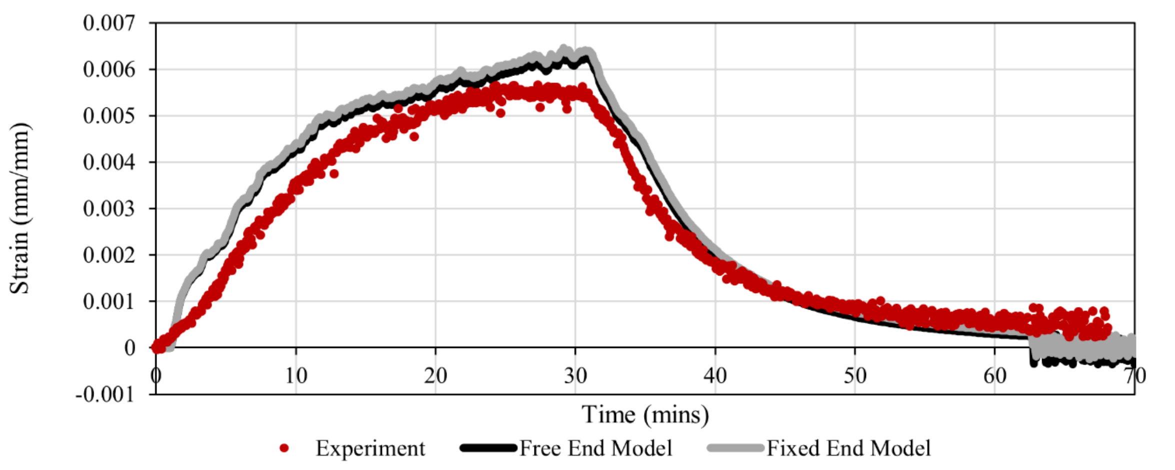

Figure 3.12: Top chord (L7) experimental and model results comparison.

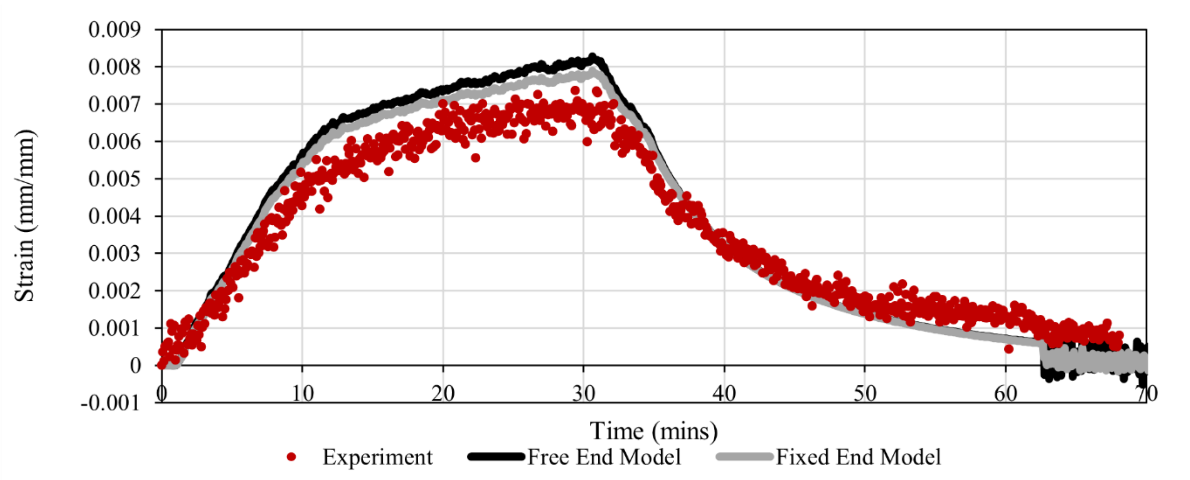

Figure 3.13: Diagonal chord (L3) experimental and model results comparison.

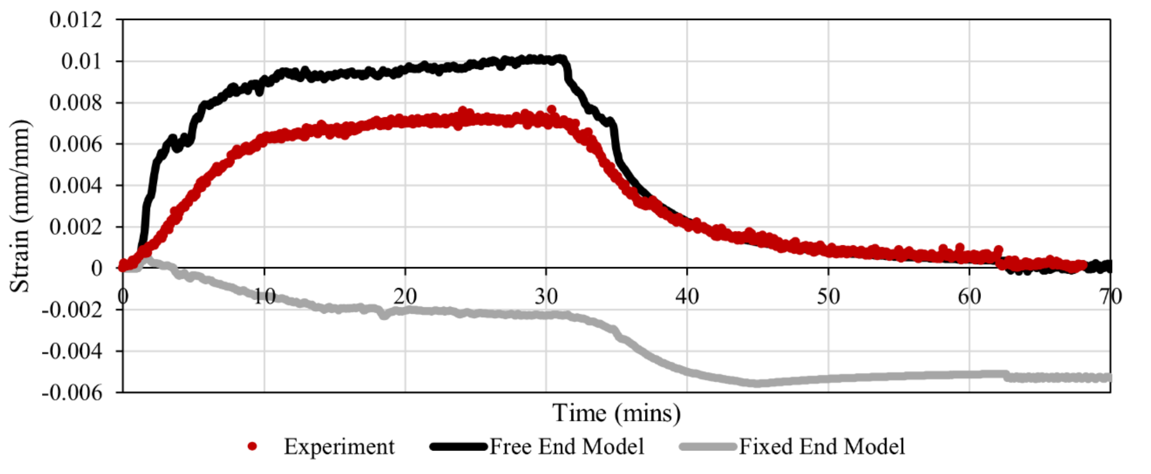

Figure 3.14: Bottom chord (L5) experimental and model results comparison.

Table 3.2: Percent difference between model and experimental results at peak thermal strain.

Chord	**Percent Difference**	
	Free End	**Fixed End**
Top	11%	13%
Diagonal	12%	7%
Bottom	28%	31%

Focusing on the top and diagonal chord results, both models conservatively predicted the thermal strain over time. The free end and fixed end models at the top and diagonal chords saw little difference in predictions. The maximum strain values at the top chord location were 0.0063, 0.0065, and 0.0057 mm/mm for the free end, fixed end and experiment results respectively. This results in a percent difference between both models (free and fixed end) and the experiment of 11% and 13% respectively. For the diagonal chord location, the fixed end model was more accurate than the free end model. The percent difference between the maximum strain value for the free end model and the experiment was 12% and the maximum strain value for the fixed end model and the experiment was 7%. Maximum strain values were 0.0083 (free end model), 0.0079 (fixed end model), and 0.0074 mm/mm (experimental).

Figure 3.14 shows the results for the bottom chord analysis, in which the impact of allowing horizontal translation is clear. In the free end model, results are conservative with the percent difference in peak strain being 28% (maximum strain value of 0.0056 mm/mm). However, when the support nodes are fully fixed, the bottom chord prediction shows negative strain values. While the trends for phases one and two are inverted, the simulation does not return strains to zero. To calculate the percent difference, the minimum strain value (-0.0102 mm/mm) was taken in this case, resulting in a value of 31%.

3.5 Discussion

3.5.1 Experiment

During the experiment, evidence of a possible chord shielding effect was found. A difference in temperature of 50 °C was found between the exposed and protected sides at the same location on the bottom chord. Therefore, it is possible that the steel itself redirects flames and heat around other parts of the truss. Future work should attempt different heat exposures and sizes of trusses to further examine this chord shielding effect.

Verification of the DIC strain results was completed because narrow spectrum illumination and DIC have not been used in tandem for a truss application. To do so, Equation 2.5 was used to compare the experimentally calculated coefficient of thermal expansion (α) to the code (CSA-S16 [10]) value. This required information regarding the maximum strain (ε_{max}) and the temperature change (ΔT) from the temperature at maximum strain to ambient (assumed to be 20 °C). All values are summarized in Table 3.3 and a sample calculation for the bottom chord is provided below. The experimental values range from 1.13E-5 to 1.33E-5 °C^{-1} while the code value is 1.4E-5 °C^{-1} [97].

Table 3.3: Coefficient of thermal expansion based on DIC results.

Chord	ε_{max}	ΔT (°C)	α (°C^{-1})
Bottom	0.00766	677.71	1.13E-5
Diagonal	0.00736	551.89	1.33E-5
Top	0.00565	431.905	1.25E-5

$$\Delta L = \alpha L_0 \Delta T$$

$$\varepsilon = \frac{\Delta L}{L_0}$$

$$\alpha = \frac{\Delta L}{L_0 \Delta T}$$

$$\alpha = \frac{\varepsilon}{\Delta T}$$

$$= \frac{0.00766}{677.71℃}$$
$$= 1.13x10^{-5}\ ℃^{-1}$$

Similar to a methodology conducted by Nicoletta et al. [89], the strain versus temperature data for each chord was plotted in Figure 3.15 using the cooling phase to limit variability that occurs during heating. This was then compared against the Eurocode 3 values which relate the coefficient of thermal expansion to thermal strain and temperature. Similar trends and magnitudes were seen at each location. L3 had the most data since it reached higher temperatures compared to the bottom and top chords. Overall, the DIC results are similar to the theoretical calculations, indicating it is suitable for this scenario.

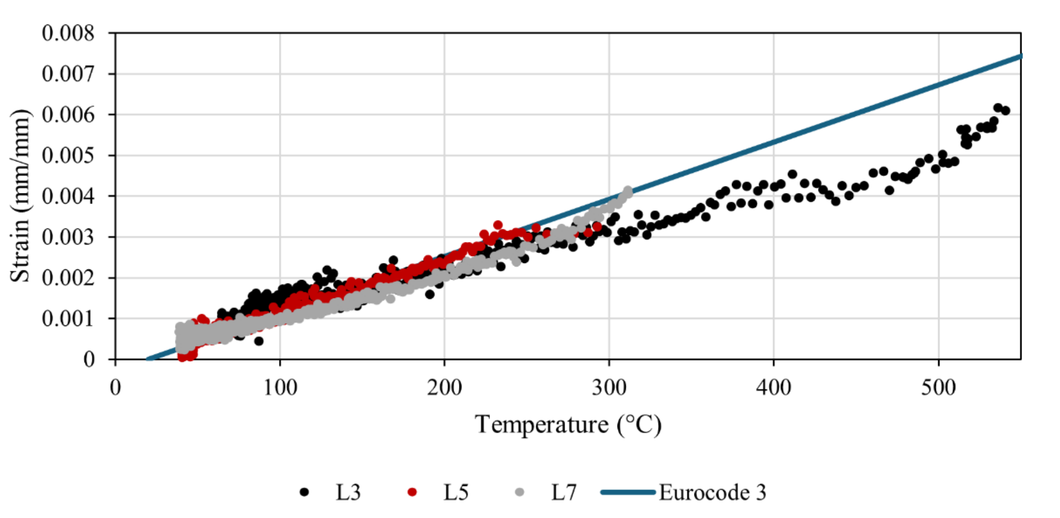

Figure 3.15: DIC validation against Eurocode 3 [97] using strain over temperature.

Other considerations include that no structural testing was performed after fire testing. Destructive testing was not conducted to preserve the specimens so they could be reheated and because the interest was for gathering information regarding the thermal mechanics of how heat is dispersed throughout the system and how that promotes thermal strains. Additionally, information from destructive tests would provide information on residual strength which was not necessary for model validation at this time. The design of the experiments also aimed to avoid any permanent mechanical damage since they were being tested multiple times, so the temperatures of the truss did not exceed 800 °C where these material changes were expected.

Future work can include using non-destructive tests to examine post fire residual strength to avoid damaging the trusses. A study by Peng et al. specifically developed a non-destructive testing technique using ultrasonic sound speed measurements to determine the elasticity of a steel beam heated and cooled [100]. Other suggestions were to conduct a metallurgical microscope test by replicating the surface microstructure. Other non-destructive tests include the investigation of magnetic steel properties to estimate yield strength and ultrasonic measurements to determine stress and strain [101].

3.5.2 Heat Transfer Model

When comparing the heat transfer model to the experimental thermocouple data (Figure 3.10 and Figure 3.11), the model simulations followed the overall trends seen in the experimental data. L1 to L5 all showed a rapid increase in temperature, followed by a period of more constant temperatures during the heating period, and then a decrease in temperature that followed an exponential decay function. L6, similar to the experimental data, had a more gradual heating and cooling, reaching much lower temperatures than the other locations.

However, while the model was able to predict general trends, it overestimates the magnitude of horizontal heat transfer but underestimates the magnitude of vertical heat transfer. A possible reason is that the thermocouples were not fully insulated and that they were affected by gas temperatures, which would impact the comparison of the model and experimental results. The installation method for the thermocouples relied on tension within the nickel-chromium wire to apply pressure on the fibre wool and the thermocouple end. This was more difficult in certain locations depending on which side of the angles the thermocouples were being mounted. If tension was lost during the application or heating, there is some possibility of the thermocouple being exposed to the air temperature as well as the steel temperature.

Other possible reasons to explain the discrepancy in the heat transfer model versus the experiment are that the geometry was oversimplified when going from a three-dimensional structure to a two-dimensional model. For vertical heat transfer, rather than representing the horizontal chords as two L-shapes, a single rectangle was used instead. Both angle members would contribute to the temperatures experienced by the diagonal chords, thus introducing more heat into the system, amplifying only the vertical heat transfer. When considering the horizontal heat transfer, it is possible that the overestimation of temperature was caused by the method in which boundary conditions were applied. As a simplification, the convective and radiative heat were applied to the section of the truss located within the width of the fuel pan (see Figure 3.7). However, the flame follows a conical, not rectangular prism shape for a localised fire. Therefore, L5 and L6 may have had more heat applied in the model than what occurred in the experiment. A more accurate method would be to calculate or measure the temperature at different distances away from the centreline.

Another observation from the heat transfer model is the rate of heating differs from the experiment. The author tested to see if it was a result of an inaccurate convective heat transfer coefficient by using a method from Eurocode 3, Section 4.2.5.1 [37]. The method predicts steel temperature development over time, requiring material input parameters such as density and specific heat capacity. The method also requires heat flux which is dependent on gas temperatures (taken from the experimental data). Results of testing values of 20, 25 (Eurocode recommended values) and 35 W/m^{2}K for the convective heat transfer coefficient can be seen in Figure 3.16. Since the temperatures are reaching similar magnitudes, it was noted that because the flames were touching the truss, the fire may be better represented as a fully developed fire, despite it being localized. Hence, the 25 W/m^{2}K value being sufficient even though it was intended for a standard fire test.

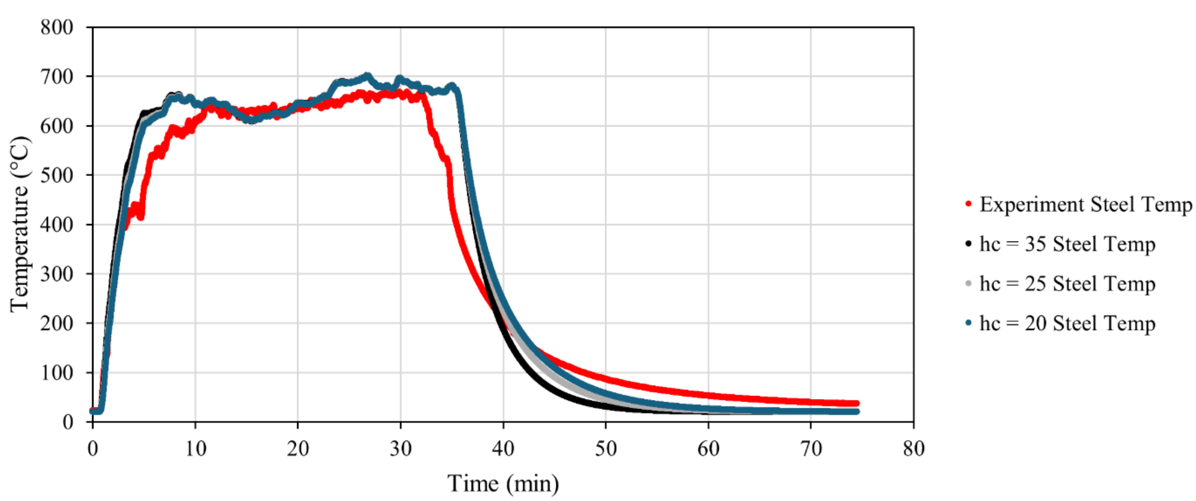

Figure 3.16: Comparison of the experimental steel temperatures versus the calculated steel temperatures using the Eurocode 3 method for steel temperature development.

Finally, as seen in Figure 3.10, the model outputs nearly the same temperatures for L1 and L2, whereas the experiment showed a difference of approximately 50°C. This may be because there is a chord shielding effect (discussed in Section 3.2 and [23]) in the experiments that is not captured in the model. Further research is required to capture this complexity. Overall, these three factors may describe the discrepancy between the experiment and heat transfer model results and thus should be better understood when developing numerical models to be used for fire safety design purposes.

3.5.3 Thermal Deformation Model

For the deformation model, the results show good comparison between experimental and model results, generally predicting around a 10% difference in maximum strain values. The models are conservative, following the correct trends and magnitudes. However, the bottom chord shows the most interesting results, highlighting the impact of the supports on thermal strain. With both supports fixed along the bottom chord, the thermal expansion caused by the fire exposure results in internal forces and negative strain.

Another observation is that for the top and diagonal chords, the fixed end model had similar or more accurate results compared the free end model. Allowing one end to freely expand and contract predicted more thermal strain than in reality. This is because the experimental setup partially restricted the horizontal translation of the truss. For the free end model, moving from the bottom chord to the top chord results, the accuracy increases. This is because the top chord was fully free to move (as represented in the model). Therefore, most differences in modelling and experiment are believed to be because the trusses in the experiments were partially restricted.

In addition, the likely reasons for the conservative results of the remaining model predictions include the method in which thermal loads were applied. As discussed in the methodology section, the highest temperature at each thermocouple location was applied to each of the 11 beam sections. If no thermocouple data was available, the highest thermocouple data from a nearby beam. The beam sections with no thermocouple data were locations further from the heat source, meaning higher than actual temperature data was applied for those sections as well.

Finally, one other consideration for factors not fully represented in the model compared to the experiment are the impact of microstructural changes and residual stresses. As discussed in Chapter 2, residual stresses are caused by uneven heating and cooling of a member without the impact of external loads [23]. During manufacturing, the process of welding the individual members to form the truss could create microstructural changes (cause phase changes in portions of the steel) and residual stresses. As well, residual stresses may have been altered during the localized heating process. Therefore, it is possible that this may impact the accuracy of the model results since they are unquantified and thus not considered in the thermal deformation analysis. However, the trusses were tested unloaded to minimize variability and results showed good correlation to experimental data.

3.6 Conclusion

This chapter focused on creating practical tools for the fire design and analysis of steel truss roofing systems. A review of current guidelines and codes shows that stadium roofs are vulnerable to fire due to their lack of required protection. This was shown through the case study, in which a localized roof fire resulted in a full evacuation of the stadium.

Literature suggested that alternative solution designs are necessary from a fire safety perspective on a stadium roof structure. Limited experimental evidence of realistic fire scenarios in stadiums exist as well as validated numerical models based on such fire scenarios and structural arrangements. Therefore, focus was placed on developing tools for alternative solutions such as performance-based design to aid in fire safety design for steel truss stadium roof systems.

In this work, four full scale experiments of steel trusses under localised pool fire scenario were carried out and are presented. These experiments were unloaded so that multiple tests can be performed on the same samples and so that the dispersion of heat and development of thermal strains could be isolated without creep strain being introduced. This was also beneficial when validating the numerical models. Steel temperatures were measured using thermocouples, ultimately finding a possible chord shielding effect. Thermal strain was measured using novel technology: narrow spectrum illumination and DIC. The strain results were successfully verified against Eurocode 3 values since narrow spectrum illumination and DIC have not been used in this application before.

Following the experiments, heat transfer and deformation models were created using LS-DYNA, replicating the experiment (based on the case study) that were conducted using two OWSJs. The heat transfer model using solid elements and simplified the geometry into a two-dimensional model to ease computational requirements. Convective and radiative boundary conditions were applied using tributary areas to represent the pool fire used in the experiment. Specific locations were observed to highlight the model's capacity to predict horizontal and vertical heat transfer. When comparing to experimental thermocouple data, findings were that the model was able to replicate general trends, however, overestimated horizontal heat transfer while underestimating vertical heat transfer. The heat transfer model helped identify areas of future research required to improve the accuracy of the results. To start, future work should include attempting a three-dimensional heat transfer model. With more accurate geometry, it is likely that the heat transfer would become a better match. This would also determine whether the software's default is to overestimate horizontal heat transfer and underestimate vertical heat transfer, which would be of use to designers.

When developing the deformation model, the truss was built using beam elements. Two cases were tested which varied the supports: one model had two fixed ends, and the other had a free and fixed end. Experimental temperature loads were applied conservatively to each member and thermal strain was observed. Results were compared to experimental DIC data and findings were that overall trends and magnitudes were accurate. With both ends fixed however, thermal expansion forces are restricted inward resulting in negative strains. The good correlation between the deformation model and experiments encourages future work to consider larger scale trusses with various connection types such as gusset plate connections. Behaviours are not always scalable, nor the same if geometry changes. In addition, structural testing (loading the trusses) should be completed, with further modelling attempts. This will take steps in achieving the ultimate goal of furthering the connection between human behaviour and structural fire design and analysis tools.

Overall, it is important to recognize that in a high occupancy, large-scale building such as stadia, there are additional considerations when designing. Stadia are an example of a structure that has overlaps in both human behaviour and structural resilience. As seen in the case study, additional time can be needed to determine whether evacuation is required, and then for the evacuation to occur. This chapter began the process of generating human behaviour and structural resilience modelling tools that can be combined to aid in design and analysis. A framework for future experiments and subsequent models was generated with the aim of assisting steel truss fire design and analysis.

Chapter 4: Cone Calorimeter Testing and Numerical Modelling of Sawn Lumber and Engineered Timber

4.1 Introduction

The previous chapter focused on the development of finite element tools for steel trusses in fire applications. The overall objective of the thesis herein is tool generation to assist in risk-based designs when using alternative design solutions (rather than a prescriptive design). Timber is considered next because it is both an old and new material but is not well understood from a fire perspective. This is a concern considering the growing interest in mass timber construction in response to the current climate crisis. With industry and government leaders committing to reduce carbon emissions by 2030, timber construction is a good alternative for traditional building materials such as concrete or steel [5]. From a sustainability standpoint, the built environment sector, including the building construction industry, contributes to over 37% of global emissions [102]. In contrast, timber is a renewable resource with the ability to sequester carbon when sustainably harvested [103].

While there are many environmental benefits, there are under researched areas including the formation of the char layer when exposed to fire [104]. Because timber is a combustible material, it undergoes pyrolysis; unburned wood is heated, releasing combustible gases and transforms into a char layer [42]. Pyrolysis changes from slow to rapid at approximately 300 °C. This char layer is significant because it impacts the structural strength of the timber member, as well as the burning rate. Char has no structural strength, meaning that as the section forms a char layer, it loses cross-sectional area and structural integrity. Furthermore, the char layer is known to have insulating properties, slowing the heat transfer of the fire source to the unburned, structurally sound wood. However, the rate in which the char layer forms, the amount it insulates the remaining wood, and what causes char fall off, are largely unknown.

This uncertainty regarding the fire performance of timber can render current codes inapplicable at times. In the context of design and industry application, alternative methods for assessing the fire performance of timber are required. Experimental testing can provide information on the behaviour of timber in fire; however, frequent large-scale testing to inform design is unrealistic. Furthermore, in the context of heritage timber buildings, in which Canada has a plethora of, it can be difficult to obtain testing materials. Therefore, there is a need for numerical modelling tools. A validated modelling methodology can be used in parametric studies to predict material behaviour, thus allowing designers to understand how possible fire events could impact a structure. This can then be considered in risk-based analyses such as risk indexing (in which designs are ranked based on probability and severity of a fire event) and assist in justifying design choices when alternative solutions are required [105]. Given the limited knowledge and design guidelines surrounding the behaviour of wood and timber in fire, research is required in order to develop an accurate, reliable, and experimentally informed modelling methodology for char formation and timber heat transfer. Therefore, the objective of this chapter is to develop modelling tools for timber in fire (spanning heritage timber to modern timber products), supported by experimental data, while also considering the unique behaviour associated with combustible materials.

4.2 Background

A literature review was conducted, expanding upon [104], with a restricted scope on finite element heat transfer models of timber in fire and the influence of key parameters (i.e., moisture evaporation and char formation) on the results. The following sections assess different finite element analyses and their ability to simulate timber behaviour in fire.

Timber as a combustible material presents a variety of new modelling challenges when compared to traditional materials such as concrete and steel, including the presence of moisture and the formation of the char layer. The moisture within the material affects the ignition time and intensity required for ignition. As the temperature increases, the water will begin to evaporate, which requires energy [42]. This energy loss must be accounted for. As well, the thermal properties of timber will change over time and temperature to account for char formation. These include its thermal conductivity, specific heat capacity and density. Therefore, the aim is to explore how literature considers moisture evaporation and char formation to determine if and how they potentially impact a heat transfer timber model.

4.2.1 Moisture Evaporation

Werther et al. conducted a parametric study to explore the ability of various softwares to model finite element heat transfer analyses for timber [106]. A series of timber structural elements were modelled using softwares SAFIR, ANSYS, and Abaqus to determine limitations and best practices. This study specifies that using the thermal conductivity, specific heat capacity and density parameters from EN 1995-1-2 (Eurocode 5) [107] allows for complex timber behaviour, such as charring, to be considered implicitly. Furthermore, the authors report that each software's sensitivity to the mesh size and timestep varies, thus making mesh and time sensitivity analyses vital. However, the main finding from this study is the development of the Latent Heat method, which allows moisture evaporation to be considered in ANSYS and Abaqus. The latter allows the user to specify the moisture content of the timber specimen and as a result, removes the peak within the specific heat capacity curve if moisture is not included in the analysis.

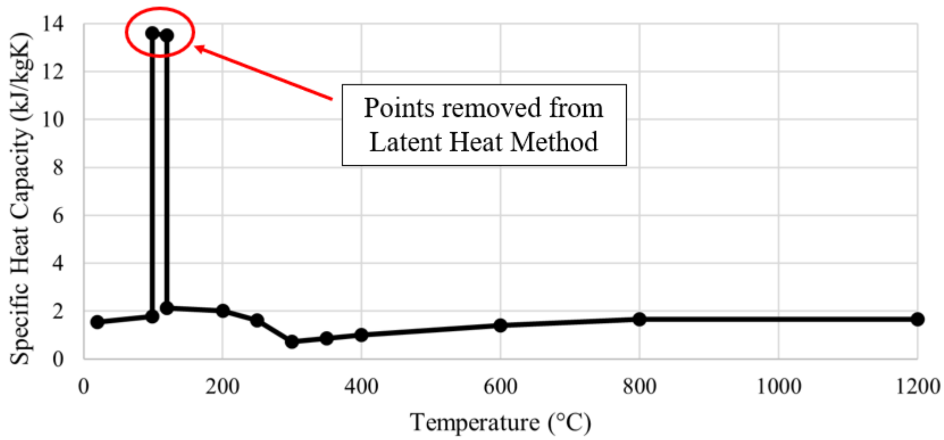

Figure 4.1: Latent Heat method [106] modified specific heat capacity over time.

The latent heat model was used in several other studies, particularly the author's research team, including Philion et al. [104] and Quiquero et al. [108]. The methodologies presented in [104] will be closely followed herein and further discussed in Section 4.2.3. Quiquero et al. [108] modelled a post-tensioned timber beam using Abaqus, applying convective and radiative heat as boundary conditions, and conduction for heat transfer. Results showed good comparison but underestimated predicted char depth.

Using MATLAB, Pečenko et al. conducted several studies including developing a simplified model for heat and moisture transfer and char formation [109], and a two-step numerical model that first modelled heat and moisture transfer and then the mechanical response [110]. Focusing solely on the heat and moisture transfer char formation model, they first coded the water to move within the cell walls using diffusion laws before using latent heat and phase change temperature calculations to account for water vaporization. Pečenko et al. determined that the initial moisture content had considerable impact on heat transfer and charring rates [109], [110].

4.2.2 Char Formation

After reviewing moisture evaporation methodologies, several studies which attempted to implement char formation into a finite element model were found [64-68]. Shen et al. [111] modelled pyrolysis in small-scale, wet wood samples by developing an energy conservation equation which ultimately showed good agreement between experimental and calculated results. Though this study did not use the finite element method, it formed the basis for the methodology referenced in several other timber pyrolysis finite element models.

Thi et al. conducted two pyrolysis finite element analysis studies [112], [113]. The first used MATLAB in a two-dimensional heating scenario and varied thermal properties such as the specific heat capacity, thermal conductivity and density inputs to represent pyrolysis. The second used Abaqus to model to simulate one-dimensional heat transfer, accounting for pyrolysis through a user defined subroutine which modified the internal thermal energy and heat flux using implicit analysis.

More recently, Tran et al. modelled the thermo-mechanical behaviour of compressed spruce wood samples tested using a cone calorimeter [114]. Testing was completed to experimentally measure the specific heat capacity and thermal conductivity with temperature since there is no available data for compressed wood. Using Abaqus, the experiments were modelled with an additional user defined subroutine to account for the pyrolysis process in three-step multi-reaction kinetics. Preliminary results of heat transfer, mass loss, and charring depths showed good agreement to experimental findings; however, additional studies are required to validate the model for high temperature fire scenarios.

As seen in these studies, more refined software and subroutines are being required to accurately represent pyrolysis in finite element heat transfer models of timber in fire. This may be representative of the fact that there have been research developments and therefore, there is more information on timber behaviour in fire and this pyrolysis process. While the first study required MATLAB only, the second and third studies required subroutines with increasing complexity.

Finally, as an alternative option, one could consider the char layer through moving boundary conditions during finite element simulations [115]. It may be possible to account for char formation by activating and deactivating elements and boundary conditions, or by adding and removing elements with varying material properties.

4.2.3 Summary

The interest in understanding both char formation and moisture migration is highlighted in the literature with most studies modelling timber heat transfer analysis using finite element method in Abaqus, MATLAB, or ANSYS. A commonly used approach for considering moisture content was the Latent Heat method [106] in which phase change temperature and latent heat of vaporization are required. From a char formation perspective, some studies relied on the Eurocode 5 inputs in which char formation and moisture migration were already incorporated for standard fire exposure. Others chose to write additional subroutines since finite element software alone did not have this capability built in. An alternative approach to these subroutines and coding thermos-chemical reactions includes implementing moving boundary conditions.

To further explore these parameters within finite element heat transfer modelling, the research herein will conduct a modelling study with complementary experimental testing to allow for validation. In a previous study by the author's research group, a modelling methodology for predicting heat transfer in timber using finite element analysis software LS-DYNA was created [104]. The model was validated against a glulam beam and heritage timber member and then applied as an apriori model to a (CLT) panel exposed to a localized fire. As a continuation and expansion of the previous scope, the objective of the chapter herein is to observe the applicability of the methodology on heritage sawn lumber (hardwood and softwood) and modern engineered timber products (glulam and CLT) at small scale radiant heat exposure. Further examination into the methodology at a small scale will allow the authors to identify important parameters for accurate models as well as possible solutions to challenges that arise with the aim of developing a higher certainty model. This study will vary only the material being studied to isolate the impact of material properties. Also, the experimental and numerical model results can begin to form a database of material information which can be referenced in future studies and industry applications.

4.3 Experimental and Numerical Methodology

4.3.1 Experiment

The experiments were conducted in a two-part series with the procedure mainly following ASTM E1354 [116]. Note that all testing was conducted with supervision from supervisorial personnel. The authors' research team conducted the first part of the experiments which tested heritage samples [104], [117] and the second part of the test series (focused on engineered timber products) was conducted and analyzed by the author and an additional collaborator (co-author of the conference paper) [118]. Methodology for sample preparation and the thermal tests are similar between the two-test series', with differences in the procedure for measuring char depth post fire test. The hardwood samples were sourced from a beam circa 1880, and the softwood heritage samples were sourced from a joist circa 1830. The glulam samples were sourced from the web of a T-beam and CLT samples from larger panels. All samples were tested using a cone calorimeter. A total of 20 hardwood heritage, 20 softwood heritage, 15 glulam and 15 CLT samples were tested at a heat exposure of 30 or 50 kW/m^2 and for durations of 3, 6, 10, 15, or 30 minutes (see Table 3.1 for the test matrix).

Table 4.1: Cone calorimeter test matrix.

Material Type	Sample Type	Heat Flux (kW/m^2)	Heat Duration (min)	Number of Samples per Duration
Heritage Timber	Hardwood	30	3, 6, 10, 15, 30	2
		50		2
	Softwood	30		2
		50		2
Mass Timber	Glulam	50		3
	CLT	50		3

The 30 and 50 kW/m^2 applied heat flux were chosen to observe a higher and a lower exposure intensity. The higher heat flux provided enough energy to cause ignition of the samples, allowing this behaviour to be explored. The lower heat duration was chosen because it had a lower likelihood of the sample igniting. Instead, this allowed the char formation when a sample was only smouldering providing useful information for a different heat exposure with different material behaviour. The durations were also chosen to track the formation of the char layer over time. The highest charring rate was expected to occur in the beginning of the experiments. Once the char layer forms, it acts as an insulating material, slowing further pyrolysis and char formation. Therefore, more short duration tests (3, 6 and 10 minutes) were completed. Once the specimens were burned, the charring depth was measured and compared.

4.3.1.1 Sample Preparation

The samples were cut to 100 x 100 x 45 mm dimensions per the size restrictions from the cone calorimeter equipment. The heritage samples were conditioned at approximately 23 °C and 50% relative humidity. The use of a moisture chamber became available for the second, engineered timber test series, so samples were stored at 21 °C and 70% relative humidity to aim for a moisture content of 12%. The hardwood samples are of an oak species and the softwood samples are of a spruce species as determined by a horticulturist. The glulam samples are Spruce Pine 20f-EX, produced from Element5, and were cut to ensure a glue line was along the midpoint of the sample (for future mechanical testing) and included two outer laminates and two core laminates of the original member (see Figure 4.2). The 20f-EX is representative of a balanced grade in which the grade of the individual laminations (i.e., strength) varies depending on the location layer (i.e., strongest laminates on the outer portion compared to the core). The CLT samples, produced from Element5, are V2 stress grade and include the outermost laminate and an approximately 10.5 mm portion of the next laminate (see Figure 4.3).

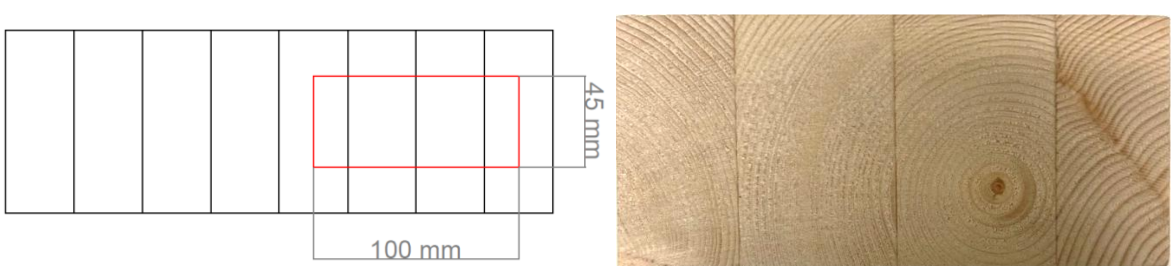

Figure 4.2: Prepared glulam sample prior to cone calorimeter testing.

Figure 4.3: Prepared CLT sample prior to cone calorimeter testing.

Prior to testing, all samples were examined to avoid large cracks or deformations, with any unusual observations, such as several knots, being recorded. From there, dimensions, weight and moisture content of the samples was measured. For the heritage samples, two hardwood and four softwood samples were used to represent their respective sample types. Moisture content was calculated by placing the samples in a furnace to dry for 24 hours at 108 °C and weighing them before and after drying. For the engineered timber samples, a Tramex moisture meter (MRH III) was used to measure the moisture content in both the side and end grain of the sample. A summary of average values for density and moisture content along with their coefficient of variation (CoV) is presented in Table 4.2 and will serve as material property inputs for the model.

Table 4.2: Average and CoV of material properties per test type.

Sample Type	Property		Heating Duration (min) 3	6	10	15	30
Hardwood	Density	*Avg. (kg/m³)*	565.91				
	Moisture Content	*Avg. (%)*	8.67				
Softwood	Density	*Avg. (kg/m³)*	355.95				
	Moisture Content	*Avg. (%)*	6.97				
Glulam	Density	*Avg. (kg/m³)*	478.70	493.01	508.14	504.71	504.59
		CoV (%)	1.80	0.73	2.47	Una*	1.47
	Moisture Content	*Avg. (%)*	9.3	10.1	10.5	10.7	9.6
		CoV (%)	9.86	Una*	Una*	Una*	1.97
CLT	Density	*Avg. (kg/m³)*	481.06	496.53	478.53	498.12	502.81
		CoV (%)	3.30	3.45	3.72	2.74	1.34
	Moisture Content	*Avg. (%)*	13.4	13.5	13.5	13.5	13.6
		CoV (%)	0.93	2.42	2.40	2.10	2.66

* Data unavailable.

4.3.1.2 Thermal Test

The thermal tests followed a modified ASTM E1354 [116] methodology using the cone calorimeter at the Waterloo Fire Research Laboratory. The cone calorimeter apparatus (seen in Figure 4.4) is a dual-cabinet model which includes a gas analyser cabinet and the cone calorimeter cabinet. The gas analyser cabinet measures the heat release rate and gas concentrations (oxygen, carbon dioxide, and carbon monoxide) throughout the tests [119]. The cone calorimeter cabinet contains the cone shaped radiant heater that uniformly heats the samples at a pre-set heat flux. These tests were completed in a well-ventilated and controlled environment with the specified heat flux applied to the top of the sample by the electric cone heater and the bottom face insulated (see Figure 4.5). No external spark ignition was used to allow the samples to self-ignite, which differed from the ASTM E1354 procedure. This was done to more accurately represent a real fire scenario. Additionally, with the higher intensity heat flux, it was hypothesized that the samples would self-ignite without the need for an external spark. This self-ignition process was also of interest to study. Finally, the cone calorimeter cabinet contains a load cell, which measured mass loss over time.

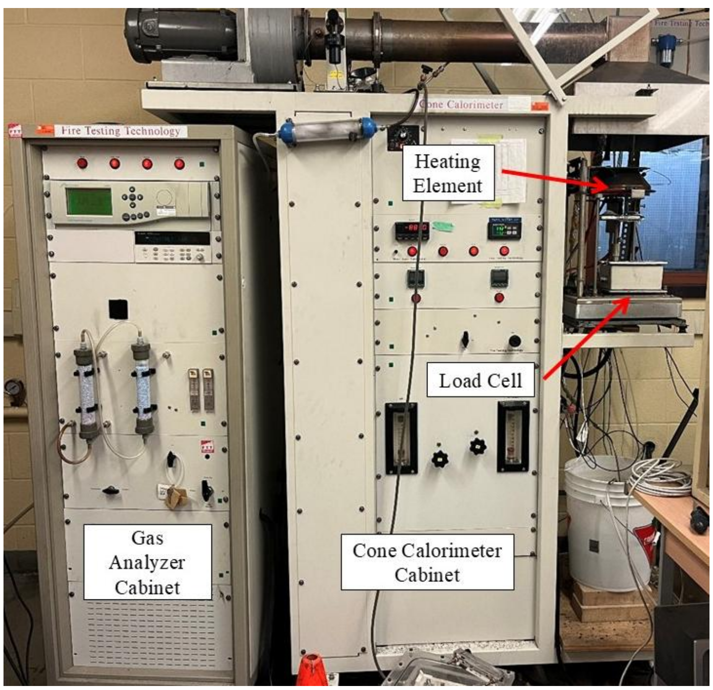

Figure 4.4: Cone calorimeter apparatus.

Figure 4.5: Cone calorimeter heating mechanism.

At the end of each test, the samples were removed and immediately sprayed with water to stop further char formation. The samples were then moved back to the moisture chamber to facilitate conditioning prior to measuring the char depth.

4.3.1.3 Measurement of Char Depth

After fire testing, and the reconditioning of the samples, the char depth of each sample was measured. Two methods for char measurement were used. For the heritage samples, the specimens were cut in half and the distance between the unexposed face to the char layer was measured. By subtracting the measurement by the original depth of the specimen, the char depth was calculated. From there, the char layer was divided by the heat duration to calculate the charring rate. Due to time constraints, a preliminary measurement for char depth of the engineered timber samples was used following Quiquero and Gales [120]. A timber frame larger than the original sample dimensions was built and holes drilled at the mid and quarter points along the centreline of each glulam lamination (see Figure 4.6). The charred sample was placed inside the frame which prevents movement of the sample, and a thin sharpened steel rod was used to probe the sample (perpendicular to the exposed face) at each specified drilled location. Because the char layer has no structural strength, the depth at which the rod reached resistance was measured and set as the char layer depth. This method was used to gain a preliminary understanding of char depth without damaging the samples. Future work will shear test and cut the samples to gain an exact measurement of the char depth.

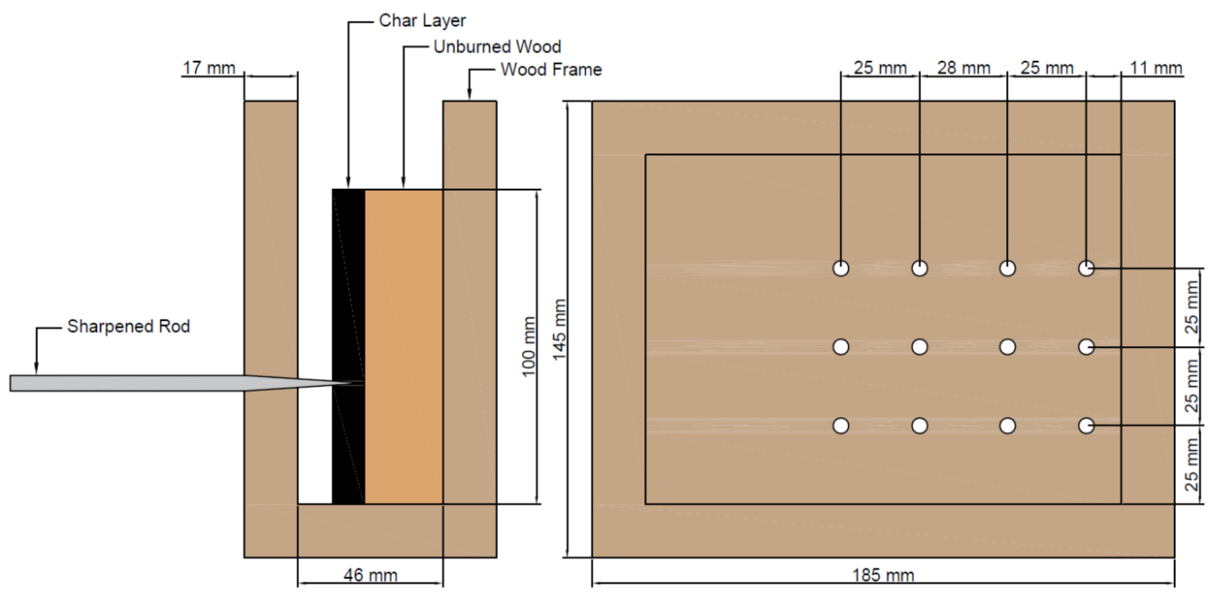

Figure 4.6: Char depth measuring apparatus and measurement locations.

4.3.2 Model

Once the material properties were measured, a numerical model using Ansys' LS-DYNA program was created by the author to replicate the experiments following the methodology from Philion et al. [104]. LS-DYNA, a finite element analysis software, was used as the numerical solver. This software was chosen because of its common use in the industry and academia for fire safety engineering analyses [46], [93], [121]. While LS-DYNA is extensively validated to model steel and concrete behaviour in high temperatures, its ability to predict timber behaviour is a relatively new research endeavour and therefore considered herein in lieu of other software packages. While the focus of the study is on identifying important parameters in timber heat transfer analysis and how best to implement these behaviours, the aim is to develop a general framework that can be adapted for use in other finite element software.

The model represents an explicit one-dimensional heat transfer of the cross-section of the testing samples (100 x 45 mm). Oasys' Primer was used the pre-processor, and the results were output and processed by Oasys' D3Plot and T/HIS software [46].

4.3.2.1 Mesh and Time Sensitivity Analyses

Initial steps taken to create the model included completing a mesh and time sensitivity analysis. Mesh sizes of 1, 3, and 5 mm solid elements were compared, as well as timesteps of 1, 5 and 10 seconds. The objective of these analyses was to choose the largest possible mesh and timestep size to reduce computing time, while maintaining the accuracy of the results. Overall, the analyses were completed using the 3-minute, 50 kW/m2 heat flux test; results indicated that the use of a 1 mm mesh size and a 10 second initial timestep were ideal (see Figure 4.7 and Figure 4.8). This can be seen through the discrepancies seen between results with 1, 3 and 5 mm, and the lack of discrepancies between the various timesteps. While the initial timestep was set, a variable timestep option was chosen, so it can increase or decrease within a range of 1.0E-6 and 30 seconds.

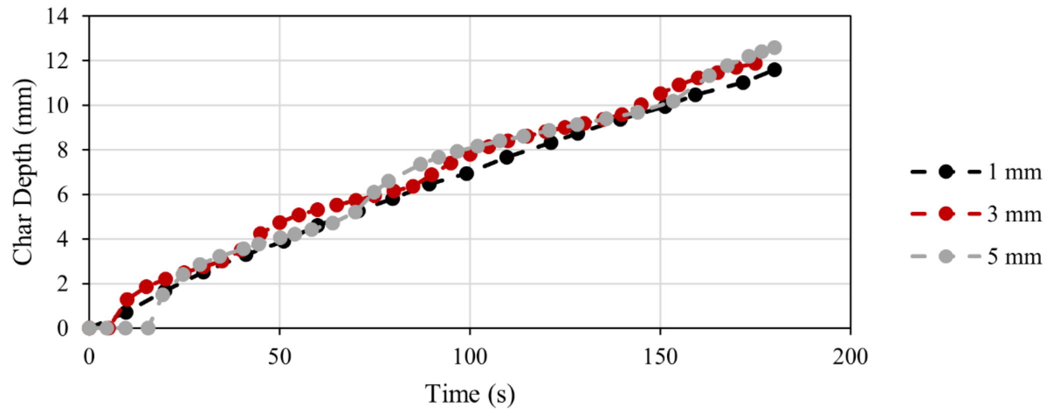

Figure 4.7: Mesh sensitivity analysis of hardwood at 50 kW/m^2 for 3 minutes.

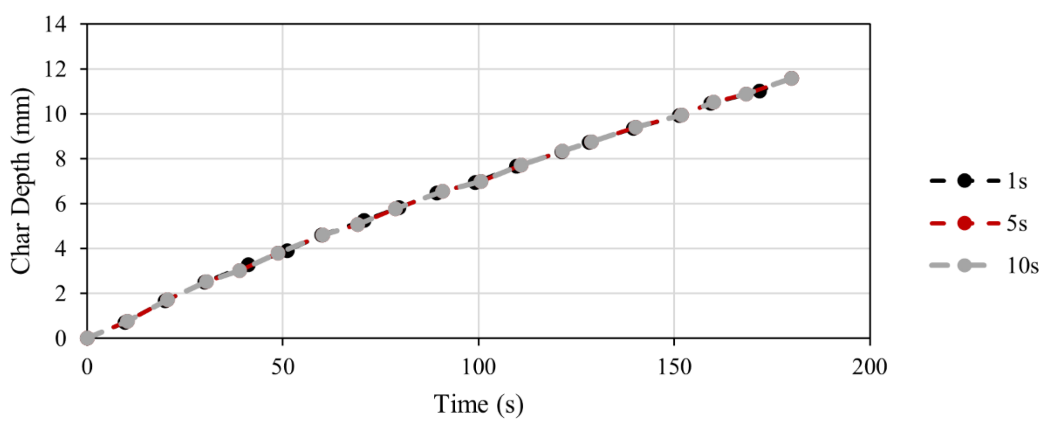

Figure 4.8: Time sensitivity analysis of hardwood at 50 kW/m^2 for 3 minutes.

4.3.2.2 Material Properties

Based on the Eurocode 5 method [107], the density, specific heat capacity and thermal conductivity of the samples were inputted. A key limitation of the software is the inability of the user to directly change the density. Instead, the bulk density (collected in Table 4.2) was taken as the single value for the duration of the simulation. This also means that the material properties cannot be simply or directly changed. Therefore, while timber changes into ash and an insulating char layer, the software only models the wood material with its associated properties. Given the configuration, it will err on the conservative side of calculating charring rate as the insulating layer will be absent.

The material type was set to be thermal isotropic, which allowed thermal conductivity and specific heat capacity curves with respect to temperature from Eurocode 5 [107] to be used. Another limitation of the software is the inability to input the multiple specific heat capacity values for a single temperature value. Therefore, the Latent Heat method per Werther et al. [106] allows the peak accounting for water evaporation between 99 and 120 °C to be removed (illustrated in Figure 4.1). Instead, to account for moisture evaporation, the phase change temperature of water and latent heat of wood were inputted. The latent heat of wood was calculated by multiplying the averaged moisture content (Table 4.2) by the latent heat of evaporation of water (2260 kJ/kg). Note however, that the Eurocode 5 thermal conductivity and specific heat capacity curves are for softwood (there are no curves for hardwoods) [107]. As these were used for both the softwood (including the engineered timber model) and hardwood models, the author understands this is a source of inaccuracy.

4.3.2.3 Thermal Properties

The initial temperature was set to be ambient temperature, assumed to be 20 °C for the heritage specimens, and the actual averaged value ranging from 23 to 25 °C for the engineered timber specimens. This is the temperature of the specimen at the start of the simulation. As per the cone calorimeter test methodology, the heating side had a boundary condition of 30 or 50 kW/m2 heat flux, and the insulated side a boundary condition of 0 kW/m2 heat flux. Heat transfer occurred through conduction.

4.4 Experimental and Numerical Results

4.4.1 Experimental

While the results of both the heritage lumber as reference samples and engineered samples will be discussed, other experimental observations will be discussed solely for the tests conducted by the author (engineered timber test series). All glulam and CLT specimens self-ignited without the use of a sparker. This confirmed the hypothesis that at a higher heat flux exposure of 50 kW/m^2, a sparker could be foregone, allowing more realistic fire scenarios and ignition.

During and after testing, some notable observations were made, including that the CLT samples did not always self-extinguish immediately post-test. This means that for some samples, the fire became self-sustaining (for the duration between stopping the tests and extinguishment), able to continue burning using the gasses produced as fuel. This was not the case for the glulam samples, with all flames immediately extinguishing once they were removed from the cone calorimeter's applied heat flux.

In addition, the CLT samples were found to have "adhesive bleeding". Examples of this can be seen in Figure 4.9 where the adhesive is seen to soften and then leak from along the glue lines. It is possible that the adhesives used for the CLT samples differed from that in the glulam samples, with one more susceptible to adhesive bleeding. Structurally this has implications since the glue bonds the timber laminates together to form a composite material. With less adhesive, the residual strength of a timber member is uncertain. Corner rounding was also seen when examining the glulam and CLT char formation after testing (more prominent in the longer duration tests). This is a common occurrence in which the corners are "subjected to two-dimensional heat transfer", causing the originally sharp corners to take on a more rounded shape [36].

Figure 4.9: Examples of adhesive bleeding occurring during the CLT cone calorimeter tests (circled in red).

Figure 4.10 shows a representative glulam and CLT charred specimen at a heating duration of six minutes, respectively. In general, more cracks were found in the glulam samples when compared to the CLT. Possible reasons may include that the glulam samples consisted of four laminates, meaning three glue lines were visible, while the exposed surface of the CLT samples was a solid piece of wood. This may indicate that the presence of glue lines results in more cracking. Further examination of experimental results including structural testing of the samples will be conducted in the future.

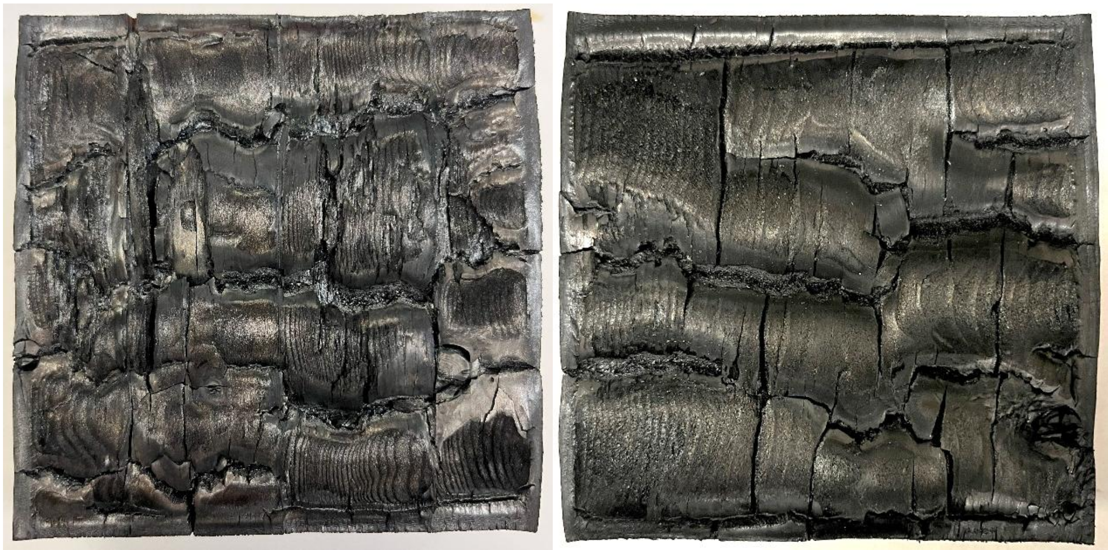

Figure 4.10: Charred glulam sample (left) and charred CLT sample (right) after a six-minute test.

Table 4.3 shows the average char depths and charring rates for the heritage hardwood and softwood samples for each test duration and heating intensity. Because the sample size was only two samples per test, no CoV is provided. The average char depths and their CoV as well as the charring rate for the glulam and CLT tests for all durations at 50 kW/m^2 heat flux are presented in Table 4.4. For the experimental data, the measured char depths of each engineered timber specimen per time duration were averaged (total of 36 measurements per specimen) and divided by the duration of the test to approximate a charring rate.

Table 4.3: Average char depth and charring rate for the heritage hardwood and softwood samples.

Sample Type	Property	Heat Intensity (kW/m^2)	Heating Duration				
			3	6	10	15	30
Heritage Hardwood	Char Depth (mm)	*30*	2.5	6.5	9.3	13.8	23.3
		50	5.8	9.8	12.5	17.8	30.8
	Charring Rate (mm/min)	*30*	0.8	1.1	0.9	0.9	0.8
		50	1.9	1.6	1.3	1.2	1.0
Heritage Softwood	Char Depth (mm)	*30*	1.8	4.0	7.8	10.2	18.3
		50	5.8	7.5	10.8	15.0	31.5
	Charring Rate (mm/min)	*30*	0.6	0.7	0.8	0.7	0.6
		50	1.9	1.3	1.1	1.0	1.1

Table 4.4: Average and CoV of char depth and average charring rate for the engineered timber glulam and CLT samples.

Sample Type	Property		Heating Duration (min) 3	6	10	15	30
Glulam	Char Depth	*Avg. (mm)*	5.43	7.50	10.24	13.92	21.01
		CoV (%)	3.82	3.57	2.49	4.11	7.57
	Charring Rate	*Avg. (mm/min)*	1.81	1.25	1.02	0.93	0.7
CLT	Char Depth	*Avg. (mm)*	5.23	7.97	10.76	14.04	23.99
		CoV (%)	6.43	4.38	2.02	3.59	4.35
	Charring Rate	*Avg. (mm/min)*	1.74	1.33	1.08	0.94	0.80

From Table 4.3 the charring rates at the lower intensity 30 kW/m^2 ranged from 0.8 to 1.1 mm/min and 0.6 to 0.8 mm/min for the heritage hardwood and softwood respectively. At a 50 kW/m^2 heat intensity, both the heritage hardwood and softwood charring rates spanned 1.0 to 1.9 mm/min. For the engineered timber samples, Table 4.4 shows the approximate charring rates ranging 1.81 to 0.70 and 1.74 to 0.80 were obtained for the glulam and CLT, respectively.

4.4.2 Numerical Model Results

For the model, the charring rate was calculated by determining the depth of the node at which the temperature reached 300 °C and dividing that by the heating duration. For simulations in which the heat exposure was predicted to have charred the entire sample, the time where charring occurred in the final node was interpolated and used to calculate the charring rate given a 45 mm char depth. Figure 4.11 visually shows the heat transfer at the end of the three-minute simulation for CLT. The depth of the black line was calculated and divided by the heating duration to calculate the charring rate. As aforementioned, the simulation is a one-dimensional heat transfer under idealized conditions. Therefore, the temperature distribution is also idealized with constant temperatures along any horizontal line.

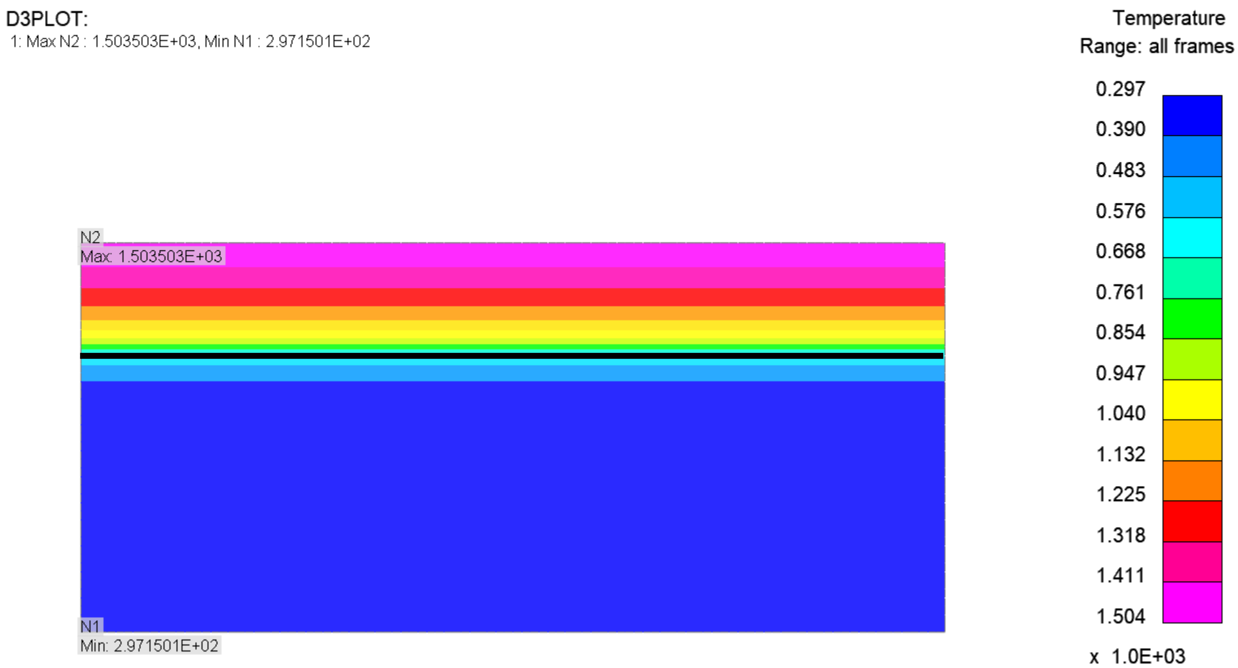

Figure 4.11: Numerical heat transfer of CLT tested for three minutes (temperature in Kelvin).

Figure 4.12 shows the experimental versus simulation char rate results for the heritage hardwoods. The hardwood modelling estimates are approximately double the experimental results on the conservative side, with a maximum model char rate of nearly 4 mm/minute. For the heritage softwood model, results show conservative charring rates with the highest charring rate being nearly 6 mm/ minute (see Figure 4.13). The trends for the 50 kW/m2 flux were followed in the model, but not for the 30 kW/m2 heat flux.

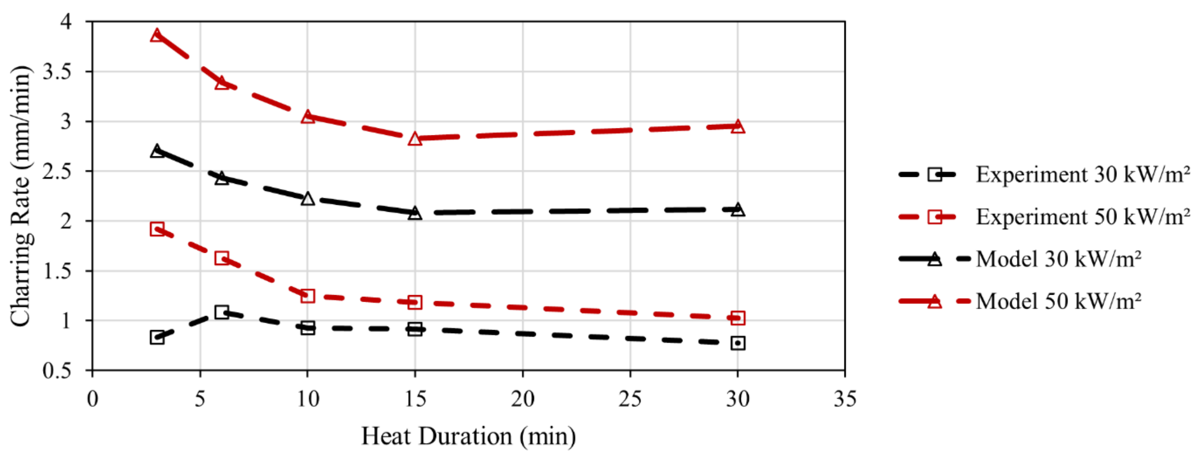

Figure 4.12: Experimental versus model charring rate for hardwood.

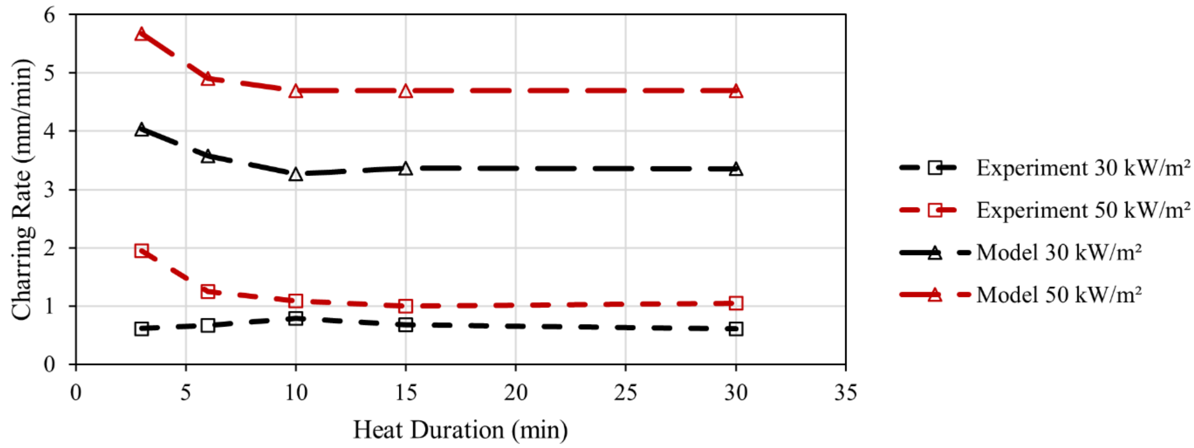

Figure 4.13: Experimental versus model charring rate for softwood

The experimental and numerical model charring rates for the engineered timber samples can be seen in Figure 4.14 and Figure 4.15 for the glulam and CLT samples respectively. The model can predict overall trends correctly with a maximum charring rate occurring at the beginning of the tests, followed by a more rapid decrease in charring rate until it begins to stabilize. However, the simulations provide an overestimation of charring rates of approximately 3.4 and 3.3 times the experimental results for glulam and CLT, respectively.

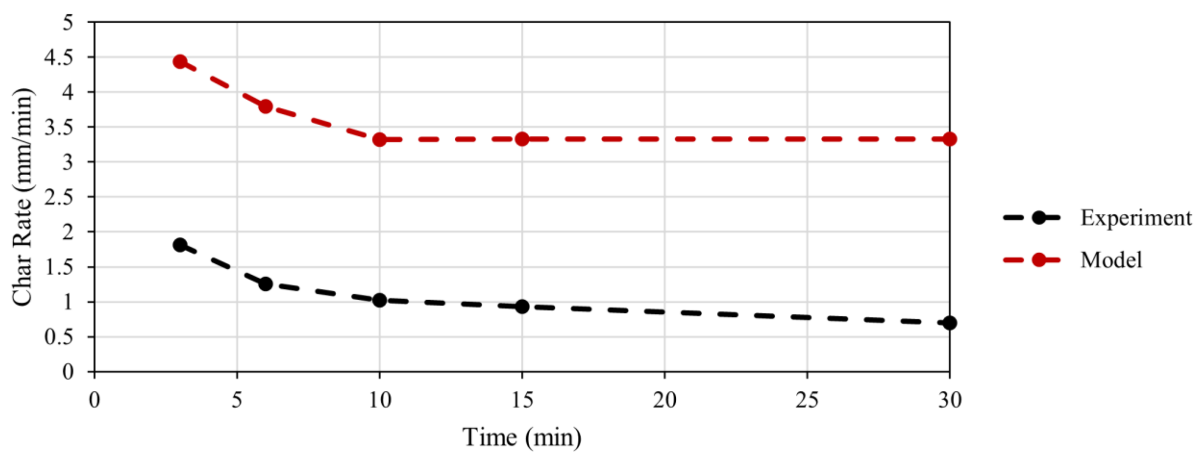

Figure 4.14: Experimental and model charring rates for the glulam samples.

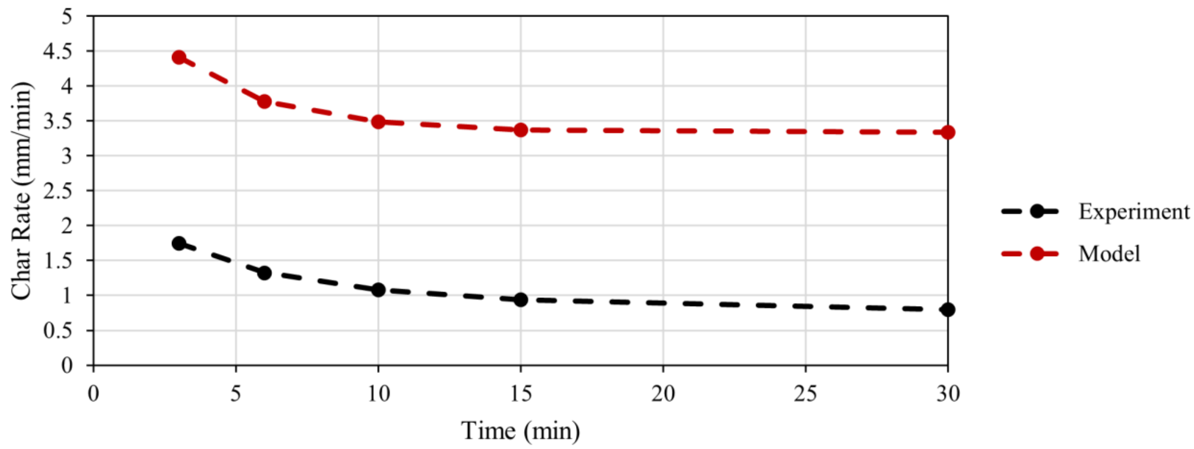

Figure 4.15: Experimental and model charring rates for the CLT samples.

From an alternate perspective, Figure 4.16 and Figure 4.17 show the differences in the model results for the lower (30 kW/m^2) and higher (50 kW/m^2) heat intensities. The model is better able to capture trends for the higher heat intensity. For the lower heat intensity tests, only some specimens ignited, while for the higher heat intensity tests, nearly all samples self-ignited. This ignition period appears in the model with the peak charring rate occurring at the start of the tests (seen in the higher heat intensity results), however, this is not the case for the lower heat intensity tests. This was understandable given that the Eurocode 5 values are intended for ignited samples.

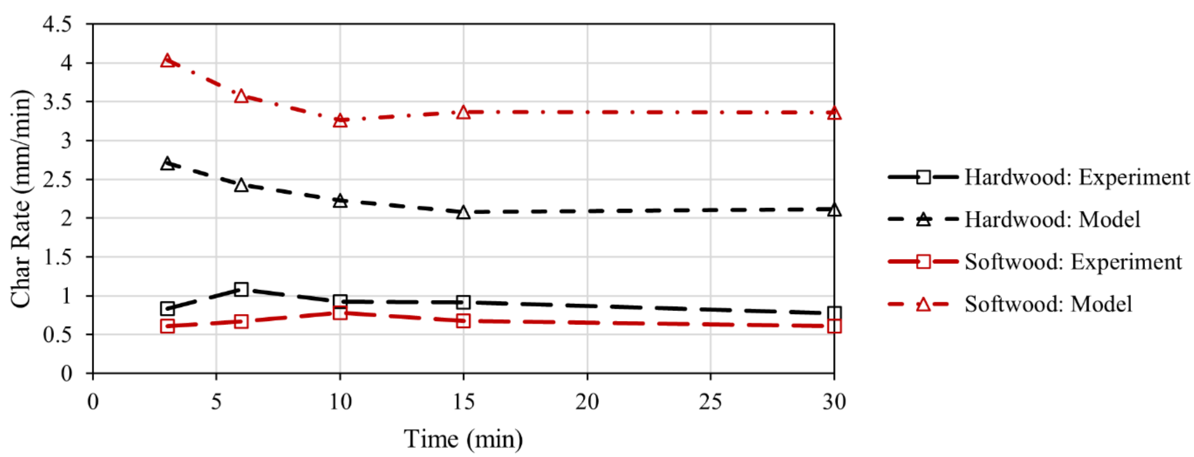

Figure 4.16: Comparison of experiment and model charring rates for 30 kW/m^2 heat intensity.

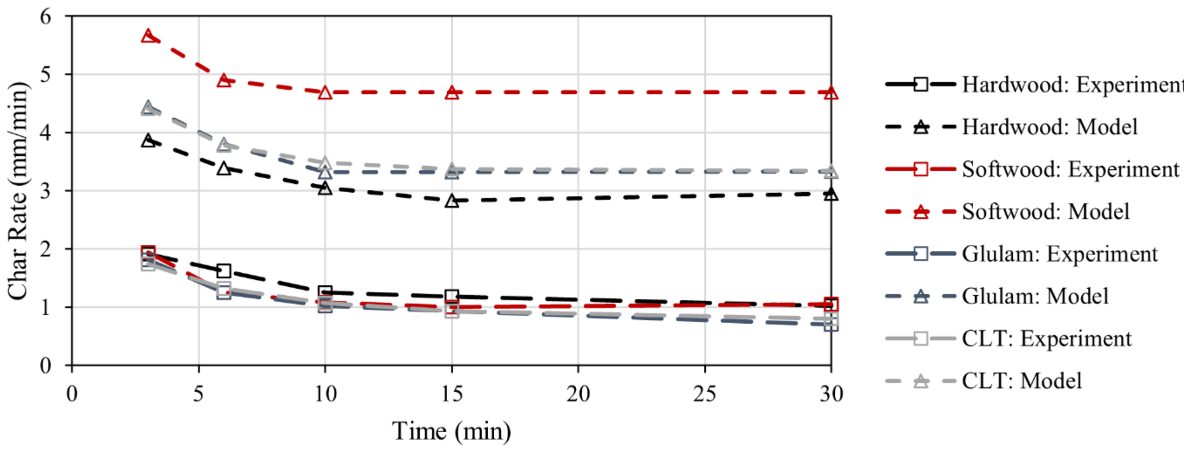

Figure 4.17: Comparison of experiment and model charring rates for 50 kW/m2 heat intensity.

It is important to note that, while the current models show conservative results, this may not always be the case for other specimens and needs further refinement and more careful research attention. Quiquero et al. [108] compared experimental and model results of a timber beam in fire using another finite element analysis software, ABAQUS. Results from this study showed an overestimation of temperatures over time, and therefore char depths, for one furnace experiment, and the opposite (an underestimation) for a second experiment of similar size. Whether this is an artifact of the model or the experiment itself needs further investigation.

4.5 Discussion

The numerical methodology is generally able to accurately predict the trend of charring rates but was overly conservative in magnitude. This indicates that the challenges associated with the modelling methodology derived in Philion et al. [104] are not material specific. Similar discrepancies between experimental and model data were found with the material type being the only variable (heritage hardwood and softwood and engineered wood products: glulam and CLT).

There are several reasons for the differences between the model and experimental results that will need addressing in second stage modelling. A likely explanation is that the material properties are not fully appropriate for the charring process taking place, thus resulting in an overestimation of predictions since the char layers insulation properties are not properly accounted for. The current model is unable to account for changes in the material characteristics as the temperature changes, as would be seen in timber undergoing pyrolysis and changes to char.

Therefore, there is no provision in the model to account for the development of the insulating char layer that would limit heat transfer through the virgin wood and temper such rapid charring. In addition, the formation of the char layer varies. Since this variability is not easily quantifiable as input into a numerical model, while it is recognized as being important, it is not being considered at the present time.

The approach in the methodology herein used the Eurocode 5 values [107] which should have accounted for moisture and char formation through the input of specific heat capacity, thermal conductivity and density with respect to temperature values. However, several issues arise with this approach. The first is that these values were prescribed for standard fire exposure as opposed to the non-standard time-temperature exposure used in the current study. Furthermore, the Eurocode 5 properties were developed for softwood (note the engineered timber samples are sourced from softwood species). Because no hardwood data was available, the Eurocode 5 values were used for all the simulations, including the hardwood heritage model. This may explain why the heritage softwood had higher charring rates than the heritage hardwood in the modelling data, whereas the opposite was found in the experiments. By using the same specific heat and thermal conductivity values, the differences between the heritage hardwood and heritage softwood models were the inputs for density and latent heat.

In addition, the specific heat capacity curve has a peak to account for moisture evaporation in which two temperatures have multiple associated specific heat capacity values. One limitation of the software, and other popular finite element programs according to Werther et al. [106] is the requirement to have a single Y ordinate per X value; therefore, the Latent Heat method was implemented [106]. The peak for moisture evaporation from the specific heat capacity curve was removed and replaced with a calculation related to energy absorption based on the latent heat of evaporation for water. In doing so, the intent of the specific heat capacity curve as included in Eurocode 5 [107] was changed and may be less representative of the material. One possible method for correcting this would be to adjust the specific heat capacity curve to the density value. Not only would this be difficult with the requirement for constant density with the current model, but preliminary results indicated even more conservative charring rates. This, as well as the other factors influencing the accuracy of the model, will form the subject of future research.

While an alternative approach was used for the moisture consideration, no alternative approaches were found to implement the temperature dependent density relationship prescribed in Eurocode 5. Another limitation of the software used in the study is the inability to vary density with temperature. This means that this consideration was not used and instead, the bulk density was used for the duration of the simulation.

To examine the impact of variable density on simulated results, a sensitivity analysis was conducted. For the heritage samples, a comparison of bulk to dry density was conducted. Using the measured average bulk density for the hardwood specimens, the charring rate for the 3-minute, 30 kW/m2 simulated exposure was 2.70 mm/min. Using the average dry density, a lower density value, the charring rate for the same simulation increased to 2.92 mm/min. Therefore, density and the charring rate are inversely proportional; as the density decreased, the charring rates increased. Since the softwood had a smaller density compared to the hardwood samples, this could explain the higher softwood charring rate seen only in the model.

For the engineered timber samples, the average bulk density, dry density, density at 800 °C (calculated from Eurocode 5 [107] as a low density), and double the bulk density were compared. Figure 4.18 shows the variability of the temperature with node location for various densities at the end of a 3-minute CLT simulation. Similarly, increased density results in lower and slower heat transfer. However, the bulk density is the maximum density at the start of the fire tests, with density decreasing eventually to zero once temperatures reach 1200 °C. Therefore, while the higher, doubled bulk density provides closer charring rates to the experimental values (2.5 versus 1.7 mm/min calculated by dividing the node depth by 3 minutes), this is unrealistic. Instead, the charring rates predicted in Section 4.4 would be even higher if the Eurocode 5 method was followed.

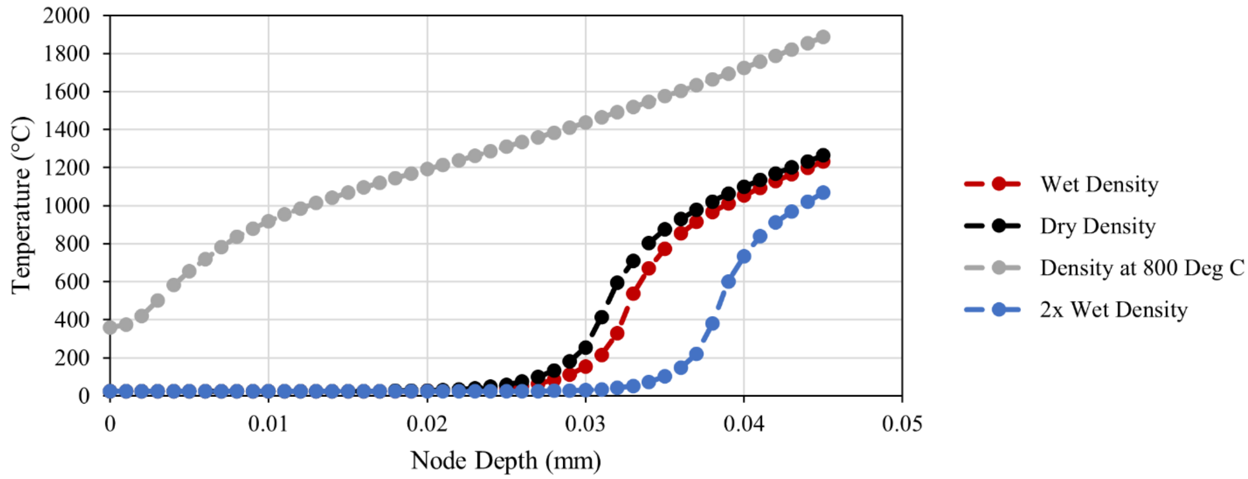

Figure 4.18: Temperature versus node depth at the end a 3-minute CLT simulation with varied density.

Results from the models and the density sensitivity analysis indicates the need for future research into alternative methods to consider char formation as it is a significant factor in heat transfer analysis. While studies in the literature review showed adequate correlation between experimental and numerical results, it is evident that the prescribed properties in Eurocode 5 are inappropriate to use in this scenario given the software's limitations. Based on the literature review, the most common option is to write pyrolysis in a subroutine and introduce them into the software. To the author's knowledge, this is not a built-in feature in various finite element softwares. Another option to be explored is the possibility of moving boundary conditions and adding char elements and removing timber elements throughout the simulation. Furthermore, studies should be conducted to explore the impact of increasing the scale of the specimens. Previous verification studies using similar methodology found good correlation for larger scale heritage and glulam members [104]. Finally, varying the type of heat exposure and intensity, for example a lower heat flux for engineered timber (to assess if the same charring rate pattern continues) or convective and radiative heat boundary condition, should be explored. These additional exploratory studies can assist in determining the current model's limitations as well as highlight the reasons behind the over conservative predictions. Overall, while models may never be able to reflect all the nuances of the pyrolysis of heritage timber, the aim is to develop a model that can be used to predict conservative char rates within a reasonable error margin. This can then be applied to risk-based methods for design and analysis in industry use.

4.6 Conclusions

In this study, heritage hardwood and softwood, and engineered glulam and CLT specimens were tested using a cone calorimeter. The heating flux intensity was 30 or 50 kW/m^2 and the duration varied between 3 and 30 minutes. This allowed for the charring rate and char formation to be tracked over time in a controlled environment. From there, numerical models were developed to replicate the experiments to determine the accuracy of current practices, and highlight future research needs to accurately predict charring rates. Based on the results several conclusions can be drawn including:

- The current modelling methodology overestimates charring rates for heritage sawn lumber as well as engineered timber products;
- Default Eurocode 5 methodology to vary specific heat capacity, thermal conductivity, and density cannot be fully implemented into LS-DYNA simulations;
- Alternative moisture content methodology was implemented which used the Latent Heat method by Werther et al. [107]; and,
- Additional considerations must be made to consider the formation of the char layer including writing external subroutines to represent pyrolysis or defining moving boundary conditions while adding and removing elements during a simulation.

Overall, this chapter provides preliminary results for a finite element heat transfer model for timber exposed to high temperatures. Further developments in modelling to gain a more accurate prediction of charring rates by better accounting for the char layer's insulating properties can result in a design and analysis tool for industry use to assist in mass timber construction.

Chapter 5: Exploratory Modelling Analyses of Thermal Material Parameters

5.1 Introduction

As a continuation of the previous chapter, Chapter 5 focuses on further developing modelling methodology for timber with the aim of increasing accuracy. As discussed in Chapters 2 and 4, the use of timber in the current industry is increasing. Major engineering companies as well as governments have committed to reducing carbon emissions and increasing sustainable practices [6], and have pivoted towards timber construction to do so. Timber's benefits include it being a renewable resource and can sequester carbon if sustainably harvested. Additionally, Canada has the added incentive to research and build with timber due to its abundance. This interest has been seen through projects such as the Canadian government led Next-Generation Wood Construction project in which personnel are being trained on building with timber and research is being conducted with guidance from industry partners. Additionally, at the time of writing, as per the Government of Canada interactive website, Canada has a total of 779 mass timber projects completed or under construction and 19 manufacturing facilities [122].

However, while there is interest in mass timber construction, it is important to highlight that timber requires more research into its behaviour in fire. Knowledge gaps means that within codes such as the Canadian Wood Design Manual [36], conservative estimates are often required regarding charring rates, and residual strength. Further research will aid in code development with complex designs often requiring alternative solutions rather than following the prescriptive codes. Once again, modelling can be used as a design tool for timber, especially given the knowledge gaps. A reliable model allows designers to conduct parametric studies since testing is expensive and not always possible given available resources (challenges with suitable lab access or access to materials for example).

Previous work conducted by the author shown in Chapter 4 used a previously developed modelling methodology to assess its applicability for small-scale cone calorimeter tests. Results were overly conservative, therefore, in this chapter, the results from the experiments and models from Chapter 4 will be compared to five new methodologies attempted herein. All new methodologies are exploratory and will alter the thermal material properties used, or the way in which they are applied. This is to gain a better understanding of which parameters are necessary for timber finite element heat transfer modelling, and their level of impact on result accuracy. This chapter aims to provide further guidance on necessary testing and model development for future works by determining the impact of thermal material properties.

5.2 Thermal Material Properties

In Chapter 4, a modelling methodology a previously developed in [104] was applied by the author to small-scale cone calorimeter tests of heritage hardwood and softwood and engineered timber glulam and CLT. The author completed majority of the engineered timber tests, built all models and validated the results. The methodology had been previously verified against larger scale specimens using a different heat exposure type. Therefore, the objective was to gain a better understanding of important parameters for a timber finite element heat transfer model by using a smaller scale sample and simplifying the type of heat exposure. Chapter 4 found that the model was able to accurately predict the trends of the charring rates for both the heritage and engineered timber products when exposed to a 50 kW/m^2 heat flux, however, magnitudes were approximately double or triple the experimental data.

Several reasons for this difference in magnitude were identified. For example, the previous chapter used the Eurocode 5 method, which considers moisture evaporation and the effects of charring within the density, thermal conductivity, and specific heat capacity curves [107]. Due to limitations in the software used, the density had to remain constant throughout the simulation and the peak in the specific heat capacity curve was removed and replaced with the Latent Heat method by Werther et al. [106]. This means that the parameters used within the previous chapter were modified and may not have been truly representative of timber behaviour. Therefore, given the limitations of the previous methodology the chapter herein will explore five additional methodologies, modifying both the approach in which thermal material properties are inputted, and the values themselves. This can improve understanding of how these parameters impact accuracy as well as determine best practices for designers and recommendations for future research.

For the chapter herein, values by Eurocode 5 [107], König and Walleij [123] and Fredlund [124] will be used. Starting with König and Walleij, the thermal material properties (specific heat capacity, density, and thermal conductivity) were calibrated through testing of timber members exposed to one-dimensional standard fire tests. While the parameters are based on standard fire tests, they did show good results for another study which validated their model against small scale

50 kW/m^2 heat flux cone calorimeter timber samples [125]. Therefore, its applicability for the study herein will be explored.

Figure 5.2 illustrates the differences between the specific heat capacity curves that will be used herein. In the previous study, the Latent Heat method [106] using the Eurocode 5 [107] specific heat capacity values were used to account for the software's inability to input more than one specific heat capacity value per temperature. Therefore, the only difference between the two specific heat capacity curves is that the Latent Heat method removes the two peak points accounting for moisture evaporation. The König and Walleij [123] values differ from the other two, with an overall lower specific heat capacity, but includes the a similar peak for moisture considerations.

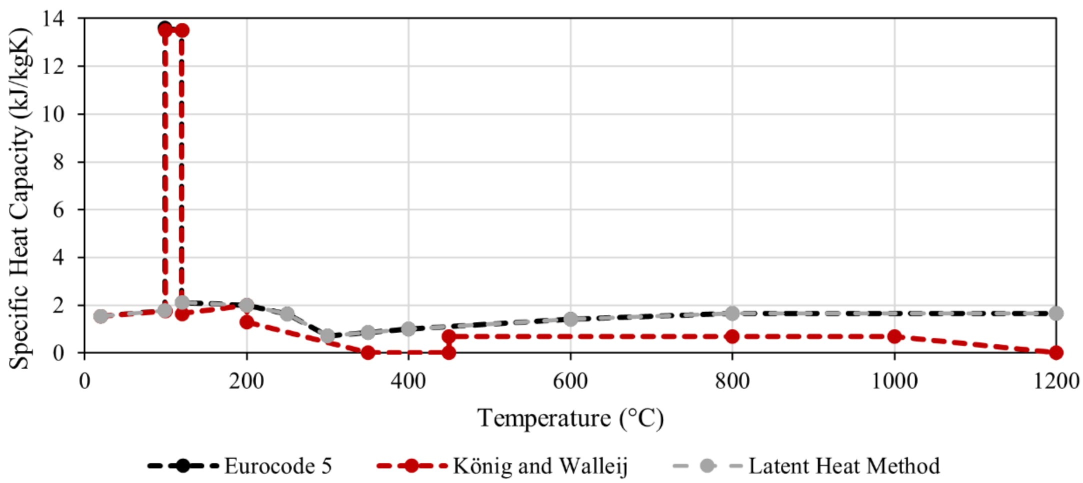

Figure 5.1: Comparison of the specific heat capacity over temperature curves for Eurocode 5 [107] and König and Walleij [123].

The variation in density over time to be used in this chapter are shown in Figure 5.2 (Eurocode 5 and König and Walleij properties). As an example, a dry density of 425 g and a moisture content of 12% was used. Note that in the simulations (discussed in later sections), the density curves inputted will be adjusted to fit the moisture content and dry density of the experimental data collected for each heat duration. The values are similar at the lower temperatures, however, the Eurocode 5 [107] values have a decrease in temperature much sooner and more rapidly compared to the König and Walleij [123] densities. Therefore, Eurocode 5 has higher specific heat capacity values requiring more energy to increase the timber temperature, but overall lower density values allowing faster heat transfer through the material.

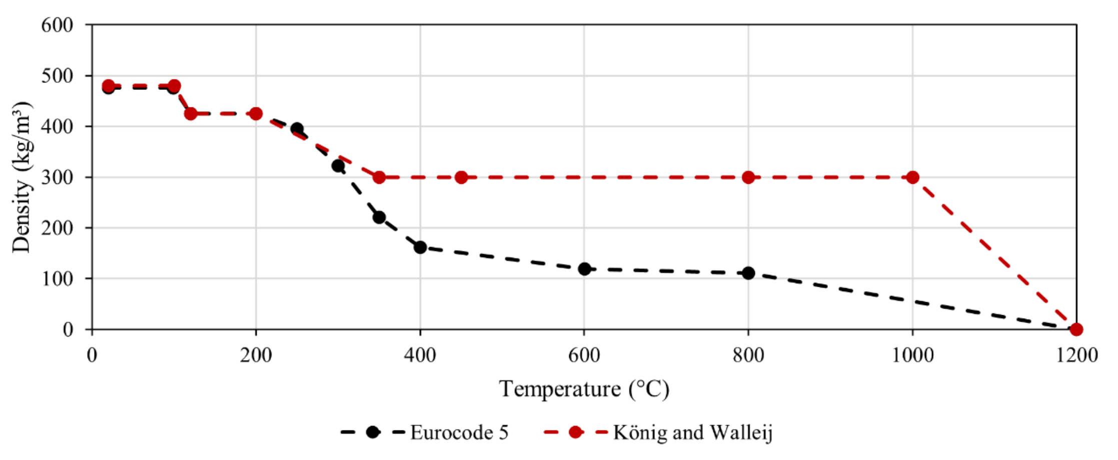

Figure 5.2: Comparison of density over temperature curves for Eurocode 5 [107] and König and Walleij [123] assuming a dry density of 425 kg/m³ and a moisture content of 12%.

Both Eurocode 5 and König and Walleij use the same thermal conductivity values. Therefore, to vary the last thermal material property, a study by Fredlund [124] was referenced. Based on the available and accessible data seen in literature, the Fredlund values were on the lower bound of thermal conductivity values [123], [126] which was believed to give a good comparison on the impact of various parameters. Fredlund developed thermal material properties based on literature and experiments with the thermal conductivity over temperature plot seen in Figure 5.3. The values are compared to Eurocode 5 [107] and König and Walleij [123]. Fredlund did have separate thermal conductivity curves for wood and char, therefore, a combined curve with the values for wood's thermal conductivity were used from 0 to 299 °C and the values for char used at 300 °C and above. This threshold is per accepted literature [42] and the combined curve was also seen in literature through studies [123], [126]. The Fredlund values are similar until approximately 500 °C where the Eurocode 5 and König and Walleij values increase at a more rapid rate. Note that the Fredlund values used herein differ slightly from the original study since the values were taken from the provided figure.

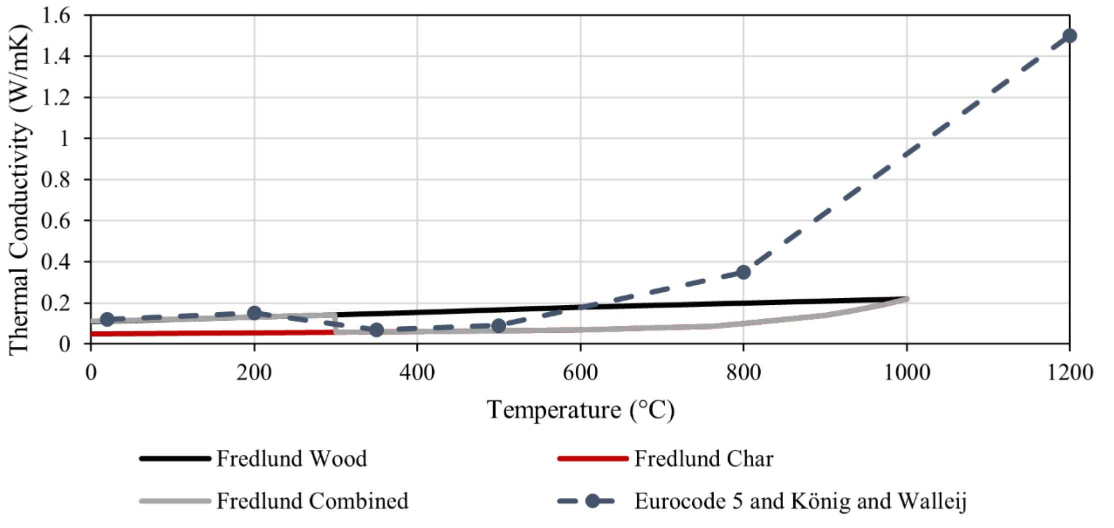

Figure 5.3: Comparison of thermal conductivity over temperature curves for Eurocode 5 [107], König and Walleij [123] and Fredlund [124].

The addition of a char layer through subroutines or adding and removing elements with a moving boundary condition was not within the scope for this chapter. In addition, given the results of the default methodology in Chapter 4, it was decided that varying scale or boundary conditions was premature at this stage. Instead, considering the aim of the thesis, the objective was to adjust methods to implement current parameters to understand their impact on model accuracy. This advances model development for use in risk analysis and risk-based design for alternative solutions.

5.3 Methodology

All modelling will be conducted using LS-DYNA as the processor with Oasys' Primer, D3PLOT and T/HIS [46] as the pre and post processors. This was to stay consistent with the previous chapter as well as to further develop the previous methodology.

5.3.1 Summary of Experiments

A full description of the experiments can be found in Chapter 4; however, a summarized version of the engineered timber tests will be discussed here. Using a cone calorimeter and following the ASTM E1354 procedure [116], 15 glulam and 15 CLT samples were tested at 50 kW/m^2 heat flux exposure. The procedure largely followed ASTM E1354 however no external spark was used to more accurately represent real fire conditions. Furthermore, a 50 kW/m^2 heat flux exposure was chosen because it was likely to cause self-ignition rendering the external spark unnecessary.

The size of the samples (100 x 100 x 45 mm) was determined by the cone calorimeter. Prior to testing, each sample was weighed, measured and the moisture content recorded. The temperature and relative humidity of the room was also measured. These values were used as input data for the model. Three samples of each material type were tested at 3, 6, 10, 15 and 30 minutes and the char layer measured and averaged to track its formation over time. The char depth results were then used as model validation data.

5.3.2 Modelling Scenarios

All models will replicate the tests however; the thermal material properties will vary. The modelling scenarios conducted in this chapter are summarized in Table 5.1. A total of six different parametric studies were conducted for the glulam and CLT samples each.

Table 5.1: Summary of the simulations conducted.

Simulation ID*	Specific Heat and Density	Latent Heat Method Used	Constant Density Used	Thermal Conductivity
1	Eurocode 5 [107]	✓	✓	Eurocode 5 [107]
2	Eurocode 5 [107]	-	✓	Eurocode 5 [107]
3	Eurocode 5 [107]	-	-	Eurocode 5 [107]
4	König and Walleij [123]	-	✓	König and Walleij [123]
5	König and Walleij [123]	-	-	König and Walleij [123]
6	Eurocode 5 [107]	-	✓	Fredlund [124]

* The simulations will have the name of 1 through 6 with G added for glulam and C added for CLT.

The first simulation is the original method used in the referenced methodology [104] and conducted in Chapter 4 in which Eurocode 5 [107] properties are used. Software limitations largely governed the modifications to the original Eurocode 5 values including the specific heat capacity and density curves. The Latent Heat method [106] was used because the software can only input a single y-coordinate for every x-coordinate. Therefore, the peak in the specific heat capacity curve was removed (as seen in Figure 5.1) and replaced with the phase change temperature of water (100 °C) and latent heat of evaporation for wood (calculated by multiplying the moisture content to the latent heat of evaporation of water). In terms of density, while Eurocode 5 prescribes a density over time curve (see Figure 5.2), this methodology maintains a constant bulk density due to software limitations. Finally, Eurocode 5 thermal conductivity properties were used.

The second and fourth simulations change only the specific heat capacity curve from simulation one while using Eurocode 5 [107] König and Walleij [123] properties respectively. In these simulations, the software's limitation of inputting a single y-coordinate per temperature value was circumvented to allow the input of a more accurate specific heat capacity curve which includes the moisture evaporation peak; therefore, the Latent Heat method is no longer required. The specific heat capacity curve was modified, assigning the second specific heat capacity value to a temperature value of one degree higher than specified. For example, Eurocode 5 has a specific heat capacity of both 1.77 and 13.6 kJ/kgK at 99 °C. In the model, the coordinates inputted were 1.77 kJ/kgK at 99 °C and 13.6 kJ/kgK at 100 °C. This method was found in a study by Chen et al. since this limitation is not software specific [127]. Finally, the simulation maintained the use of the constant bulk density.

The third and fifth simulations build from the second and fourth scenarios in which variable density is now introduced. The same methodology of modifying the temperature values of the specific heat capacity curve was used for this simulation as well. However, the density value cannot be modified throughout a simulation. Therefore, an alternative method was developed by a colleague and applied and analyzed by the author herein. A sample calculation can be seen below assuming Eurocode 5 values at 20 °C, a bulk density of 481.06 g, a moisture content of 13.37% and a factor of 10 (Equations 5.1 and 5.2). A corresponding specific heat capacity curve in

Table 5.2 can also be seen. As seen in Equation 2.9, the density value is multiplied by the specific heat capacity when calculating heat transfer. Therefore, because the specific heat capacity value can be variable throughout the simulation, the ratio of dry density to density was multiplied by the specific heat capacity curve and divided by additional factor of 10. The additional factor was also multiplied by the dry density and inputted as a constant. Essentially, the variability of the density curve was incorporated into the specific heat capacity curve.

$$Density_{Input} = \frac{Density_{Bulk}}{1 + \frac{MC}{100}} * Factor \tag{5.1}$$

$$= \frac{481.06\ g}{1 + \frac{13.37}{100}} * 10$$

$$= 4243.274\ g$$

$$C_{input} = \frac{\rho}{\rho_{dry}} * \frac{C}{Factor} \tag{5.2}$$

$$= \left(1 + \frac{MC}{100}\right) * \frac{\left(\frac{1.53}{1000}\right)}{10}$$

$$= \left(1 + \frac{13.37}{100}\right) * \frac{\left(\frac{1.53}{1000}\right)}{10}$$

$$= 173.46 \frac{J}{m^3 K}$$

Table 5.2: Example of model input specific heat capacity curve after density modification.

Temperature (°C)	Ratio of Density to Dry Density	Specific Heat Capacity (kJ/kgK)	Model Input Specific Heat Capacity (J/m^{3}K)
20	1.1337	1.53	173.4561
99	1.1337	1.77	200.6649
100	1.1337	13.6	1541.8320
120	1	13.5	1350.0000
121	1	2.12	212.0000
200	1	2	200.0000
250	0.93	1.62	150.6600
300	0.76	0.71	53.9600
350	0.52	0.85	44.2000
400	0.38	1	38.0000
600	0.28	1.4	39.2000
800	0.26	1.65	42.9000
1200	0	1.65	0.0000

Finally, the sixth simulation varies the final thermal property thermal conductivity. The simulation is the same as simulation two, where Eurocode 5 [107] values are used for specific heat capacity and a constant bulk density is used, however, the Fredlund thermal conductivity combined curve shown in Figure 5.3 was used instead of Eurocode 5 prescribed values. This allowed direct comparison of simulations two and six, changing only the thermal conductivity while the other parameters remain the same.

5.3.3 Model Parameters

Using Primer, the glulam and CLT samples were represented by solid elements with a 1 mm by 1 mm mesh to maintain consistent with the research in Chapter 4. The simulation was a one-dimensional heat transfer of a 100 by 45 mm rectangle to represent a cross-section of the experiment specimens. Material parameters such as density, specific heat capacity, thermal conductivity, phase change temperature or latent heat of evaporation were inputted using the various approaches discussed in Section 5.3.2.

Once the mesh and material properties were assigned, boundary conditions were inputted. The initial temperature was set to the average ambient temperature of the three experiments, ranging from 22 to 25 °C. Boundary conditions replicating the experimental study included a constant heat flux exposure of 50 kW/m^2 on the exposed surface and a heat flux exposure of 0 kW/m^2 on the insulated face.

Initially when conducting these simulations, they would break using the original convergence parameters in Chapter 4. These included a convergence tolerance of 1E-6, a maximum temperature difference of 50 K, and a maximum and minimum timestep of 30 and 1E-6 s respectively. The author attempted to manipulate these individually and in various combinations to allow the simulations to converge. The most successful method was to increase the convergence tolerance to one. This means that the solution will be less accurate as the values from one iteration on the same timestep to another only has to have the same value to the accuracy of one digit. The software was less sensitive to manipulation maximum temperature difference and timesteps and these values needed to change drastically in order to make an impact. Once the values were changed significantly, it began to immediately impact the results, getting very high or very low unrealistic temperature values. Note that some models still did not converge and therefore, the data was omitted from the following section.

5.4 Results

The results for the comparison of the simulations to the experimental values can be seen in Figure 5.4 and Figure 5.5. Complete datasets were gathered for simulations 1G, 2G, 6G, 1C, 2C and 6C. Simulations 3 and 5 G and C which included the variable density method did not converge, often having thermal changes between the minimum timestep larger than the allowable. When the maximum temperature change and minimum timestep was changed, the results were no longer viable. Simulation 4 G and C used the König and Walleij [123] thermal material properties and a constant density. Conclusions from the simulations using König and Walleij [123] with the model herein is that is not appropriate. Additionally, while varying the density of the timber material throughout the simulation is more scientifically accurate, it also has additional challenges with the current model. With this method, different factors (from Equation 5.1 and 5.2) were also attempted, however this did not appear to impact convergence to a significant level.

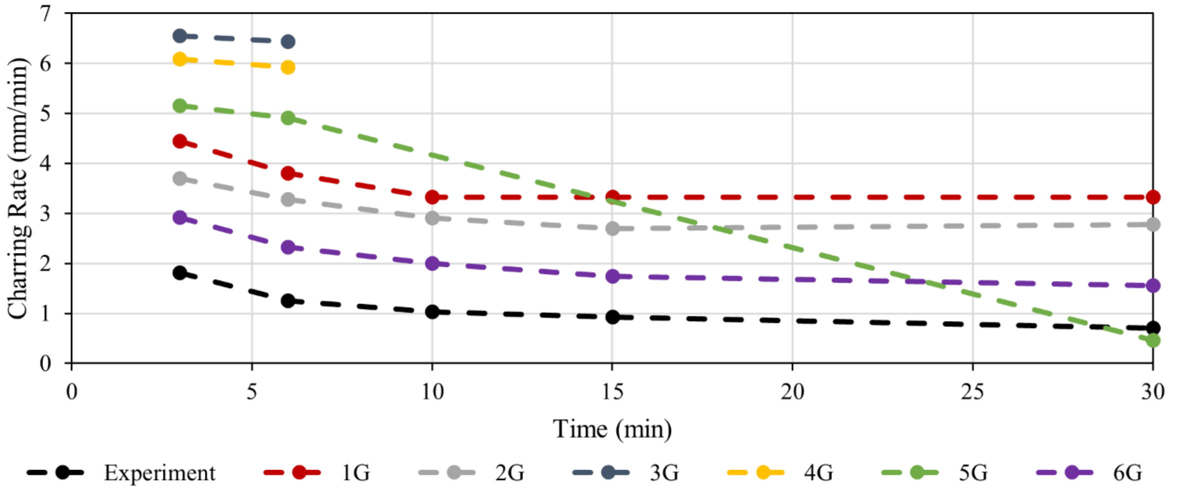

Figure 5.4: Comparison of charring rates from glulam experiments and simulations.

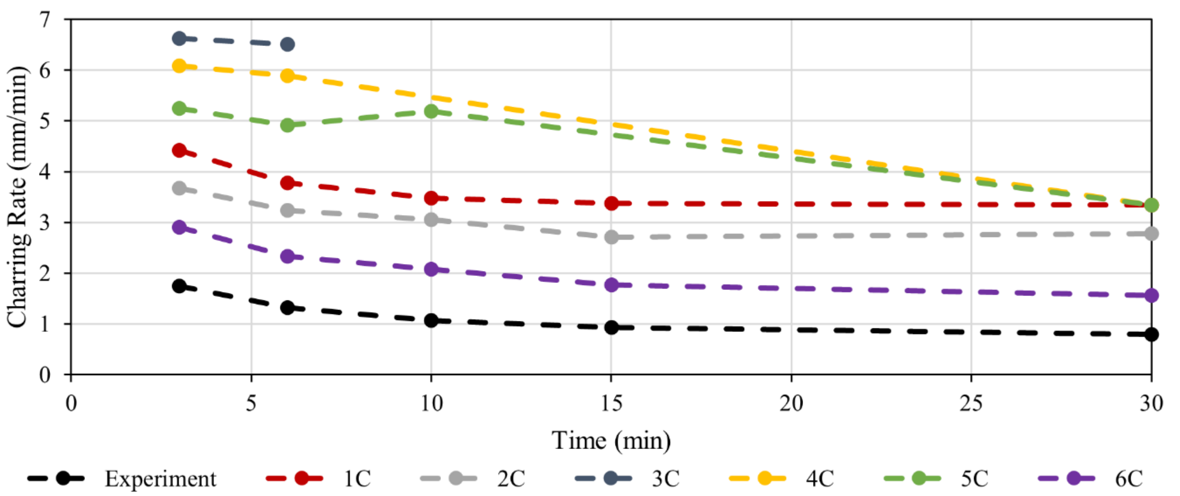

Figure 5.5: Comparison of charring rates from CLT experiments and simulations.

Simulations 2 and 6 G and C converged with an increased tolerance of 1 and all other convergence parameters the same as simulation 1 (previous default model in Chapter 4). Table 5.3 shows the difference between simulation and experimental results through an average factor. Simulation 2 maintained a constant density, but the specific heat capacity curve was truer to code, including the moisture consideration peak instead of using the Latent Heat method [106]. While the reliability of the results is lower, the results were closer to the experimental values compared to the default with values differing by a factor of 2.87 and 2.75 versus 3.41 and 3.28. Similarly, Simulations 6 G and C had lower reliability but showed the closest comparison to the experimental data that was on average under double the experimental charring rates. This scenario was the same as Simulation 2 G and C but used the lower thermal conductivity values determined by Fredlund [124].

Table 5.3: Average factor between experimental and numerical results.

Simulation	Material	
	Glulam	CLT
1	3.41	3.28
2	2.87	2.75
6	1.90	1.84

Additional visualizations can be seen in Figure 5.6 which shows the temperature over time at specific node locations for a 3-minute simulation of 1C and 6C. Temperatures do reach higher maximums in 6C compared to 1C for the nodes closer to the exposed face (0.045 to 0.04 m), however, simulation 6C does have slower thermal conduction between nodes as seen through the much slower charring rate (indicated by the time at which node reaches 300 °C).

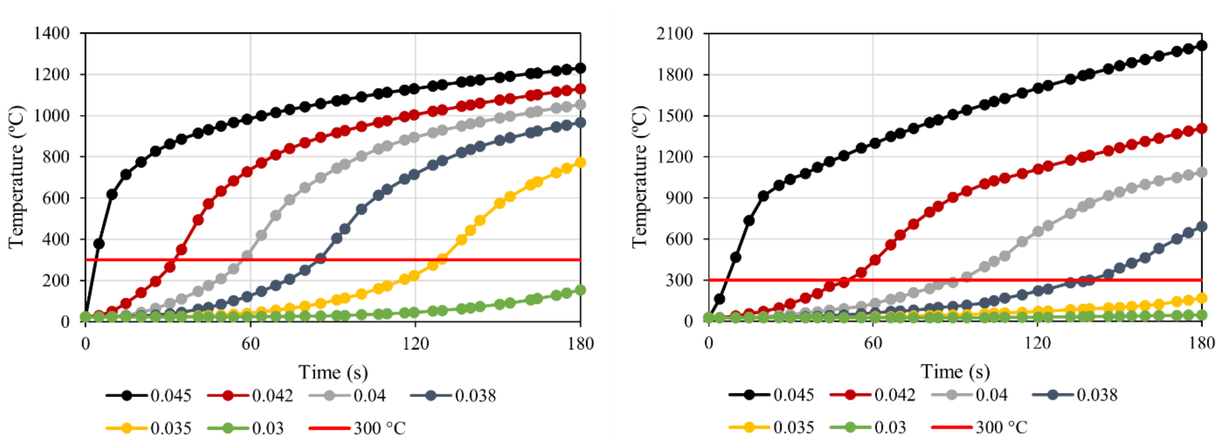

Figure 5.6: Temperature over time at various nodes for a 3-minute CLT test using Simulation 1C (left) and 6C (right).

Overall, Simulations 1, 2, and 6 for the glulam and CLT samples followed the correct trends despite the variable properties. The most accurate results found were Simulation 6 where a more accurate specific heat capacity curve, constant bulk density, and lower thermal conductivity were used. However, this had a lower reliability compared to the default methodology used in Simulation 1 and Chapter 4.

5.5 Discussion

When comparing the thermal material properties for Eurocode 5 [107] to König and Walleij [123], Eurocode 5 prescribes a higher overall specific heat capacity but lower density. For this modelling methodology with the given software, it appears that the Eurocode 5 values have found a more accurate balance between the two. Additionally, its ability to converge more easily compared to König and Walleij also makes it more useful. The Fredlund thermal conductivity values [124] however, resulted in more accurate charring rate predictions while still maintaining the correct trend patterns.

Some factors to consider from observations of the results herein include the importance of cone calorimeter specific thermal material properties for timber and the ability of the model to converge. While the author was unable to find cone calorimeter specific thermal material parameters, this is something to consider. From the experiments, the heat release rate and mass loss rate are measured. Volume loss can be estimated using the char depth measurements through the various experiments. In the future, measuring surface temperatures of the specimens may also be useful to attempt to calculate proper specific heat capacity, thermal conductivity and density curves. Given the available data, this study did provide information on the impact of the various thermal material properties. One key finding was that implementing the correct specific heat capacity curve from Eurocode 5 [107] and the thermal conductivity properties of Fredlund [124] did result in simulated charring rates closer to experiments at the expense of modelling reliability convergence.

Overall, the results do indicate that it may be possible to continue to refine accuracy through the modification of existing thermal material properties. Future work should continue to explore convergence parameters to ensure a higher model reliability, as well as developing non-standard fire material properties that would be more appropriate for the scenario herein. Additionally, inputting a char layer with insulating properties through subroutines or moving boundary conditions with elements being added and removed was outside of the scope of the chapter herein. However, this should be explored in future studies as well to provide an alternative or improved methodology.

5.6 Conclusions

This study continued to explore the thermal material properties of timber in finite element heat transfer models with the objective of identifying important parameters and quantifying their impact on simulated predictions of charring rates. With Chapter 4 being used as the basis for this chapter, thermal material properties and methodologies for inputting them were modified individually; this was based on identified challenges and software limitations.

A total of six simulations were conducted for CLT and glulam each, the first being the default methodology referenced in Chapter 4. From there, Simulation 2 went on to modify first the specific heat capacity curve (to include the moisture evaporation peak) and Simulation 3, based on Simulation 2 but further adjusting the methodology to allow for variable density. Simulations 4 and 5 were similar to 2 and 3, only parameters from a different study by König and Walleij [123]. Because Simulations 1 through 5 used the same thermal conductivity values, an additional study by Fredlund [124] was referenced to examine the impact of this final thermal material property.

Key findings include that the model failed to converge using the original parameters in Simulation 1. For simulations 2 and 6, full datasets were gathered by changing the convergence tolerance to 1 rather than 1E-6, meaning that the results are less reliable. Simulations 3 to 5 broke despite the increased tolerance and further changes to other convergence parameters (timestep range and maximum temperature change per timestep) resulted in unrealistic results. Increased accuracy was found by implementing a slightly modified specific heat capacity curve compared to using the Latent Heat method [106], however again, this is at the expense of the convergence tolerance. When comparing the available data for Eurocode 5 to König and Walleij, the Eurocode 5 values could converge more easily and had more appropriate input parameters based on simulated charring rate results. Furthermore, modifying the specific heat capacity curve based on the ratio of density to dry density (Simulations 3 and 5) would not converge. The most accurate model was Simulation 6 in which the specific heat capacity modification in Simulation 2 was paired with a lower thermal conductivity curve in a different study.

Therefore, recommendations include further work on developing cone calorimeter or constant heat exposure thermal material properties for timber. Cone data does collect some relevant information such as heat release rate and mass loss rate that may be useful for this. However, it is important to recognize that the parameters found for this chapter were largely based on standard fire exposure. Additionally, as discussed in Chapter 4, while varying thermal material properties does seem to be a possible solution for more accurate simulated charring rates, alternative options for considering adding a char layer should still be researched.

Overall, the aim of this study was to explore various parameters in the model to examine their impact on accuracy and provide a guideline for future work. Numerical modelling tools are important in the context of alternative solutions since they can provide the basis for informed decision making through processes such as risk-based analysis. Timber is a complex material with several research gaps still to be addressed. Experimental data is necessary to continue to inform modelling methodologies to develop the industry and allow for safe and sustainable mass timber construction.

Chapter 6: Conclusions and Recommendations

6.1 Summary

From building fires to wildfires, fire poses hazards requiring Fire Safety Engineering. Society has pushed structural engineering to new innovative, sustainable designs, using materials in new configurations and purposes. This has resulted in more alternative solution designs rather than relying on prescriptive designs, focusing more on fire resilience versus resistance. It was determined that steel and timber both have the basis for designing with alternative solutions. However, a review of current guidance within building codes highlighted a need for more tools and development to increase use and confidence of alternative solution designs. One method to so is through numerical modelling. Development of validated modelling methodology allows for designers to predict how structural systems will behave under various fire scenarios. This can inform the performance of a structure structurally given heat transfer information is known. The predictive scenarios can be placed within a risk-based analysis to determine the optimal solution. Also, the optimal solution can be compared to the prescriptive solution to ensure it meets code compliance. However, the development of these reliable modelling tools is hindered by specific research gaps for steel scenarios and broader research gaps for timber topics. Therefore, the objectives of this thesis were to increase knowledge of steel and timber fire resilience when exposed to non-standard fire exposure with data and information being used to develop and validate modelling tools for the promotion of using alternative solutions in design applications. The aim is to determine best practices for modelling and identify key parameters for modelling each material.

Chapter 2 provides a review of topics and concepts required to understand the thesis. This included a description of prescriptive design and alternative solutions, with overall highlights pointing mainly to achieving fire resistance versus fire resilience. From there, heat transfer was reviewed highlighting the need for fuel, heat, and oxygen for a fire with heat transfer mechanisms being conduction, convection, and radiation. In terms of material behaviour, steel in fire loses strength around 800 °C and experiences thermal expansion and contraction. Timber in fire undergoes pyrolysis, forming a char layer with no structural strength but has some insulating properties. It also experiences moisture evaporation which impacts heat transfer as water within the timber cells evaporates at increased temperatures. Finally, the finite element method which is used in the thesis herein was reviewed starting from the user inputs in the pre-processor, then to the method in which the solver produces results, and last to organizing the data in the post-processor.

Chapter 3 provides experimental testing and numerical modelling of steel trusses for stadium roof applications but can be extrapolated for other truss roof systems. The study was based off a case study in which uncertainty of steel truss roof systems exposed to a localized fire resulted in nearly an hour-long pre-evacuation time and financial losses for a nearby stadium. Investigation into international fire codes shows little to no guidance, often citing the designer should make an engineering decision on if fire protection is necessary. Therefore, if fire protection is deemed necessary, then it must be an alternative solution design. Methanol pool fire tests were conducted on unloaded small-scale steel trusses of similar chemical composition to the case study. Instrumentation included thermocouples to track the steel temperature over time and narrow spectrum illumination used to capture clear images for digital image correlation to record thermal strain over time. Both heat transfer and deformation analyses were completed and validated. Six temperature locations were reviewed with an overestimation of heat transfer in the horizontal direction but an underestimation of heat transfer in the vertical direction. For the thermal deformation model, results showed good correlation between experimental and modelling results. Recommendations for methodologies were noted as well as experimental and software limitations.

Chapter 4 then pivoted to the heat transfer modelling of sawn lumber from hardwood and softwood heritage structures and engineered glulam and CLT specimens. The push for mass timber construction requires better understanding of pyrolysis and moisture considerations. Similar to steel, experimental data was generated for model input and validation. A cone calorimeter was used to provide a controlled environment and constant heat exposure of either 30 or 50 kW/m^2 for the sawn lumber samples, and 50 kW/m^2 for the engineered timber samples. To track the development of the char layer over time, the specimens were tested at 3, 6, 10, 15, and 30 minutes with the sawn lumber tested twice at each heat flux intensity and duration, and the engineered timber samples tested thrice per duration. The dimensions, moisture content and weight were measured prior to testing for model input data and char depth and rates were measured and averaged post test for model validation. The model followed a methodology from an apriori study in which char and moisture considerations were implicitly considered through the Eurocode 5 thermal conductivity, specific heat capacity and density parameters. Software limitations meant that an alternative approach called the Latent Heat method for moisture evaporation was used, however, no alternative was found for variable density, meaning a constant bulk density was used. Results showed overly conservative charring rate estimations compared to the experimental data, though overall trends were followed.

Because of the discrepancies between model and experimental results, Chapter 5 completed exploratory analyses of the thermal material parameters used in the previous chapter. One study showed good results for cone calorimeter finite element heat transfer simulations using alternative properties by König and Walleij [123]. Therefore, since the author was unable to find properties specifically for constant heat flux exposure, values from König and Walleij [123] were used. Additionally, the thermal conductivity parameters by Fredlund [124] were also used since the original Eurocode 5 method and the König and Walleij [123] method were the same. A total of six simulation series were conducted for both the glulam and CLT samples from Chapter 4. Each simulation varied slightly whether it be through the parameters used, or the methodology used. For example, one simulation used the Eurocode 5 values but incorporated a variable density through the specific heat capacity curve. Overall results showed that the software had difficulty converging, requiring an increase in convergence tolerance. It also showed the sensitivity of the model to varying parameters with trends once again remining promising and varying amounts of conservatism in the simulations. Chapters 4 and 5 are preliminary models mainly highlighting key parameters for modelling, software limitations, and areas requiring future research.

6.2 Conclusions

The main conclusion from the thesis herein is that alternative solution designs can optimize the amount of materials or fire protection used, decreasing financial and environmental costs. However, this requires a strong basis of material behaviour and tools for predictive analyses. Experimental and numerical modelling studies were conducted for both steel and timber.

Novel conclusions from Chapter 3 include:

- Experimental testing of steel trusses exposed to a localized fire showed a possible chord shielding effect in which the bottom chord redirects heat around parts of the truss, decreasing heat exposure;

- It is important to measure cooling behaviour after testing, something that is not considered when using standard fire exposure;
- Heat and flames in a localized fire are found well beyond the base of the fire requiring the use of tributary area heating boundary conditions;
- DIC and narrow spectrum illumination technologies showed similar coefficient's of thermal expansion when verified against code values. This indicates it is a viable alternative method to using strain gauges;
- Heat transfer models of steel overestimated horizontal heat transfer but underestimated vertical heat transfer;
- It is more appropriate to use the free end model when replicating the experiment since fixing both ends does not allow for thermal expansion, resulting in negative strains; and
- Good correlation for trends and magnitudes was found for the deformation analysis. The percent difference between the model and experimental results at peak thermal strain had a minimum value of 7%.

Novel conclusions from Chapter 4 include:

- The modelling methodology predicts the correct charring rate trends but overestimates them for heritage sawn lumber and engineered timber products (model challenges are not material specific);
- The methodology uses the Eurocode 5 method which implicitly considers charring and moisture evaporation through thermal material properties;
- Software limitations mean that an alternative method called the latent heat method for moisture evaporation was used which allowed for the removal of the peak in the specific heat capacity curve;
- The software also limits the simulation to a constant density value, so the bulk density was used with no alternative method. This showed the closest prediction of charring rates when compared in a density sensitivity analysis;
- It is likely that the method is unable to accurately capture the chemistry and pyrolysis process correctly at this stage for this scenario.

Novel conclusions from Chapter 5 include:

- The model failed to converge for all simulations except for Simulation 1 when using the original convergence criteria;
- Increasing the convergence tolerance from 1E-6 to 1 was the optimal method for encouraging convergence of simulations;
- Increased accuracy in charring rate predictions was found when implementing a truer specific heat capacity curve rather than using the Latent Heat method at the expense of the convergence tolerance;
- The Eurocode 5 values showed better convergence and results compared to the simulations using König and Walleij thermal material parameters; and
- The most accurate model was Simulation 6 which used a constant bulk density, Eurocode 5 specific heat capacity (no latent heat method), and Fredlund thermal conductivity values.

6.3 Research Recommendations

Some research recommendations after completing the steel truss study in Chapter 3 include:

- Attempting to replicate the heat transfer model in a three-dimensional analysis to determine if the model is able to capture more nuance with a more accurate geometry. This would also determine if the software defaults to overestimating horizontal heat transfer and underestimating vertical heat transfer which would be useful for designers;
- Destructive techniques should be completed to determine residual strength and exposure temperature. This should also be done in tandem to heating the system to explore creep effects; and
- Larger-scale tests should be completed with different connection types because behaviours are not always scalable in both experiments and modelling.

Based on Chapter 4, future work should include:

- Conducting more tests on various specimen types, scales and heat exposures to continue to build available charring data for industry use;
- Analysis of thermally tested engineered timber samples including observations into adhesive bleeding, char patterns, and structural testing particularly along glue lines;
- Validating the methodology at a larger scale and for a different heat exposure; and

- Attempting to better represent the impact of char whether that be through writing a subroutine or attempting to have moving boundary conditions elements that activate or deactivate based on a set criteria.

The following research recommendations were gained from Chapter 5:

- Future work should attempt different approaches to encourage convergence of simulations;
- Thermal material parameters should be developed specifically for constant heat flux exposure since using parameters specifically for the standard fire appears to be inappropriate; and
- Alternative methods for implementing the char layer and its properties in this software should still be considered.

6.4 Design Recommendations

From this thesis, several design recommendations or best practices have been identified. From Chapter 3, it is evident that one must consider the true evacuation time (including time of uncertainty) in structural design or there is a credible threat to life safety. Therefore, it is important for structural and human behaviour fields to work in tandem. For timber, while it has many benefits including its sustainable nature, it is important to realize there are major research gaps still. This can be seen through the difficulty in developing a finite element heat transfer model of timber. Therefore, designers must remain conservative in mass timber construction and understand the limitations of what science is currently available. More experimental data is necessary for the development of both modelling tools and alternative solution designs.

Overall, this thesis focused on conducting experiments to gather data for the development of numerical modelling methodologies. Both experimental data and modelling tools can be used to further the progress of alternative solutions, shifting focus to fire resilience rather than fire resistance. This thesis increased knowledge of steel and timber as building materials in fire, providing key conclusions and recommendations for industry and future research work.

References

[1] Statistics Canada, "Table: 35-10-0192-01 - Incident-based fire statistics, by type of fire incident and type of structure."

[2] T. Gernay, "Performance-based design for structures in fire: Advances, challenges, and perspectives," *Fire Saf J*, vol. 142, Jan. 2024, doi: 10.1016/j.firesaf.2023.104036.

[3] A. Alvarez, B. J. Meacham, N. A. Dembsey, and J. R. Thomas, "Twenty years of performance-based fire protection design: Challenges faced and a look ahead," Nov. 2013. doi: 10.1177/1042391513484911.

[4] V. K. R. Kodur, "Guidelines for Fire Resistance Design of High-strength Concrete Columns," *Journal of Fire Protection Engineering*, vol. 15, no. 2, pp. 93–106, May 2005, doi: 10.1177/1042391505047740.

[5] UN Environment Programme, "The Buildings Breakthrough: Global push for near-zero emission and resilient buildings by 2030 unveiled at COP28." Accessed: Sep. 25, 2024. [Online]. Available: https://www.unep.org/news-and-stories/press-release/buildings-breakthrough-global-push-near-zero-emission-and-resilient#:~:text=The%20new%20initiative%20aims%20to,in%20all%20regions%20by%202030.#:~:text=The%20new%20initiative%20aims%20to,in%20all%20regions%20by%202030.#

[6] United Nations Climate Change Global Innovation Hub, "UN Climate Change Global Innovation Hub COP26 Event Report," Glasgow, 2022.

[7] Wood for Good, "COP26." Accessed: Sep. 25, 2024. [Online]. Available: https://woodforgood.com/cop26

[8] F. Richter, P. Kotsovinos, E. Rackauskaite, and G. Rein, "Thermal Response of Timber Slabs Exposed to Travelling Fires and Traditional Design Fires," *Fire Technol*, vol. 57, no. 1, pp. 393–414, May 2021, doi: 10.1007/s10694-020-01000-1.

[9] J. Gales, B. Chorlton, and C. Jeanneret, "The Historical Narrative of the Standard Temperature–Time Heating Curve for Structures," Mar. 01, 2021, *Springer*. doi: 10.1007/s10694-020-01040-7.

[10] Canadian Standards Association, "Annex K: Structural Design for Fire Conditions," in *S16:19 Design of Steel Structures*, National Standards of Canada, 2019.

[11] Canadian Standards Association, "Annex B: Fire Resistance of Large Cross-Section Wood Elements," in *O86-14 Engineering Design in Wood*, CSA Group, 2017.

[12] J. C. Yang, M. F. Bundy, J. L. Gross, A. P. Hamins, F. H. Sadek, and A. Raghunathan, "International R and D Roadmap for Fire Resistance of Structures Summary of NIST/CIB Workshop," Gaithersburg, MD, Jun. 2015. doi: 10.6028/NIST.SP.1188.

[13] M. Smith and J. Gales, *Design of Steel Structures in Canada Using Annex K (Under Review)*. 2025.

[14] "Test Methods for Fire Tests of Building Construction and Materials," May 01, 2020, *ASTM International, West Conshohocken, PA*. doi: 10.1520/E0119-20.

[15] International Organization for Standardization, "Fire-resistance tests - Elements of building construction," Nov. 1975. [Online]. Available: https://standards.iteh.ai/catalog/standards/sist/9f6ee18c-6c7a-465c-b3e9-

[16] Canadian Commission on Building and Fire Codes and National Research Council of Canada, *National Fire Code of Canada 2020*, 11th ed. Canadian Commission on Building and Fire Codes, 2022.

[17] K. Himoto, "Conceptual framework for quantifying fire resilience – A new perspective on fire safety performance of buildings," *Fire Saf J*, vol. 120, p. 103052, Mar. 2021, doi: 10.1016/j.firesaf.2020.103052.

[18] A. Davidson and J. Gales, "BIM and Fire Safety Engineering – Overview of State of The Art," *International Journal of High-Rise Buildings*, vol. 10, no. 4, pp. 251–263, Jan. 2021, doi: 10.21022/IJHRB.2021.10.4.251.

[19] C. Jeanneret, “Alternative Solutions for Canadian Fire Engineering Design,” York University, Toronto, 2021.

[20] A. Chakrabarty, S. Mannan, and T. Cagin, “Process Safety,” in *Multiscale Modeling for Process Safety Applications*, Elsevier, 2016, pp. 5–110. doi: 10.1016/B978-0-12-396975-0.00002-4.

[21] D. Drysdale, *An Introduction to Fire Dynamics: 3rd Edition*. Wiley, 2011.

[22] P.-C. Chiang and S.-Y. Pan, “Iron and Steel Slags,” in *Carbon Dioxide Mineralization and Utilization*, Singapore: Springer Singapore, 2017, pp. 233–252. doi: 10.1007/978-981-10-3268-4_11.

[23] T. Tankova *et al.*, “Residual stresses in welded I section steel members,” *Eng Struct*, vol. 197, p. 109398, Oct. 2019, doi: 10.1016/j.engstruct.2019.109398.

[24] K. Pańcikiewicz, M. Maślak, M. Pazdanowski, M. Stankiewicz, and P. Zajdel, “Changes in the microstructure of selected structural alloy steel grades identified after their simulated exposure to fire temperature,” *Case Studies in Construction Materials*, vol. 18, p. e01923, Jul. 2023, doi: 10.1016/j.cscm.2023.e01923.

[25] R. Wickens, “Fundamentals of Carbon Steel Part 1 - Phases & Microstructures,” LFF Group. Accessed: Jun. 09, 2025. [Online]. Available: https://www.lffgroup.com/posts/carbon-steel-fundamentals-part-1

[26] D. I. Nwosu and V. K. R. Kodur, “Steel Structures Exposed to Fire: A State-of-the-art Report,” Dec. 1997. doi: https://doi.org/10.4224/20337843.

[27] J. Chipman, “Thermodynamics and Phase Diagram of the Fe-C System,” *Metallurgical and Materials Transactions B*, vol. 3, pp. 55–64, 1972.

[28] R. Wickens, “Fundamentals of Carbon Steel Part 2 - Heat Treatment,” LFF Group. Accessed: Jun. 12, 2025. [Online]. Available: https://www.lffgroup.com/posts/fundamentals-of-carbon-steel-part-2

[29] Standards Council of Canada, “Design of steel structures - CSA S16:19 National Standards of Canada,” 2019. [Online]. Available: www.csagroup.org/legal

[30] A. S. Usmani, J. M. Rotter, S. Lamont, A. M. Sanad, and M. Gillie, “Fundamental principles of structural behaviour under thermal effects,” *Fire Saf J*, vol. 36, no. 8, pp. 721–744, Nov. 2001, doi: 10.1016/S0379-7112(01)00037-6.

[31] S. Venkatachari and V. K. R. Kodur, “Effect of transient creep on fire induced instability in steel framed structures,” *J Constr Steel Res*, vol. 181, p. 106618, Jun. 2021, doi: 10.1016/j.jcsr.2021.106618.

[32] M. Biron, “Advanced Mechanical Properties,” in *Material Selection for Thermoplastic Parts*, Elsevier, 2016, pp. 407–455. doi: 10.1016/B978-0-7020-6284-1.00010-6.

[33] G. T. Tsoumis, “wood,” Encyclopedia Britannica. Accessed: May 31, 2025. [Online]. Available: https://www.britannica.com/science/wood-plant-tissue/Microstructure

[34] Architizer Editors, “Architectural Material Guide: Hardwood vs. Softwood,” Architizer. Accessed: May 31, 2025. [Online]. Available: https://architizer.com/blog/practice/materials/softwood-cladding/

[35] G. Harun, B. Chorlton, F. Richter, and J. Gales, “The effects of radial cracks on the fire performance of heritage timber,” *Fire Mater*, vol. 47, no. 3, pp. 386–399, Apr. 2023, doi: 10.1002/fam.3104.

[36] Canadian Wood Council, “Wood Design Manual - Volume 2,” Ottawa, 2017.

[37] “Lumber,” Canadian Wood Council. Accessed: Jun. 08, 2025. [Online]. Available: https://cwc.ca/articles/lumber/

[38] “Mass Timber,” Canadian Wood Council. Accessed: Jun. 01, 2025. [Online]. Available: https://cwc.ca/articles/mass-timber-2/

[39] “Glulam,” Canadian Wood Council. Accessed: Jun. 08, 2025. [Online]. Available: https://cwc.ca/articles/glulam/#:~:text=Used%20for%20members%20stressed%20principally,without%20affecting%20the%20strength%20characteristics.

[40] “CLT,” Canadian Wood Council. Accessed: Jun. 08, 2025. [Online]. Available: https://cwc.ca/articles/cross-laminated-timber-clt/

[41] J. Thibodeau, M. Désilets, M. Brien, and C. Gosselin, "Fact sheet: Pyrolysis," Government of Canada. Accessed: May 31, 2025. [Online]. Available: https://gost.tpsgc-pwgsc.gc.ca/tfs.aspx?ID=58&lang=eng#infoMenu1

[42] A. I. Bartlett, R. M. Hadden, and L. A. Bisby, "A Review of Factors Affecting the Burning Behaviour of Wood for Application to Tall Timber Construction," Jan. 15, 2019, *Springer New York LLC*. doi: 10.1007/s10694-018-0787-y.

[43] C. Di Blasi, "Modeling chemical and physical processes of wood and biomass pyrolysis," *Prog Energy Combust Sci*, vol. 34, no. 1, pp. 47–90, Feb. 2008, doi: 10.1016/j.pecs.2006.12.001.

[44] H. Mitchell, R. Amin, M. Heidari, P. Kotsovinos, and G. Rein, "Structural hazards of smouldering fires in timber buildings," *Fire Saf J*, vol. 140, p. 103861, Oct. 2023, doi: 10.1016/j.firesaf.2023.103861.

[45] L. Schmidt, R. M. Hadden, and D. Fernando, "Observations and impact of char layer formation and loss for engineered timber," *Fire Saf J*, vol. 147, Jul. 2024, doi: 10.1016/j.firesaf.2024.104196.

[46] Oasys, "Oasys LS-DYNA Environment," Nov. 21, 2024, *Oasys*: 21.

[47] "Advanced Simulation Software," Oasys. Accessed: Jun. 01, 2025. [Online]. Available: https://www.oasys-software.com/dyna/software/

[48] M. Elchalakani, B. Yang, K. Mao, and T. Pham, "Numerical methods," in *Geopolymer Concrete Structures with Steel and FRP Reinforcements*, Elsevier, 2023, pp. 491–583. doi: 10.1016/B978-0-443-18876-3.00001-3.

[49] C. Zhang, X. Chen, Z. Shao, C. Xu, and J. Wang, "Simulation and optimization of the molecular weight distribution in a non-ideal polymerization reactor," 2016, pp. 565–570. doi: 10.1016/B978-0-444-63428-3.50099-0.

[50] Livermore Software Technology, "LS-DYNA Keyword User's Manual Volume 1," Sep. 2021.

[51] J. N. Reddy and D. K. Gartling, *The Finite Element Method in Heat Transfer and Fluid Dynamics*, 3rd ed. Boca Raton: CRC Press, 2010.

[52] "What are the differences between implicit and explicit?," LS-DYNA Support. Accessed: Jun. 02, 2025. [Online]. Available: https://www.dynasupport.com/faq/general/what-are-the-differences-between-implicit-and-explicit

[53] HM Government, "The Building Regulations 2010 - Fire Safety - Approved Document B," 2010. [Online]. Available: www.gov.uk/guidance/building-regulations-

[54] Sports Ground Safety Authority, *Guide to Safety at Sports Grounds*, 6th ed. London, 2018.

[55] Australian Building Codes Board, "National Construction Code - Volume One: Building Code of Australia," 2022.

[56] National Fire Protection Association, *NFPA 101 Life Safety Code*. Quincy, 2024.

[57] Associated Press, "Superdome Roof Catches Fire, One Injured with Minor Burns," *Sports Illustrated*, Sep. 21, 2021. Accessed: Aug. 28, 2024. [Online]. Available: https://www.si.com/nfl/2021/09/21/superdome-roof-catches-fire-new-orleans-one-injured

[58] A. Ortiz, "Fire Breaks Out at New Texas Rangers Stadium," *The New York Times*, Dec. 14, 2019. Accessed: Aug. 28, 2024. [Online]. Available: https://www.si.com/nfl/2021/09/21/superdome-roof-catches-fire-new-orleans-one-injured

[59] Daily Finland Report, "Football stadium gutted in fire in Helsinki," *Daily Finland*, Jul. 14, 2024. Accessed: Aug. 28, 2024. [Online]. Available: https://www.dailyfinland.fi/national/38563/Football-stadium-gutted-in-fire-in-Helsinki

[60] The Canadian Press, "Raptors game vs. Indiana suspended due to speaker fire, resumes without fans," *Toronto Star*, Mar. 26, 2022. Accessed: Mar. 18, 2024. [Online]. Available: https://www.thestar.com/news/gta/raptors-game-vs-indiana-suspended-due-to-speaker-fire-resumes-without-fans/article_5313743c-479a-51d8-951e-b932cb874871.html

[61] J. Teitelbaum, B. Knight, and Forbes Staff, "The Most Valuable NBA Teams 2024," Forbes. Accessed: Jan. 15, 2025. [Online]. Available:

https://www.forbes.com/sites/justinteitelbaum/2024/10/24/the-most-valuable-nba-teams-2024/

[62] "NBA Attendance Report 2022," ESPN. Accessed: Jan. 15, 2025. [Online]. Available: https://www.espn.com/nba/attendance/_/year/2022/sort/allAvg

[63] Postmedia News, "MLSE seeks $3M in damages for fire that disrupted Raptors game: Report," Toronto Sun. Accessed: Jan. 20, 2025. [Online]. Available: https://torontosun.com/sports/basketball/nba/toronto-raptors/mlse-seeks-3m-in-damages-for-fire-that-disrupted-raptors-game-report

[64] C. Jeanneret, K. Chin, M. Smith, P. Kotsovinos, and J. Gales, "Design of Bi-Linear Steel Connectors for Fire Loading," in *International Fire Safety Symposium (IFireSS 2025) - 5th Edition*, Belfast, Jun. 2025.

[65] G. C. Clifton *et al.*, "Post-Fire Evaluation of the New Zealand International Convention Centre," *Fire Technol*, 2023, doi: 10.1007/s10694-023-01516-2.

[66] C. Muñoz Blanc, A. Obiol Sánchez, and I. Fortea Navarro, "Evaluation of steel structures integrity in a post-fire condition: Case study of the Serradells sports centre in Andorra," *Fire Saf J*, vol. 133, Oct. 2022, doi: 10.1016/j.firesaf.2022.103668.

[67] F. M. Block and N. A. Butterworth, "The Definition of Fire Resistance Requirements for Stadium and Arena Developments Based on Risk," *Steel Structures*, vol. 9, pp. 39–46, 2009.

[68] L. Lu, G. Yuan, Z. Huang, Q. Shu, and Q. Li, "Performance-based analysis of large steel truss roof structure in fire," *Fire Saf J*, vol. 93, pp. 21–38, Oct. 2017, doi: 10.1016/j.firesaf.2017.08.002.

[69] M. Salminen and J. Hietaniemi, "Performance-based fire design of steel structures of Helsinki Olympic Stadium," in *Applications of Structural Fire Engineering*, Czech Technical University in Prague, 2017. doi: 10.14311/asfe.2015.016.

[70] G. Zhang, G. Zhu, G. Yuan, and Q. Li, "Stability analysis of large-span steel truss structure under local cooling from fire extinguishing system," *Structural Design of Tall and Special Buildings*, vol. 27, no. 6, Apr. 2018, doi: 10.1002/tal.1451.

[71] E. Ozyurt and Y. C. Wang, “Effects of truss behaviour on critical temperatures of welded steel tubular truss members exposed to uniform fire,” *Eng Struct*, vol. 88, pp. 225–240, Apr. 2015, doi: 10.1016/j.engstruct.2015.01.032.

[72] K. Kubicka and U. Radoń, “Proposal for the Assessment of Steel Truss Reliability Under Fire Conditions,” *Archives of Civil Engineering*, vol. 61, no. 4, pp. 141–154, Dec. 2015, doi: 10.1515/ace-2015-0041.

[73] S. Jiang, S. Zhu, X. Guo, and Z. Li, “Full-scale fire tests on steel roof truss structures,” *J Constr Steel Res*, vol. 169, Jun. 2020, doi: 10.1016/j.jcsr.2020.106025.

[74] S. Jiang, S. Zhu, X. Guo, C. Chen, and Z. Li, “Safety monitoring system of steel truss structures in fire,” *J Constr Steel Res*, vol. 172, Sep. 2020, doi: 10.1016/j.jcsr.2020.106216.

[75] G. Q. Li, J. Li, and S. Zhu, “An approach for early-warning collapse of planar steel trapezoid trusses exposed to fire,” *Fire Saf J*, vol. 137, May 2023, doi: 10.1016/j.firesaf.2023.103778.

[76] R. Sibil and E. Ozyurt, “A Numerical Study to Evaluate the Changes in Dynamic Properties of Various Steel Truss Types Under Fire Conditions,” *International Journal of Steel Structures*, vol. 23, no. 6, pp. 1476–1489, Dec. 2023, doi: 10.1007/s13296-023-00782-8.

[77] R. Kallada Janardhan, S. Shakil, W. Lu, S. Hostikka, and J. Puttonen, “Coupled CFD-FE analysis of a long-span truss beam exposed to spreading fires,” *Eng Struct*, vol. 259, May 2022, doi: 10.1016/j.engstruct.2022.114150.

[78] E. G. Hantouche, K. K. Al Khatib, and M. A. Morovat, “Modeling creep of steel under transient temperature conditions of fire,” *Fire Saf J*, vol. 100, pp. 67–75, Sep. 2018, doi: 10.1016/j.firesaf.2018.07.006.

[79] P. Fedczuk and W. Skowroński, “Non-Linear Analysis of Plane Steel Prestressed Truss in Fire,” *Journal of Civil Engineering and Management*, vol. 8, no. 3, pp. 177–183, Jan. 2002, doi: 10.1080/13923730.2002.10531274.

[80] J. Gales, L. Robertson, and L. Bisby, “Creep of prestressing steels in fire,” *Fire Mater*, vol. 40, no. 7, pp. 875–895, Nov. 2016, doi: 10.1002/fam.2345.

[81] B. Nicoletta, J. Gales, P. Kotsovinos, and B. Weckman, “Experimental Thermal Performance of Unloaded Spiral Strand and Locked Coil Cables Subject to Pool Fires,” *Structural Engineering International*, vol. 32, no. 3, pp. 392–410, Jul. 2022, doi: 10.1080/10168664.2021.1881943.

[82] H. Carton, A. Davidson, L. Mladenova, J. Gales, and R. AL-Hamd, “Advancements in the Characterization of Structural Material High-Temperature Deformation,” in *4th International Conference on Structural Safety Under Fire & Blast Loading*, London, 2024.

[83] European Commission, “Temperature assesment of a vertical steel member subjected to localised fire,” 2017.

[84] John Gales, “Unbonded Post-Tensioned Concrete Structures in Fire,” Doctoral, University of Edinburgh, Edinburgh, 2013.

[85] C. M. Smith and M. S. Hoehler, “Imaging Through Fire Using Narrow-Spectrum Illumination,” *Fire Technol*, vol. 54, no. 6, pp. 1705–1723, Nov. 2018, doi: 10.1007/s10694-018-0756-5.

[86] S. Gatien, T. Young, M. S. Hoehler, and J. Gales, “Application of narrow-spectrum illumination and image processing to measure surface char formation in lateral ignition and flame spread tests,” *Fire Mater*, vol. 43, no. 4, pp. 358–364, Jun. 2019, doi: 10.1002/fam.2706.

[87] W. Chu, J. Fang, R. Zhou, and Y. Wang, “A Novel Methodology to Gauge and Quantify the Surface Cracks of Burning Timber,” *Fire Technol*, May 2025, doi: 10.1007/s10694-025-01761-7.

[88] S. Stanier, A. Take, J. Blaber, and D. White, “GeoPIV-RG,” 2015.

[89] T. McAllister, W. Luecke, M. Iadicola, and M. Bundy, “Measurement of Temperature, Displacement, and Strain in Structural Components Subject to Fire Effects: Concepts and Candidate Approaches,” Gaithersburg, MD, Nov. 2012. doi: 10.6028/NIST.TN.1768.

[90] L. Bisby, J. Gales, and C. Maluk, “A contemporary review of large-scale non-standard structural fire testing,” *Fire Sci Rev*, vol. 2, no. 1, p. 1, 2013, doi: 10.1186/2193-0414-2-1.

[91] V. Kodur, M. Z. Naser, and H. S. Kim, "Testing Protocols and Procedures for Undertaking Fire Resistance Tests on Concrete Structures Incorporating Fiber-Reinforced Polymers," *Polymers (Basel)*, vol. 17, no. 3, p. 404, Feb. 2025, doi: 10.3390/polym17030404.

[92] E. Rackauskaite, P. Kotsovinos, and G. Rein, "Model parameter sensitivity and benchmarking of the explicit dynamic solver of LS-DYNA for structural analysis in case of fire," *Fire Saf J*, vol. 90, pp. 123–138, Jun. 2017, doi: 10.1016/j.firesaf.2017.03.002.

[93] E. Rackauskaite, G. Flint, A. Maani, A. Temple, and P. Kotsovinos, "Use of LS-DYNA for Structural Fire Engineering," in *12th European LS-DYNA Conference*, Koblenz, 2019.

[94] S. Watson, B. Nicoletta, P. Kotsovinos, R. Al Hamd, and J. Gales, "Modelling Thermal Performance of Unloaded Spiral Strand and Locked Coil Cables Subject to Pool Fires," *Structural Engineering International*, 2022, doi: 10.1080/10168664.2022.2101969.

[95] A. Temple, G. Walker, G. Flint, Y. Panev, and P. Kotsovinos, "Verification of 2D heat transfer models developed in LS-DYNA for structural fire engineering applications," in *Applications of Fire Engineering - Proceedings of the International Conference of Applications of Structural Fire Engineering, ASFE 2017*, CRC Press/Balkema, 2018, pp. 367–377. doi: 10.1201/9781315107202-39.

[96] Canadian Institute of Steel Construction, "Handbook of Steel Construction 12th Edition," Toronto, 2021.

[97] European Committee for Standardization, "EN 1993-1-2: Eurocode 3: Design of steel structures - Part 1-2: General rules - Structural fire design," 2005.

[98] C. Jeanneret, K. Chin, P. Kotsovinos, and J. Gales, "Chord Shielding Effect in Steel Trusses when Exposed to a Localized Fire," in *CSCE Annual Conference*, Moncton, 2023.

[99] K. Chin, C. Jeanneret, P. Kotsovinos, and J. Gales, "Experimental and Numerical Response of Steel Trusses Exposed to a Localized Fire," in *13th International Conference on Structures in Fire*, Coimbra, 2024, pp. 1117–1126. [Online]. Available: https://orcid.org/0009-0008-0848-8393

[100] P.-C. Peng, J.-H. Chi, and J.-W. Cheng, "A study on behavior of steel structures subjected to fire using non-destructive testing," *Constr Build Mater*, vol. 128, pp. 170–175, Dec. 2016, doi: 10.1016/j.conbuildmat.2016.07.056.

[101] M. S. Doktor, C. Fox, W. Kurz, and J.-P. Stockis, "Characterization of steel buildings by means of non-destructive testing methods," *J Math Ind*, vol. 8, no. 1, p. 10, Dec. 2018, doi: 10.1186/s13362-018-0052-5.

[102] United Nations Environment Programme and Yale Center for Ecosystems + Architecture, "Building Materials and the Climate: Constructing a New Future." Accessed: Sep. 25, 2024. [Online]. Available: https://wedocs.unep.org/handle/20.500.11822/43293

[103] Canadian Wood Council, "Wood Products and Carbon Sequestration." Accessed: May 16, 2025. [Online]. Available: cwc.ca/wp-content/uploads/2013/11/WOOD-Products-and-Carbon-Sequestration.pdf

[104] E. Philion, B. Chorlton, J. Gales, and P. Kotsovinos, "Structural Fire Modeling Strategies for Exposed Mass Timber Compartments and Experimental Gaps for Model Validation," *Journal of Performance of Constructed Facilities*, vol. 36, no. 6, Dec. 2022, doi: 10.1061/(asce)cf.1943-5509.0001761.

[105] A. Law, "The role of modelling in structural fire engineering design," *Fire Saf J*, vol. 80, pp. 89–94, Feb. 2016, doi: 10.1016/j.firesaf.2015.11.013.

[106] N. Werther *et al.*, "Parametric Study of Modelling Structural Timber in Fire with Different Software Packages," Zurich, 2012.

[107] European Committee for Standardization, "EN 1995-1-2: Eurocode 5: Design of timber structures - Part 1-2: General - Structural fire design," Brussels, 2004.

[108] H. Quiquero, J. Gales, A. Abu, and R. Al Hamd, "Finite Element Modelling of Post-tensioned Timber Beams at Ambient and Fire Conditions," *Fire Technol*, vol. 56, no. 2, pp. 737–767, Mar. 2020, doi: 10.1007/s10694-019-00901-0.

[109] R. Pečenko, S. Svensson, and T. Hozjan, "Modelling heat and moisture transfer in timber exposed to fire," *Int J Heat Mass Transf*, vol. 87, pp. 598–605, May 2015, doi: 10.1016/j.ijheatmasstransfer.2015.04.024.

[110] R. Pečenko, I. Planinc, S. Svensson, and T. Hozjan, “Implementing coupled heat and moisture transfer model in the fire analysis of timber beams,” *Fire Saf J*, vol. 107, pp. 170–178, Jul. 2019, doi: 10.1016/j.firesaf.2018.11.007.

[111] D. K. Shen, M. X. Fang, Z. Y. Luo, and K. F. Cen, “Modeling pyrolysis of wet wood under external heat flux,” *Fire Saf J*, vol. 42, no. 3, pp. 210–217, 2007, doi: 10.1016/j.firesaf.2006.09.001.

[112] V. D. Thi, M. Khelifa, M. El Ganaoui, and Y. Rogaume, “Finite element modelling of the pyrolysis of wet wood subjected to fire,” *Fire Saf J*, vol. 81, pp. 85–96, Apr. 2016, doi: 10.1016/j.firesaf.2016.02.001.

[113] V. D. Thi, M. Khelifa, M. Oudjene, M. El Ganaoui, and Y. Rogaume, “Finite element analysis of heat transfer through timber elements exposed to fire,” *Eng Struct*, vol. 143, pp. 11–21, Jul. 2017, doi: 10.1016/j.engstruct.2017.04.014.

[114] T. T. Tran *et al.*, “Fire structural performance of thermo-mechanically compressed spruce timber by means experiments and a three-step multi-reactions pyrolysis 3D-finite element modelling,” *Constr Build Mater*, vol. 320, Feb. 2022, doi: 10.1016/j.conbuildmat.2021.126100.

[115] S. Šulc, V. Šmilauer, and F. Wald, “Thermal model for timber fire exposure with moving boundary,” *Materials*, vol. 14, no. 3, pp. 1–10, Feb. 2021, doi: 10.3390/ma14030574.

[116] ASTM International, “Standard Test Methods for Fire Tests of Building Construction and Materials,” ASTM E119-22. Accessed: Apr. 07, 2024. [Online]. Available: https://www.astm.org/e0119-22.html

[117] E. Philion, K. Chin, P. Kotsovinos, B. Weckman, and J. Gales, “An Analysis of the Fire Performance of Small-Scale Canadian Heritage Hardwood and Softwood,” *Structural Engineering International*, vol. 32, no. 2, pp. 253–264, Jun. 2024, doi: 10.1080/10168664.2024.2340566.

[118] K. Chin, A. Lau, D. Lacroix, and J. Gales, “Numerical Modelling of Charring in Engineered Timber,” in *International Fire Safety Symposium (IFireSS 2025) - 5th Edition*, Belfast, Jun. 2025.

[119] NIST, “Cone Calorimeter,” NIST. Accessed: Apr. 23, 2025. [Online]. Available: https://www.nist.gov/laboratories/tools-instruments/cone-calorimeter

[120] H. Quiquero and J. Gales, “Behaviour of Fire-Damaged Engineered Timber Beams,” in *5th International Structural Specialty Conference of the Canadian Society of Civil Engineers*, London: CSCE, Jun. 2016, pp. 993–1.

[121] H. Quiquero, M. Smith, and J. Gales, “Developing fire safety engineering as a practice in Canada,” 2018, *Canadian Science Publishing*. doi: 10.1139/cjce-2016-0552.

[122] “State of Mass Timber in Canada,” GC Wood. Accessed: Jun. 18, 2025. [Online]. Available: https://experience.arcgis.com/experience/58e313c4ac0247138ba5057d655ed1d4

[123] J. König and L. Walleij, “One-Dimensional Charring of Timber Exposed to Standard and Parametric Fires in Initially Unprotected and Postprotection Situations,” 1999.

[124] B. Fredlund, “Modelling of Heat and Mass Transfer in Wood Structures During Fire,” *Fire Saf J*, vol. 20, pp. 39–69, 1993.

[125] M. Létourneau-Gagnon, C. Dagenais, and P. Blanchet, “Fire performance of self-tapping screws in tall mass-timber buildings,” *Applied Sciences (Switzerland)*, vol. 11, no. 8, Apr. 2021, doi: 10.3390/app11083579.

[126] C. Maraveas, K. Miamis, and C. E. Matthaiou, “Performance of Timber Connections Exposed to Fire: A Review,” *Fire Technol*, vol. 51, no. 6, pp. 1401–1432, Nov. 2015, doi: 10.1007/s10694-013-0369-y.

[127] Z. Chen, C. Ni, C. Dagenais, and S. Kuan, “WoodST : A Temperature-Dependent Plastic-Damage Constitutive Model Used for Numerical Simulation of Wood-Based Materials and Connections,” *Journal of Structural Engineering*, vol. 146, no. 3, Mar. 2020, doi: 10.1061/(ASCE)ST.1943-541X.0002524.